Master's thesis

NTNU
Norwegian University of Science and Technology
Faculty of Engineering
Department of Geoscience and Petroleum

Haissam Rabih Sakr

A coupled wellbore-reservoir modelling approach to showcase the effect of CO_2 injection on flow behavior in a saline aquifer

Master's thesis in Petroleum Engineering
Supervisor: Ashkan Jahanbani Ghahfarokhi
Co-supervisor: Alv-Arne Grimstad
June 2024

NTNU
Norwegian University of
Science and Technology

Haissam Rabih Sakr

A coupled wellbore-reservoir modelling approach to showcase the effect of CO_2 injection on flow behavior in a saline aquifer

Master's thesis in Petroleum Engineering
Supervisor: Ashkan Jahanbani Ghahfarokhi
Co-supervisor: Alv-Arne Grimstad
June 2024

Norwegian University of Science and Technology
Faculty of Engineering
Department of Geoscience and Petroleum

NTNU
Norwegian University of
Science and Technology

Acknowledgement

I would like to start by expressing my sincere gratitude to my supervisor Ashkan Jahanbani Ghahfarokhi for his continuous support throughout this semester, and to my co-supervisor Alv-Arne Grimstad for his critical contributions which made this study feasible. Your technical proficiency, academic guidance, and motivation were significant in the completion of this study.

Furthermore, I extend my appreciation to the Department of Geoscience and Petroleum at the Norwegian University of Science and Technology for their assistance in facilitating technical support, enabling me to conduct this research effectively with their instant follow-ups.

Summary

Carbon capture and storage (CCS) is on the rise as a solution for reducing the amount of carbon dioxide (CO_2) in the atmosphere, which is considered the main reason behind global warming. To safely store CO_2 in a prospective site, for a long period without causing any adverse effects on the integrity of the wellbore and formation, a comprehensive study should take place to account for all the possible challenges and complications faced during and after injection. This study investigates the effect of CO_2 injection on flow behavior, using a coupled wellbore-reservoir modeling approach, considering two targeted sites: a saline aquifer and a depleted gas field. Key findings from the simulation results include the efficiency of different trapping mechanisms. Structural trapping showed effectiveness in confining CO_2 within geological formations, residual trapping caused 40% of CO_2 to be immobilized in deeper pore spaces, solubility trapping enhanced the retention of CO_2 by significantly increasing CO_2 mole fractions in water, and mineral trapping showed efficiency in capturing up to 5% of injected CO_2 over a span of 200 years. In addition, fracture pressure for Bryne and Sandnes formations was calculated using Eaton's method at 515 bara, ensuring safe injection rates below this constraint, similarly for the Frigg depleted field where the fracture pressure was calculated at 150 bara. Step-rate injection test was done to identify the optimal rate of CO_2 injection of 10,000 m^3/day, balancing both storage efficiency and formation integrity. Thermal simulations were also run and showed that temperature variations impact CO_2 phase behavior. This affects for example the solubility of CO_2 in brine, the geochemical reactions, the density and viscosity of both CO_2 and brine, and the porosity of the formation. Phase diagrams were generated to examine the phase changes of CO_2 under different conditions to better understand their effect on storage efficiency, and pressure and temperature profiles. Finally, a sensitivity analysis was carried out to conclude an optimal scenario for CO_2 storage. It indicated that lower reservoir pressure, higher porosity, and lower initial water saturation increased the storage capacity by around 60%. This study offers a comprehensive framework for optimizing CO_2 injection strategies in CCS projects, understanding how CO_2 is behaving under different conditions, and ensuring the integrity of geological formations.

Keywords: CO_2 injection, coupling approach, thermal effects.

Sammendrag

Karbonfangst og -lagring er i framgang som en løsning for å redusere mengden karbondioksid (CO_2) i atmosfæren, som regnes som hovedårsaken til global oppvarming. For å trygt lagre CO_2 på et potensielt sted over en lang periode, uten å forårsake noen negative effekter på integriteten til brønnbanen og formasjonen, bør en omfattende studie gjennomføres for å ta hensyn til alle mulige utfordringer og komplikasjoner som kan oppstå under og etter injeksjon. Denne studien undersøker effekten av CO_2-injeksjon på strømningsadferd, ved bruk av en koblet brønnbane- og reservoarsmodelleringstilnærming med tanke på to bestemte steder: en saltvannsakvifer og et utarmet gassfelt. Viktige funn fra simuleringsresultatene inkluderer effektiviteten av ulike fangstmekanismer. Strukturell fangst viste seg å være effektiv i å innesperre CO_2 i geologiske formasjoner, residualfangst førte til at 40% av CO_2 ble immobilisert i dypere porerom, løselighetsfangst økte retensjonen av CO_2 ved å betydelig øke CO_2-molekylfraksjonene i vann, og mineralfangst var effektiv i å fange opp til 5% av injisert CO_2 over en periode på 200 år. I tillegg ble bruddtrykket for Bryne- og Sandnes formasjonene beregnet ved bruk av Eatons metode til 515 bara, noe som sikrer trygge injeksjonshastigheter under denne grensen. Tilsvarende ble bruddtrykket for det utarmede Frigg-feltet beregnet til 150 bara. Trinnvise injeksjonstester ble utført for å identifisere den optimale CO_2-injeksjonshastigheten på 10,000 m^3/dag, som balanserer lagringseffektivitet og formasjonens integritet. Termiske simuleringer ble også utført, og viste at temperaturvariasjoner påvirker CO_2-faseatferd. Det påvirker for eksempel løseligheten av CO_2 i saltvann, de geokjemiske reaksjonene, tettheten og viskositeten til både CO_2 og saltvann, og porøsiteten til formasjonen. Fasediagrammer ble generert for å se på faseendringene til CO_2 under ulike forhold for å bedre forstå effekten på lagringseffektivitet, samt trykk- og temperaturprofiler. Til slutt ble en følsomhetsanalyse gjennomført for å konkludere med optimale forhold for lagring av CO_2. Den indikerte at lavere reservoartrykk, høyere porøsitet og lavere initiell vannmetning økte lagringskapasiteten med rundt 60%. Denne studien tilbyr et omfattende rammeverk for optimalisering av CO_2-injeksjonsstrategier i CCS-prosjekter, forståelse for hvordan CO_2 oppfører seg under forskjellige forhold, og sikring av integriteten til geologiske formasjoner.

Nøkkelord: CO_2-injeksjon, koblingstilnærming, termiske effekter.

Contents

List of Figures

1 Introduction

The excess of greenhouse gas emissions in the atmosphere is causing a threat to humanity. A report to the United Nations General Assembly stated that the human-induced climate change is the largest, most pervasive threat to the natural environment and societies the world has ever experienced, and the poorest countries are paying the heaviest price [3].

The increase in greenhouse gases in our atmosphere is the main reason behind global warming. A greenhouse gas is any gaseous compound in the atmosphere that is capable of absorbing infrared radiation, such as carbon dioxide CO_2, methane CH_4, and nitrous oxide N_2O, therefore trapping and holding heat in the atmosphere [14].

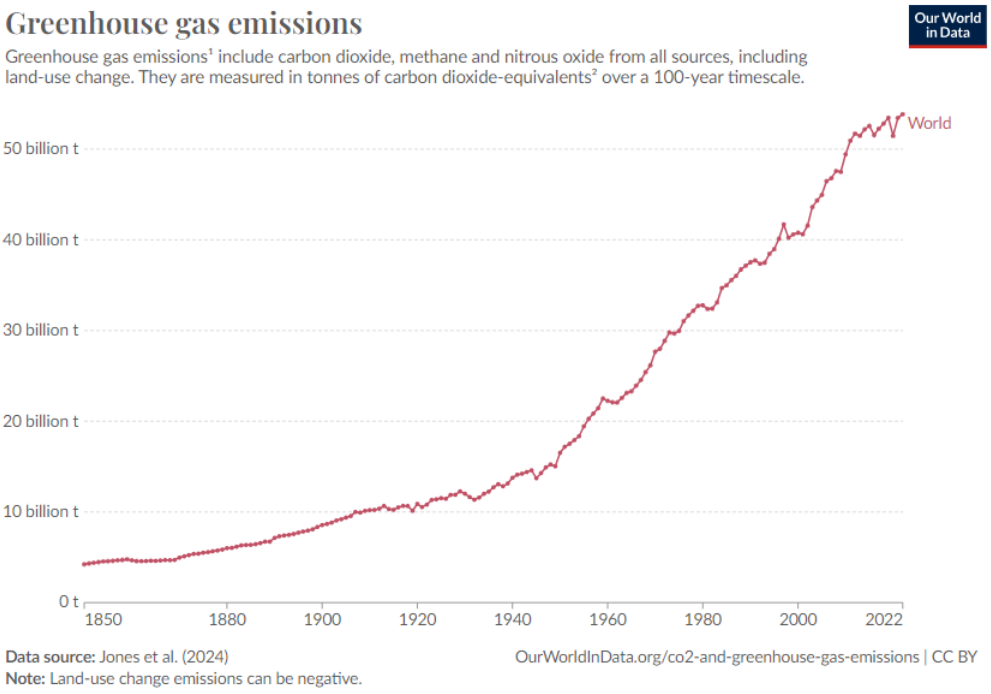

Figure 1: Global Greenhouse Gas Emissions in tonnes of CO_2 equivalents [16].

Carbon dioxide (CO_2) is the predominant greenhouse gas produced as a result of fossil fuels burning, significantly linked to petroleum activities, industrial production, and land use change. Many believe that oil and gas companies are the main contributors to climate change and that they should be held responsible for years of their petroleum activities.

However, it is not widely known that major oil and gas companies like Equinor, BP, Total-Energies, ExxonMobil, and Royal Dutch Shell are paving the way to other companies and investors to contribute to carbon capture and storage projects (CCS).
ExxonMobil, for example, is investing $20 billion in lower-emission investments from 2022 through 2027, including CCS projects like the Baytown facility in Texas and the Houston carbon capture hub [6]. In addition, Equinor is developing a full-scale CCS value chain in Europe, the Northern Lights initiative in Norway, which operates alongside Shell and TotalEnergies aiming to store CO_2 captured from industrial sources across the continent. For the substantial investments being put into CCS projects, numerous academic and industry research papers are being published each year. Excessive studies have been carried out to optimize the injection of CO_2 and to understand the behavior of CO_2 under different conditions.

Some complications that are faced in CO_2 injection projects include: vaporization of CO_2 causing changes in thermodynamic properties as a result of CO_2 injection in a dense state into a low-pressure reservoir, pressure control issues as a result of vaporization of CO_2 increasing the flow velocity and potential formation of hydrates, and compromised wellbore integrity.
In addition, a number of challenges are encountered in CCS projects such as: inducing fractures or re-activating existing faults, potentially leading to leakage as a result of high CO_2 injection rates, predicting and understanding the movement and behavior of the CO_2 plume within the aquifer and the complex interactions between the CO_2, brine, and rock, and CO_2 dissolution and mineralization, where CO_2 reacts with the rock in a saline aquifer to form carbonates, a process that can alter the porosity and permeability of the reservoir [2].

This master's thesis tackles a number of challenges and complications of CO_2 injection mentioned above, in a comprehensive study by applying a coupled wellbore-reservoir modeling approach. A wellbore model was built first on PIPESIM and then integrated into CMG GEM™ where a reservoir model was built simulating Bryne and Sandnes formations (potential saline aquifer storage site) and then Frigg formation (potential depleted gas field storage site). The main objective of this thesis aims to employ a coupled wellbore-reservoir modeling approach to evaluate the overall suitability of chosen formations for long-term CO_2 storage.

The study reflects how different CO_2 injection rates affect the pressure profiles of the system and integrity of storage formation. It also presents the dominant trapping mechanisms in various geological settings, the impact of temperature variations on CO_2 phase behavior and storage efficiency, and the optimal conditions for maximizing CO_2 storage capacity while ensuring geological integrity.

The methodologies employed to identify an optimal injection rate include calculating the fracture pressure using Eaton's method, and step-rate injection testing. In addition, more methodologies are applied to assess the flow behavior of CO_2 like visualising the CO_2 trapping mechanisms and evaluating the thermal effects on CO_2, brine, and formation rock. Finally a sensitivity analysis was done to evaluate the best storing conditions of CO_2 in a saline aquifer. All of the mentioned methodologies provide a comprehensive framework for optimizing CO_2 injection strategies and understanding CO_2 behavior under different conditions in two different prospective sites.

2 Theory

To assess the behavior of CO_2 in the near well-bore region, and to showcase the effects of different CO_2 injection scenarios on the studied system using a wellbore-reservoir coupled approach, a variety of theories must be presented.

2.1 Trapping Mechanisms of CO_2

Structural trapping, residual trapping, solubility trapping, and mineral trapping are the four trapping mechanisms of CO_2. Understanding these mechanisms is essential for any CCS project.

Structural trapping represents the physical trapping of CO_2 in geological formations, where CO_2 is trapped under seal-like impermeable rock layers, preventing the CO_2 from migrating further to the surface and then into the atmosphere. Structural trapping is the first mechanism for CO_2 containment that happens right after injection. Therefore, identifying suitable geological formations with effective cap rocks is crucial for long-term and safe CO_2 storage [1].

Residual trapping takes place when the capillary forces immobilizes the CO_2 in the pore spaces of the rock. As CO_2 spreads through the porous rock, a fraction of it gets trapped in the pores as disconnected bubbles. This mechanism adds security to the containment of CO_2 by immobilizing a portion of it and reducing the risk of leakage over time, even if structural trapping fails [8].

Solubility trapping implies the dissolution of CO_2 into the formation water (typically brine), forming a denser CO_2-water mixture which is less likely to migrate upwards, consequently affecting the behavior of CO_2 in the system and the shape of the plume. This mechanism requires a suitable pressure and temperature for the dissolution to take place, and needs more time compared to the previous mechanisms [15].

Mineral trapping occurs when the dissolved CO_2 reacts with minerals in the formation rock, forming stable carbonate minerals. This mechanism takes the most time but can permanently immobilize CO_2 as solid mineral phases, ensuring long-term sequestration [7].

2.2 Fracture Pressure

The fracture pressure is the pressure required to create a fracture in the formation [4]. Taking account for fracture pressure is a key element in CO_2 injection projects, as breaching the fracture pressure can cause uncontrolled fracturing of the cap rock or storage formation, compromising the integrity of the storage site. Therefore estimating the fracture pressure helps in optimizing the injection of CO_2, as CO_2 storage would be maximized when the injection is done at pressures close to but below the fracture pressure.

Eaton's (1969) [5] method to calculate the fracture pressure gradient uses Poisson's ratio of the formations based on the concept of the minimum injection pressure proposed by Hubbert and Willis (1957) [10]:

$$FG = \frac{\nu}{1-\nu}(OBG - P_{\mathrm{p}}) + P_{\mathrm{p}} \tag{1}$$

Where ν is Poisson's ratio, which can be calculated from the compressional and shear velocities (Vp and Vs) using the equation below:

$$\nu = \frac{0.5((V_{\mathrm{p}}/V_{\mathrm{s}})^2 - 1}{(V_{\mathrm{p}}/V_{\mathrm{s}})^2 - 1} \tag{2}$$

Eaton's method could be used to calculate the fracture gradient by incorporating different lithologies through Poisson's ratio. For example, for shales a Poisson's ratio of 0.43 is typically used, whereas a Poisson's ratio of 0.3 is used for sandstones [21]. Nevertheless, in this study Poisson's ratio was calculated using the compressional and shear wave velocities obtained from the sonic logs corresponding to representative wells from each formation.

2.3 Injection Rate Optimization

Step-Rate Injection Test

This test is used to estimate the optimal injection rate that the system can handle without causing any induced fractures. Therefore, this test helps in planning the injection of CO_2 in CCS project to maximize the storage efficiency while maintaining the integrity of the system. It consists of setting an injection schedule with gradual increase in CO_2 injection rate in specific steps to be defined. The bottomhole pressure is monitored all along, any spikes or unusual trends would be analyzed. [18].

Usually this test is used to estimate the fracture pressure of the system. However, this won't be the case as the fracture pressure will be obtained using a different method.

2.4 Thermal Effects of CO_2 Injection into a Saline Aquifer

It is important to understand what happens when cold CO_2 is injected into a warmer formation, as several significant effects can take place due to heat exchange.

Thermal Contraction and Expansion

Thermal gradients get created when cold CO_2 is injected into a warmer system. This could cause contraction and then expansion of the rock matrix, potentially changing the porosity and permeability of the aquifer. As a result of injecting cold CO_2, cooling of the surrounding formation could lead to possible thermal fracturing [20].

Effects on fluid properties

The viscosity and density of both CO_2 and brine are affected by thermal changes, and this could greatly affect the flow dynamics. As a cooler environment can increase the viscosity of brine, reducing its mobility and potentially leading to changes in the migration patterns of the injected CO_2 [12].

Effects on solubility and mineral reactions

When cold CO_2 is injected into a warmer aquifer, the solubility of CO_2 in brine gets higher as long as it is still cold. However, as the CO_2 warms up, its solubility decreases. In addition, temperature changes results in various geochemical reactions, such as the dissolution of minerals and the precipitation of carbonates, which affects the porosity and permeability of the formation.

Carbonic acid is formed when CO_2 reacts with brine , lowering the pH of the aquifer. This acidic environment causes the dissolution of carbonate minerals (like calcite and dolomite) and the precipitation of secondary minerals such as siderite over time [13].

All the chemical reactions and their effects on the storage of CO_2 are explained in section 4.5.4.

2.5 Previous Work

A number of studies have been done to assess the effects of CO_2 sequestration by applying wellbore-reservoir coupling approach. For example, an article by Hussein Hoteit, Marwan Fahs, and Mohamad Reza Soltanian [9] investigated how to address flow-assurance issues during the injection of CO_2 into depleted gas reservoirs by using a coupled approach, to understand the CO_2 flow behavior within the wellbore and to find solutions for the challenges caused by the liquid-to-gas transition of CO_2 under these conditions. The methodology that they followed consist of applying a coupled approach to integrate multiphase flow within both the wellbore and the reservoir. They built a 3D radial compositional reservoir simulator using Eclipse by Schlumberger incorporating detailed grid properties to simulate the impact of temperature variations on CO_2 phase behavior. One proposed solution in the article involves heating CO_2 at the wellhead to have it in supercritical state, reducing the likelihood of vaporization and pressure gaps along the wellbore.

A similar approach was adapted in this thesis where the injected CO_2 was in the supercritical conditions to avoid any complications in the saline aquifer. However, the fact that both models are built using different simulators, and that they use different values for formation properties as well as different depths and lithologies, requires an updated approach.

Another article by Seyed Mostafa Jafari Raad, Don Lawton, Greg Maidment, and Hassan Hassanzadeh [11] investigated the effect of transient behavior of wellbore parameters during CO_2 injection on the overall injection performance. The methodology that they adapted is a coupled well-reservoir model to overcome the complications caused by the presence of gas-liquid transient flow in the wellbore causing significant changes in the wellbore dynamics and the increase in bottomhole pressure caused by the accumulation of liquid CO_2 in the wellbore. They used CMG STARS™, a non-isothermal transient multiphase flow simulator, to simulate wellbore and reservoir interactions. A sensitivity analysis was done to understand the impact of several reservoir parameters on wellbore transient flow behavior, such as permeability. The model was validated using history matching and showed that it is reliable to optimize CO_2 injection tests, improving the efficiency and safety of storage operations.

In this thesis CMG GEM™ was used instead, to take into account the different trapping mechanisms of CO_2 and the geochemical reactions. However, there are similarities with the mentioned article as the flow behavior of CO_2 was analyzed using different techniques.

Finally, both articles contribute valuable insights into CO_2 injection processes using wellbore-reservoir coupling approach, but from different perspectives. This thesis would include methodologies from both articles to tackle the flow-assurance and structural integrity issues, while assessing the transient behaviors and their implications for injection performance and optimization. The thesis will offer a comprehensive understanding of the challenges and solutions in CO_2 injection into a saline aquifer and a depleted gas reservoir.

3 Methodology

Knowing the significance of carbon capture and storage, and based on the objective of this study, to couple the wellbore data with a reservoir simulator to study the behavior of CO_2 under different conditions, a reservoir simulator must be chosen to be suitable to perform all the analyses needed.

PIPESIM, a steady-state wellbore simulator, was chosen in the previous study to assess its limitations in showcasing the effect of different CO_2 injection scenarios on flow behavior in a wellbore. A series of results were obtained from running a sensitivity analysis on multiple parameters. However, some limitations had to be overcome by coupling with a reservoir simulator.

The chosen reservoir simulator for this study is CMG GEM™ . CMG is a software by Computer Modelling Group Ltd. that consists of 8 different simulators and tools listed in Figure 2, GEM™ is one of the simulators.

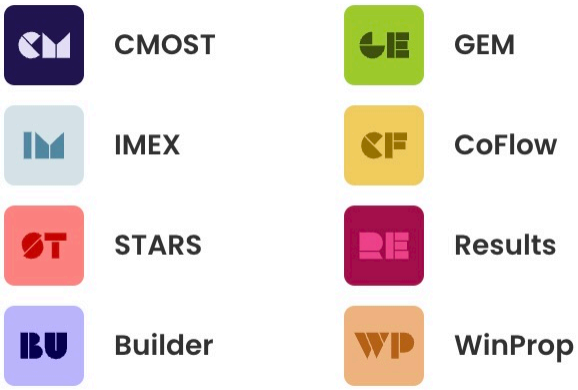

Figure 2: CMG simulators and tools.

There are two simulators that are most used when it comes to CO_2 sequestration simulation, GEM™ and STARS™. GEM™ is a compositional and unconventional simulator, it is widely used to capture unconventional shale liquids production and to simulate CO_2 and H_2 storage processes. However, STARS™ is a thermal and advanced processes simulator, it could be used to simulate CO_2 storage processes for the fact that it includes complex wellbore modelling (FlexWell), but it is mostly used for modelling of recovery processes involving steam, solvents, air and chemicals.

At this level, using GEM™ is more convenient to achieve the objectives of this study without indulging in complex processes, especially that GEM™ is able to simulate some simple thermal processes and has a wellbore model option which is needed to couple with PIPESIM.
In addition, GEM™ has a unique built-in process wizard that could be used explicitly for CCS purposes, such as adding the trapping mechanisms needed for a better simulation of CO_2 storage.

The models are built using CMG BUILDER™, it is a pre-processor simulation model building tool. It is an interactive interface which enables the design and preparation of simulation models for all CMG simulators.
WINPROP™ is a fluid property characterization tool used to create detailed fluid property descriptions for CMG simulators. The WINPROP™ file is added to BUILDER™ to fill the components section needed to validate the model.
After finishing building the whole model, GEM™is used to run the simulation and when the results are done, they can be visualized using RESULTS™, a post-processor visualization and analysis tool. The whole cycle or process could be simplified in Figure 3 below.

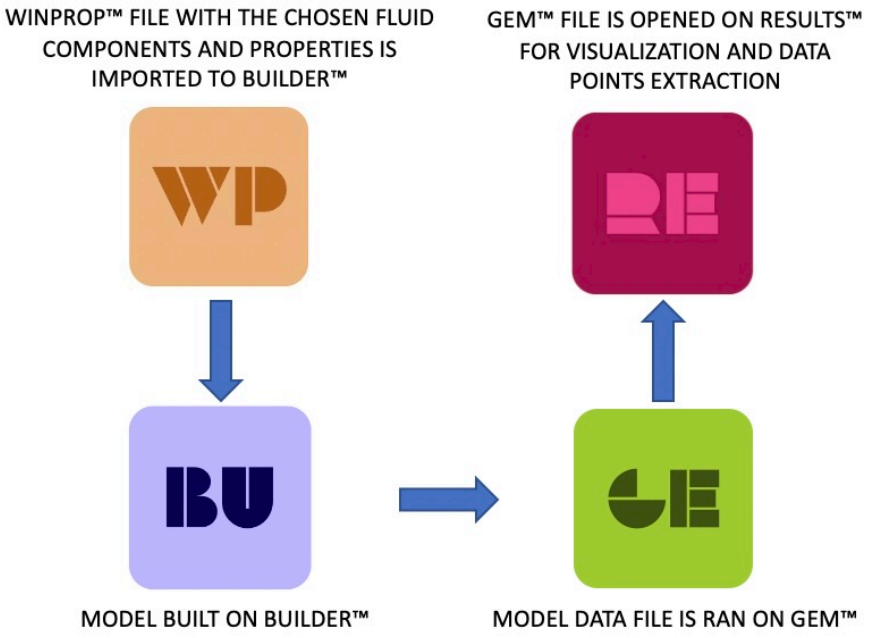

Figure 3: CMG cycle.

The coupling approach used to achieve the objective of this study is one-way coupling, see Figure 4. This type of coupling is based on using the output from the wellbore model (PIPESIM) as input for the reservoir model (CMG GEM™) without any iterative loop. However, some simple iterations could be done when needed. For example, some initial guesses from PIPESIM might not go well with the system built on GEM™ considering more precise data are used and considering that GEM™ accounts for transient effects unlike PIPESIM. Therefore, a change is done on PIPESIM and then the new data could be tried again on GEM™.
This approach is less computationally intensive, but it may not capture the dynamic interactions between the wellbore and the reservoir as effectively as an intensive iterative coupling approach.

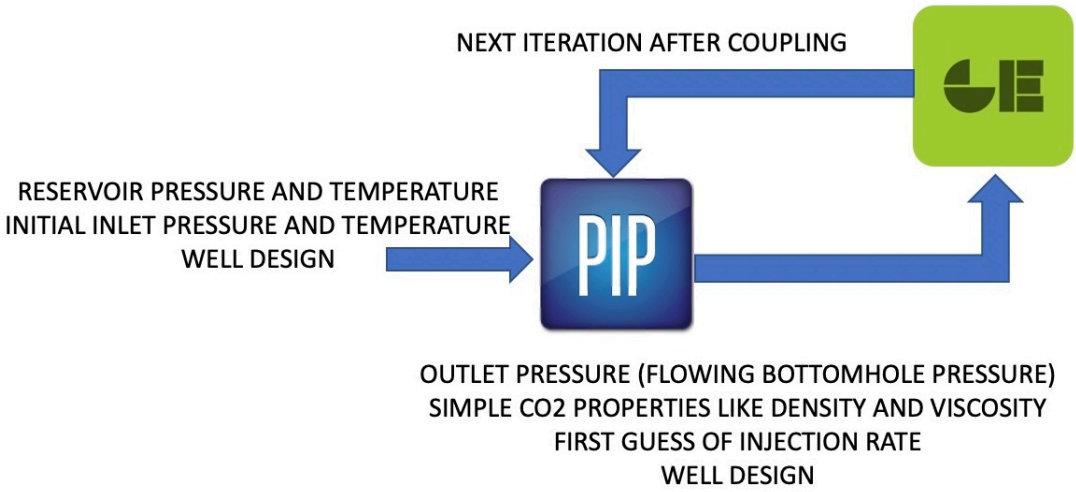

Figure 4: One-way coupling.

Three models will be introduced later in the next section. The first is a simple 2D cartesian model built solely to get familiar with CMG and perform a simple simulation on trapping mechanisms with the some general and default data.
The second model is a also a 2D cartesian model, it represents Bryne and Sandnes formations with all the available data. Will be used as a reference to every upcoming analysis.
The third model represents the Frigg depleted field, and will be used to compare the results with the previous study done on PIPESIM where a pressure surge occurred.

3.1 Model 1: Simple 2D Model

3.1.1 Choosing the model's grid and properties

As mentioned earlier, this model is built only to get familiar with CMG BUILDER™ and to run simple simulation showing the trapping mechanisms of CO_2.
It is a 2D cartesian grid model, 100 blocks in 'i' direction, 1 block in 'j' direction, and 20 blocks in 'k' direction, resulting in a total of 2000 blocks.
The thickness of every block in 'i' and 'j' directions is 10 meters to have a width of 1000 meters, and in 'k' direction it is 5 meters to have a thickness of 100 meters.
The reservoir properties are distributed equally along the whole grid as follows:

- Permeability in i, j and k directions: 100 mD
- Porosity: 0.18
- Grid top: 1200 m
- Rock compressibility 5.8e-07 1/kPa

3.1.2 Fluid components

In this section, WINPROP™ is used to generate the fluid components file. By using the library in WINPROP™, CO_2 and CH_4 were added to the model. CO_2 to be injected with 1 mole fraction, and CH4 as a tracer component but with a 0 mole fraction.
Some parameters were needed to do that, such as:

- Reservoir temperature: 50°C
- Water density: 1020 kg/m^3
- Water compressibility: 4.5e-07 1/kPa
- Reference pressure of water: 131 bara

This model represents a saline aquifer.

3.1.3 Rock-Fluid interactions

In this section, a new rock type must be identified and relative permeability tables must be input. Stone's Second Model is the method selected to evaluate the 2-phase relative permeabilities.
For water-oil table and liquid-gas table a random set of relative permeabilities was used as shown in Tables 1 and 2 :

	Sw	**krw**	**krow**
1	0.2	0	1
2	0.29	0.002	0.677
3	0.38	0.018	0.415
4	0.47	0.061	0.218
5	0.56	0.144	0.0833
6	0.65	0.291	0.012
7	0.7	0.411	0
8	0.74	0.486	0
9	0.82	0.771	0
10	0.91	0.95	0
11	1	0.99	0

Table 1: Water-oil table

	Sg	**krg**	**krog**
1	0.0008	0	1
2	0.06	0	0.89
3	0.0889	0.001	0.71
4	0.1889	0.01	0.48
5	0.2667	0.03	0.31
6	0.3556	0.05	0.26
7	0.4444	0.1	0.18
8	0.5666	0.33	0.091
9	0.6711	0.55	0.0376
10	0.73	0.66	0.011
11	0.8	0.99	0

Table 2: Liquid-gas table

Hysteresis was also added in the same section by defining a maximum residual gas saturation of 0.4.

3.1.4 Initial conditions

Setting the initial conditions is considered an important step in building the model, as it defines how the calculations are going to be performed. For this simple level of analysis, 'Vertical Depth Average' was used. It means that the block calculations will be done at each grid block average over the depth interval. For this, a reference pressure of 118 bara and a reference depth of 1200 m, which is the grid top, were chosen.

3.1.5 Wells & Recurrent

At this step, defining the simulation period and adding a well is required.
A simulation period of 200 years (from 1/1/2024 to 1/1/2224) was chosen to take account for any mineral interactions with CO_2. The well added is an injector with two operational constraints:

- Maximum bottomhole pressure: 445 bara
- Maximum surface gas rate: 10,000 m^3/day

The wellbore model was ignored at this level, and the injected fluid chosen is pure CO_2. The bottomhole perforations were done on grid blocks [1,1,18], [1,1,19], and [1,1,20]. The injection of 10,000 m^3/day of CO_2 will be held for 1 year, and the rest 199 years will be used for monitoring purposes. Finally, Figure 5 shows how model 1 will look like in 3D.

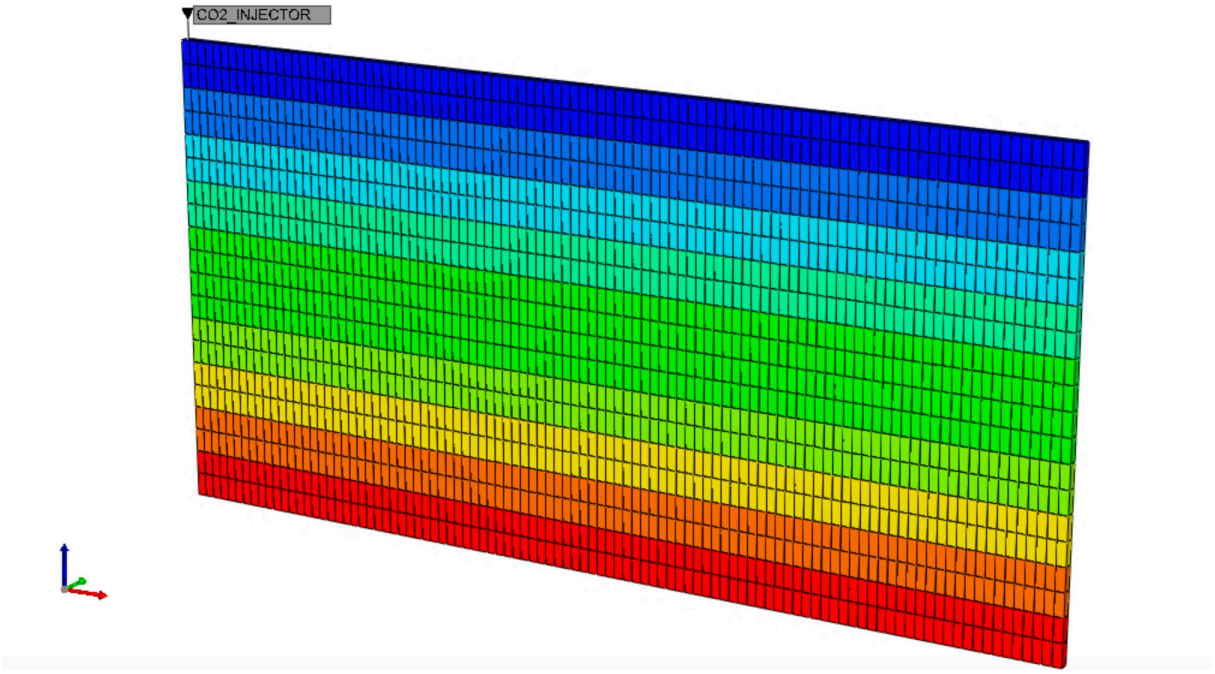

Figure 5: 3D view of model 1.

To this point, the only trapping mechanisms that will be shown are structural and residual trapping, as no solubility calculations has been done, and no mineral reactions have been introduced to the model.

To add the solubility trapping mechanism, a new WINPROP™ file should be used where Harvey's Method (1996) is turned on under Henry's Law Constant Correlation tab. The solubility parameters could then be calculated by inputting the reservoir pressure and temperature and then imported to CMG BUILDER™.

For the mineral trapping mechanism, a series of reactions should be input by using a feature in CMG GEM™ called process wizard.

Some of the aqueous reactions added are:

$$CO_2 + H_2O \longrightarrow H^+ + HCO_3^- \tag{3}$$

$$H^+ + OH^- \longrightarrow H_2O \tag{4}$$

$$CO_3^- + H^+ \longrightarrow HCO_3^- \tag{5}$$

Some of the mineral reactions added are:

$$CaAl_2Si_2O_8 + 8.0\,H^+ \longrightarrow 4.0\,H_2O + Ca^{2+} + 2.0\,Al^{3+} + 2.0\,SiO_2(aq) \tag{6}$$

$$CaCO_3 + H^+ \longrightarrow Ca^{2+} + HCO_3^- \tag{7}$$

$$Al_2Si_2O_5(OH) + 6.0\,H^+ \longrightarrow 5.0\,H_2O + 2.0\,Al^{3+} + 2.0\,SiO_2(aq) \tag{8}$$

With reactions 3, 4, 5, 6, 7, and 8 mineral trapping will be taken into consideration in further simulations.

3.2 Model 2: Refined 2D Cartesian Model of Bryne and Sandnes Formations

This section is considered the key element in preparation for a series of analyses, as this model will be the reference for every simulation to come considering that saline aquifers are the most targeted formations in current CCS projects. They provide larger storage capacity and are the preferred choice for projects focusing purely on CO_2 storage.
This model represents the Bryne and Sandnes formations, which are considered prospective formations for storing CO_2 captured from industrial sources in Norway and other parts of Europe, in a mission to mitigate global warming and reduce the atmospheric emissions of CO_2.
Bryne and Sandnes formations are part of the Lower Jurassic sandy sequence laying in the southern part of the Norwegian North Sea. The Sandnes formation is a developed, sorted and widely distributed sand, above the Bryne formation which is a thick silt and sandstone formation. Together they form a prospective saline aquifer that has promising properties for long-term CO_2 storage.
The final version of the model was validated after a sequence of iterative steps taken for calibration. Such as adjusting the size of the grid, performing some grid refinement, and choosing a suitable well placement. All based on the fact that the model should be a host to a significant amount of CO_2, and taking into account the petrophysical data available and the operational constraints of the system. In addition, the injection rate was chosen after running a step-rate injection test, and validated by performing other pressure transient analysis techniques.
This model will eventually help achieve the objectives of this study: investigating the effect of CO_2 injection in the near-wellbore region and assessing the flow behavior under different CO_2 injection scenarios. This is done by analysing the data points obtained from CMG RESULTS™, and running some pressure transient analysis. In addition, the optimization of CO_2 injection rates for maximum safe storage, and understanding the impact of each scenario on the system's pressure response and formation properties was done on this model.
A critical part in building a simulation model is gathering the necessary data. For this case, some reservoir data like porosity, permeability, formation pressure, and temperature conditions were obtained from the Norwegian Offshore Directorate. Furthermore, the wellbore data was collected from information on wellbore geometry, material properties, and existing downhole conditions also from the Norwegian Offshore Directorate.

3.2.1 Choosing the model's grid and properties

Similar to model 1, this model is also a 2D cartesian grid, composed of 200 blocks in 'i' direction, 1 block in 'j' direction, and 20 blocks in 'k' direction, resulting in a total of 4000 blocks.
The thickness of every block in 'i' and 'j' directions is 10 meters to have a width of 2000 meters, and in 'k' direction it is 5 meters to have a thickness of 100 meters, which is the same as the Bryne and Sandnes formations' thickness.
The initial grid properties are distributed equally along the whole grid as follows:

- Grid top: 3500 m
- Grid thickness in K direction: 5 m
- Porosity: 24%
- Permeability in I and J directions: 150 mD
- Permeability in K direction: 0.15 mD (because of the presence of some coal layers in most of the formation)
- Rock compressibility 5.8e-07 1/kPa

Later on, some grid refinement was added around the wellbore for some accurate representation. The grid refinement simulates some fractures with high porosity and very low permeabilities that could be encountered in real life.
The refined blocks are distributed randomly around the wellbore, with porosity ranging from 0.2 to 0.55, and permeability ranging from 0.001 to 150 mD.
Figure 6 shows how model 2 will look like after creating the grid, inputting the needed data, and refining some random blocks. Assuming that the CO_2 injector will be placed in the middle of the model and perforated at the last 3 layers.

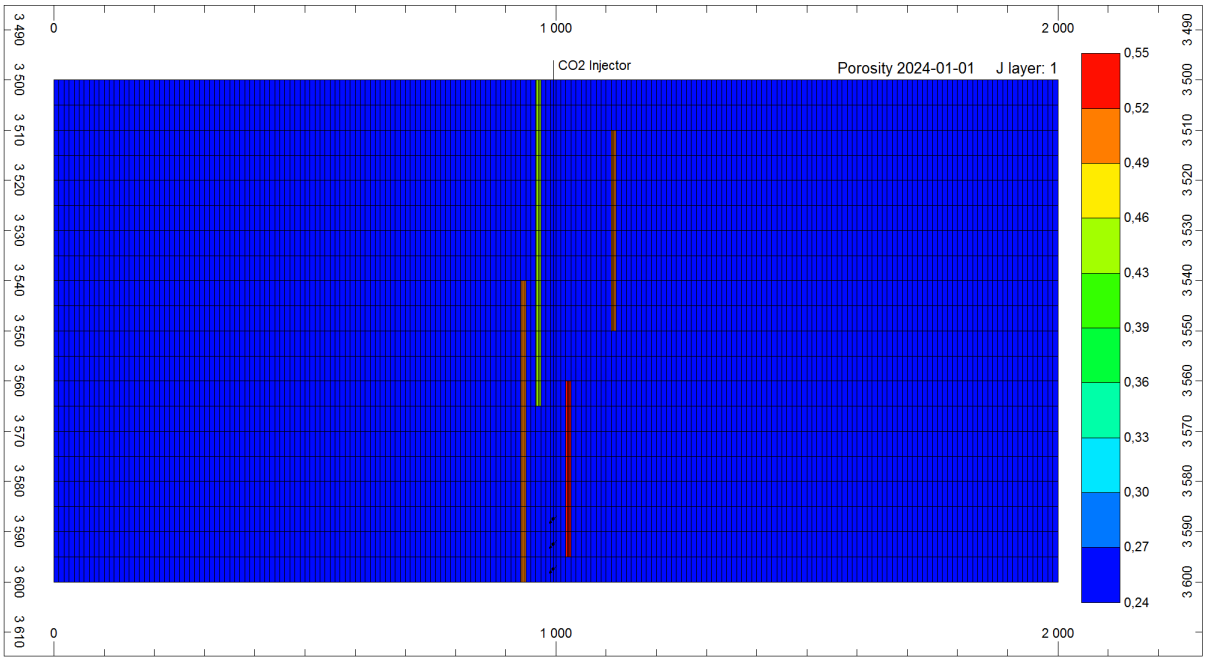

Figure 6: IK-2D view of model 2.

3.2.2 Fluid components

The fluid components are also generated using WINPROP™ by using reservoir temperature 110°C, water density 1020 kg/m^3, and water compressibility 4.5e-07 1/kPa. At this level process wizard was also used to add a CCS process, which will include gas trapping hysteresis CO_2 solubility in water, ionic dissolution, and mineral trapping using geochemistry in the simulation.
The mineral and aqueous reactions added are the same as the one added to model 1, in addition to some other mineral input needed such as:

- Volume fraction of Calcite: 0.0088
- Volume fraction of Kaolinite: 0.0.0176
- Volume fraction of Anorthite: 0.0088

3.2.3 Rock-fluid interactions

The relative permeability tables were generated using built-in correlations and presented in Tables 3 and 4 below:

Sw	krw	krow
0.2	0.0	1.0
0.232258	0.002583715	0.875515
0.264516	0.0093513	0.759276
0.280645	0.01414848	0.70425
0.312903	0.02641694	0.600388
0.345161	0.04211377	0.504782
0.377419	0.06111538	0.417438
0.441935	0.108671	0.267553
0.474194	0.137084	0.205026
0.506452	0.16851	0.150785
0.554839	0.221196	0.08497739
0.587097	0.259958	0.05149133
0.619355	0.301586	0.02632944
0.651613	0.346049	0.009510579
0.683871	0.393315	0.001064414
0.7	0.417991	0.0
0.732258	0.469412	0.0
0.764516	0.523571	0.0
0.796774	0.580444	0.0
0.829032	0.640011	0.0
0.86129	0.702251	0.0
0.893548	0.767145	0.0
0.909677	0.800581	0.0
0.925806	0.834674	0.0
0.958065	0.904821	0.0
0.974194	0.940871	0.0
1.0	0.9999	0.0

Table 3: Water-oil relative permeability

Sg	krg	krog
0.0006	0.0	1.0
0.022093	0.0	0.926691
0.05	0.0	0.836126
0.063953	0.0	0.792784
0.09186	9.636479e-06	0.709941
0.133721	0.0001544405	0.595157
0.161628	0.0004884455	0.524854
0.189535	0.001193133	0.459444
0.203488	0.001747266	0.42855
0.231395	0.003409855	0.370338
0.259302	0.00604612	0.316824
0.287209	0.009977872	0.267925
0.315116	0.01557301	0.223551
0.343023	0.02324555	0.18361
0.398837	0.04670942	0.116615
0.412791	0.05464856	0.102471
0.440698	0.07351818	0.07720342
0.496512	0.125459	0.03827668
0.580233	0.249583	0.006431884
0.60814	0.306461	0.002025317
0.636047	0.372548	0.000168731
0.65	0.40934	0.0
0.677907	0.491029	0.0
0.705814	0.584378	0.0
0.761628	0.810343	0.0
0.775581	0.875833	0.0
0.8	0.9999	0.0

Table 4: Liquid-gas relative permeability

3.2.4 Initial conditions

In this section, a type of reservoir initialization calculation must be chosen. In model 1, the 'Vertical Depth Average' was chosen, and reference pressure and depth were specified to perform the calculations. However, it is important in this section to compare the two options available for initialization calculations, as this model will be a reference for all the sensitivity and pressure transient analyses.
Two different options were tried in this section, one is the 'Vertical Depth Average' option, it indicates that the pressures will be calculated from the hydrostatic equation and saturation from the capillary pressure tables. Also, the block saturation will be assigned as an average of the corresponding saturation over the depth interval spanned by the grid block. This option requires an initial input of reference depth and pressure. The other option is 'USER INPUT' , where pressure, water saturation and global composition of fluids are specified at each grid block, and the saturation calculation will be done by applying flash calculations. Both options were simulated separately, using a specific set of data.
For 'Vertical Depth Average':

- Reference depth: 3500 m (grid top)
- Reference pressure: 325 bara (coupled from PIPESIM model as an outlet pressure at this depth considering a reservoir pressure of 375 bara and an injection rate of 10,000 m^3/d)

For 'USER INPUT':

- Reservoir pressure: 375 bara
- Water saturation: 0.8 (Assumption)
- Global composition of CO_2: 1
- Global composition of CH4: 0

The results were compared and presented in the results section 4.3.1, and the chosen option to continue with further simulations was the 'USER INPUT'.
A saline aquifer would typically have a water saturation equals to 1.
However, an assumption of S_w=0.8 was chosen as the saturation could be affected by production history in nearby formations and possible migration of some formation fluids. In the sensitivity analysis part in section 4.6.4 , a saturation of 1 was evaluated.

3.2.5 Wells and recurrent

Simulation dates were set to be from 1/1/2024 to 1/1/2034, a period of 10 years, with a plan to CO_2 inject the first 5 years, and to monitor the system the other 5 years.
An injector well was created to inject CO_2 into the aquifer, with the following wellbore model used in PIPESIM:

- Tubing depth and length: 3600 m
- Tubing relative roughness: 0.254
- Wellhead temperature: 30°C
- Bottomhole temperature: 100°C
- Wellbore radius: 0.10795 m

The perforations in the bottomhole were done on grid blocks [i, j, k] = [100,1,18], [100,1,19], [100,1,20], with a perforation radius of 0.0762 m. This implies that the well is vertical and placed in the middle of the aquifer, and the injection will occur at the deepest layers. This was chosen after several iterations on well placement, the comparison results are presented in section 4.3.2.
To complete the wells and recurrent part, operational constraints must be defined. The three key constraints in this model are maximum bottomhole pressure, maximum surface gas rate, and minimum wellhead pressure. To choose each, a series of calculations and analyses were done.
The maximum bottomhole pressure constraint should always be less than the system's fracture pressure, to ensure a safe CO_2 injection. The steps taken to calculate the fracture pressure will be demonstrated in section 3.4.
The maximum surface gas rate is directly related to the system's ability in handling a specific amount of CO_2, to avoid any fracturing and leaking of CO_2. However, at the beginning of the project there could be a margin of rates that could be assessed in accordance with the formation's storage capacity.
Data from the Norwegian Offshore Directorate was used to calculate the possible injection rate of CO_2 that suits the capacity of the targeted formation.
As taken from the Norwegian Offshore Directorate website, the storage capacity of Bryne and Sandnes formations is 1 Gt, with a storage efficiency of 4.5%, which is equivalent to 45 Mt. Hence, injecting around 1.5 Mt per year for 30 years would be promising.

To calculate the flowrate in m^3/day, assuming a density value of 850 kg/m^3, the following equation will be used:

$$q_{\text{Injection}} = \frac{M_{CO_2} * 10^9}{\rho_{CO_2} * 365} = \frac{1.5 * 10^9}{850 * 365} \approx 5000\, m^3/day \tag{9}$$

Nevertheless, a range of injection rates will be assessed in an optimization strategy detailed in section 3.5, to choose the most suitable rate for the system. The value of the minimum wellhead pressure is obtained from coupling with PIPESIM. This is done by inputting some parameters in PIPESIM and running a system analysis to estimate the wellhead pressure. For an initial guess, after inputting the reservoir pressure at 375 bar, the target flowrate at 10,000 m^3/day and specifying the wellbore model, the system analysis suggests a minimum wellhead pressure of 102 bar, this is shown in Figure 7 below:

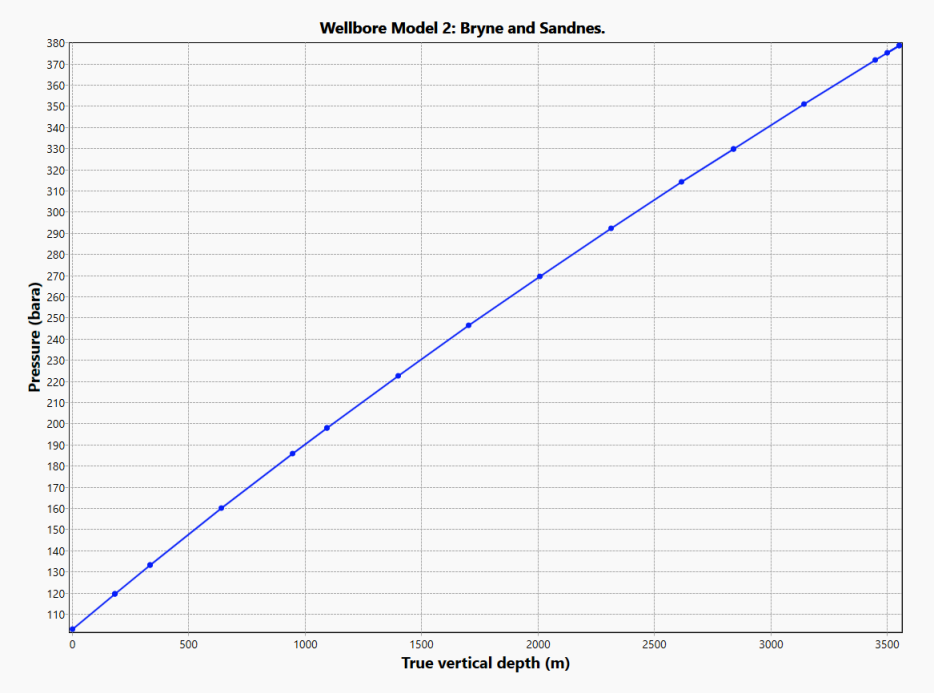

Figure 7: PIPESIM wellhead pressure estimation.

The well's diagram is shown in Figure 65 in Appendix .1.

3.3 Model 3: 2D Cartesian Model of the Frigg Formation

Model 3 representing the Frigg formation was built on CMG to compare the system's pressure response to that of PIPESIM. As in the previous study, the flow behavior of CO_2 wasn't adequately presented in the pressure plots generated on PIPESIM, especially when gas-to-liquid transition happened inside the wellbore [17].
The bottomhole pressure surge shown in Figure 8, implies that the wellhead pressure cannot be controlled properly enough to achieve a smooth behavior in the bottomhole pressure. As a solution, it was proposed in the previous study to couple the wellbore model with a reservoir simulator to try and observe the transient effects using a relatively complex model.

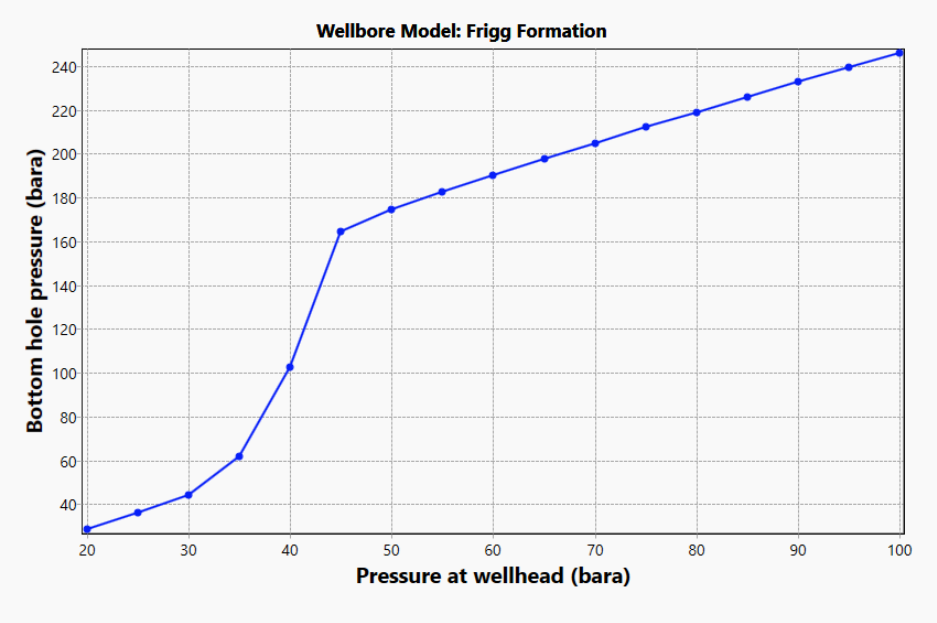

Figure 8: Bottomhole pressure with respect to wellhead pressure plot from PIPESIM.

The Frigg depleted field is a prospective CO_2 storage site due to the remaining gas in the formation, and to its connection to a huge aquifer. The field has been abandoned since 2004 after 27 years of gas production. The Frigg formation is around 2000 meters deep and consists of an unconsolidated sand with an average porosity of 30% and an average permeability of 2000 mD. The reservoir has a pressure of 30 bara after production, and a temperature of 90°C. The initial water saturation is assumed at 0.3, and the injection rate chosen is 100,000 m^3/day. The same data has been used to generate the plot from PIPESIM shown in Figure 8.

The cartesian grid (200x1x20), fluid components, rock-fluid interactions, and initial conditions calculations chosen for this model are the same as for model 2 for simplicity. However, the wellbore model is different considering new PIPESIM coupling data.
The wellbore model coupled from PIPESIM is listed below:

- Tubing depth and length: 2000 m
- Tubing relative roughness: 0.0254
- Wellhead temperature: 6°C
- Bottomhole temperature: 90°C
- Wellbore radius: 0.0889 m

The perforations in the bottomhole were done on grid blocks [i, j, k] = [100,1,18], [110,1,19], [120,1,20], with a perforation radius of 0.0762 m. This means that the well is deviated and placed in the middle of the system, and the injection will occur at the deepest layers. The well's diagram is shown in Figure 66 in Appendix .1.
This model will not be used for sensitivity analysis or injection rate optimization, as it will be limited to analyzing pressure profiles and comparing the transient effects with the previous study.

3.4 Fracture pressure calculation method

Fracture pressure is the pressure at which the formation rock breaks or fractures, causing the CO_2 that is being injected to get leaked to the surface again, which is an unfavorable scenario. Therefore, estimating the fracture pressure is necessary and could be done in a number of ways, such as using numerical modeling, fracture gradient plots, or empirical correlations. There is no consensus on how to calculate fracture gradient in the oil and gas industry, thus some assumptions should be made in this section.
Eaton's method will be used to calculate the fracture pressure using equation 10.
Eaton (1969) used Poisson's ratio of the formation to calculate fracture gradient based on the concept of the minimum injection pressure proposed by Hubbert and Willis (1957) [21]:

$$FG = \frac{\nu}{1-\nu}(OBG - P_{\mathrm{p}}) + P_{\mathrm{p}} \tag{10}$$

Where ν is Poisson's ratio, which can be obtained from the compressional and shear velocities (Vp and Vs) using equation 11 below:

$$\nu = \frac{0.5((V_{\mathrm{p}}/V_{\mathrm{s}})^2 - 1}{(V_{\mathrm{p}}/V_{\mathrm{s}})^2 - 1} \tag{11}$$

The compressional velocity is obtained from sonic logs available in the Norwegian Offshore Directorate for each formation, and shear velocity is calculated assuming a ratio of Vp= 1.75 Vs.
OBG is the overburden pressure gradient calculated using equation 12 below:

$$P_{ob}(z) = \int_0^z \rho_{\mathrm{formation}}(z) \cdot g \cdot dz \tag{12}$$

P_{p} is the pore pressure gradient, however, hydrostatic gradient will be calculated instead for simplicity using equation 13 below:

$$P_{\mathrm{p}} = \rho_{\mathrm{fluid}} \cdot g \cdot z \tag{13}$$

$\rho_{\mathrm{formation}}$ is the density of the formation and ρ_{fluid} is the density of the injected CO_2.
All the results will be presented in section 4.2

3.5 Injection rate optimization strategy for Model 2

The target for CO_2 storage in the Bryne and Sandnes formations is 45 Mt, with an operational constraint of having a flowing bottomhole pressure less than the fracture pressure (515 bara later calculated in section 4.2). Based on this goal, an injection rate optimization strategy was needed to know at which rate the injection of CO_2 will happen and over what period of time.

3.5.1 Step-Rate Injection Testing

As mentioned in the theory part, the step-rate injection test is used to determine the optimal injection rate of CO_2.
An initial injection rate as low as 100 m^3/d, will be injected for 4 hours to prepare the system for pressure response, followed by 9 increments to the rate, until reaching a maximum rate of 15,000 m^3/day. Each increment has a time-step of 2 hours. The total injection time is 24 hours, and the monitoring period after shut-in is 48 hours.
Simple analysis of the bottomhole pressure curve was done to evaluate the response of the system to the gradually increasing injection rates. Finally, a fixed injection rate will be chosen based on the analysis of the pressure response to further continue in the study.

3.6 Sensitivity Analysis for model 2

A series of parameters are altered to assess how they affect the efficiency of CO_2 injection in model 2. Model 2 representing the Bryne and Sandnes formations is a reference for this analysis, aiming to highlight the optimal CO_2 storage conditions.
Four parameters are analyzed: reservoir pressure, porosity, permeability, and initial water saturation. Each parameter is analyzed for three values, low, medium, and high as follows:

- Reservoir pressure: 60 bara - 150 bara - 375 bara
- Porosity: 10% - 24% - 40%
- Permeability: 50 mD - 150 mD - 300 mD
- Water saturation: 0.6 - 0.8 - 1.0

The main output parameters to record and compare are the cumulative CO_2 injected in model 2, and the time needed to reach the operational constraint (maximum bottomhole pressure). After analyzing each parameter independently, a radar plot was created on Excel to present the optimal CO_2 storage conditions considering all the possible options.

4 Results and Discussion

4.1 Trapping mechanisms observed from Model 1

4.1.1 Structural trapping

CO_2 saturation before injection shown in Figure 9, and after 1 year of injection and 199 years of monitoring shown in Figure 10.

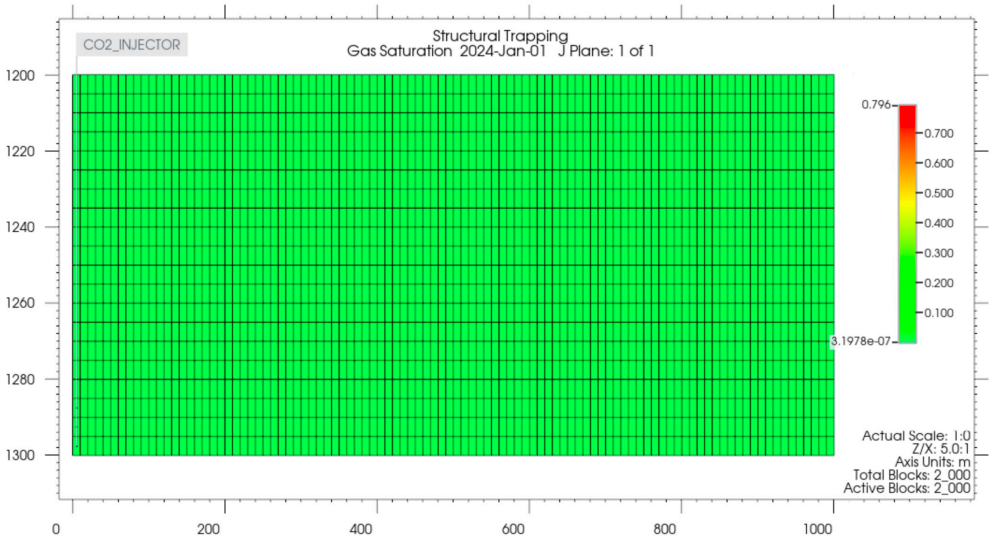

Figure 9: CO_2 saturation at year 2024 before structural trapping.

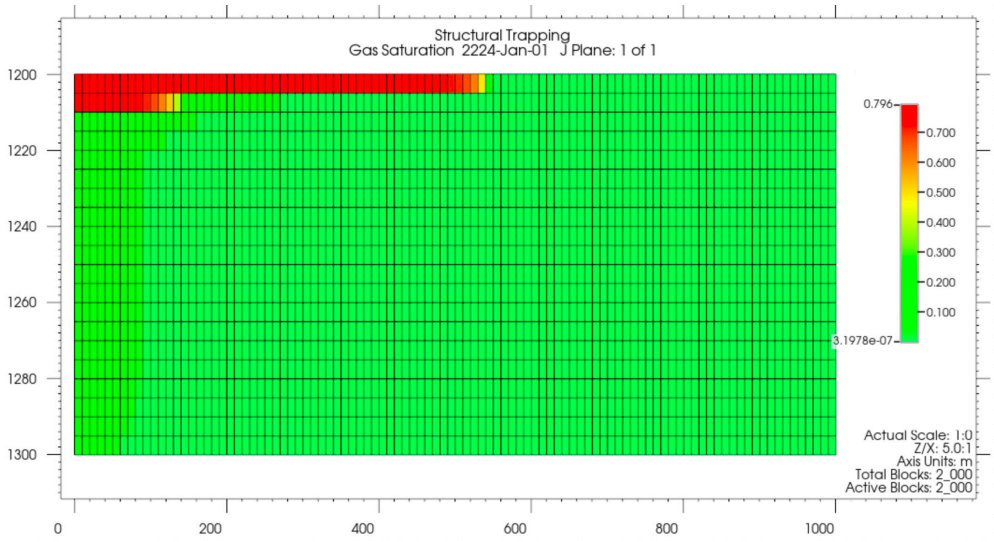

Figure 10: CO_2 saturation at year 2224 after structural trapping.

The CO_2 mole fraction before CO_2 injection shown in Figure 11, and after injection shown in Figure 12. Showing exactly the traces of CO_2 in the system, regardless of the saturation in each block.

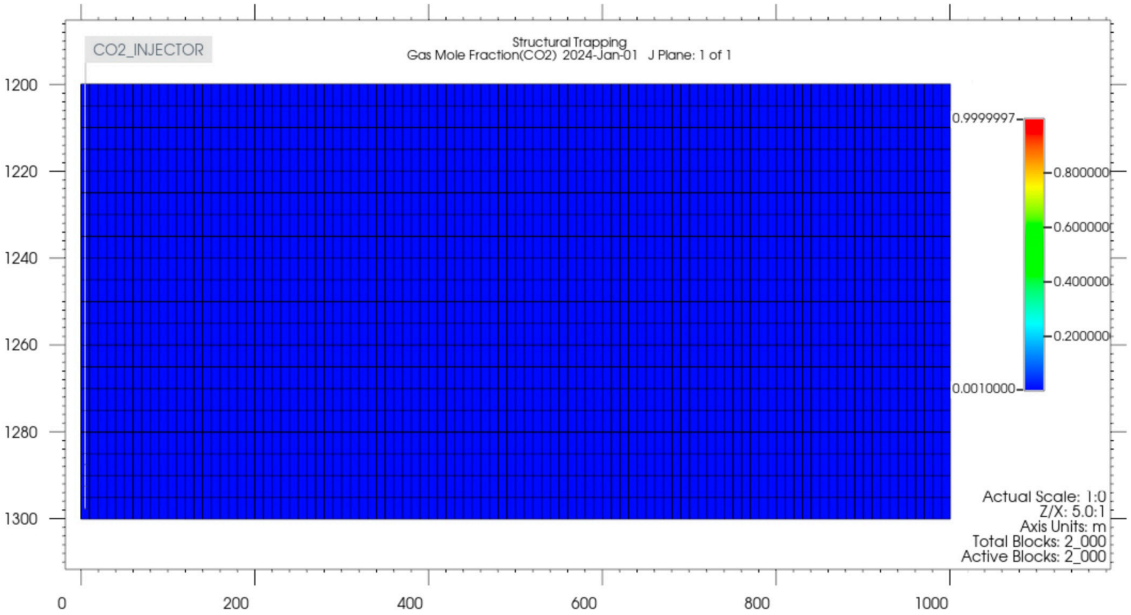

Figure 11: CO_2 mole fraction at year 2024 before structural trapping.

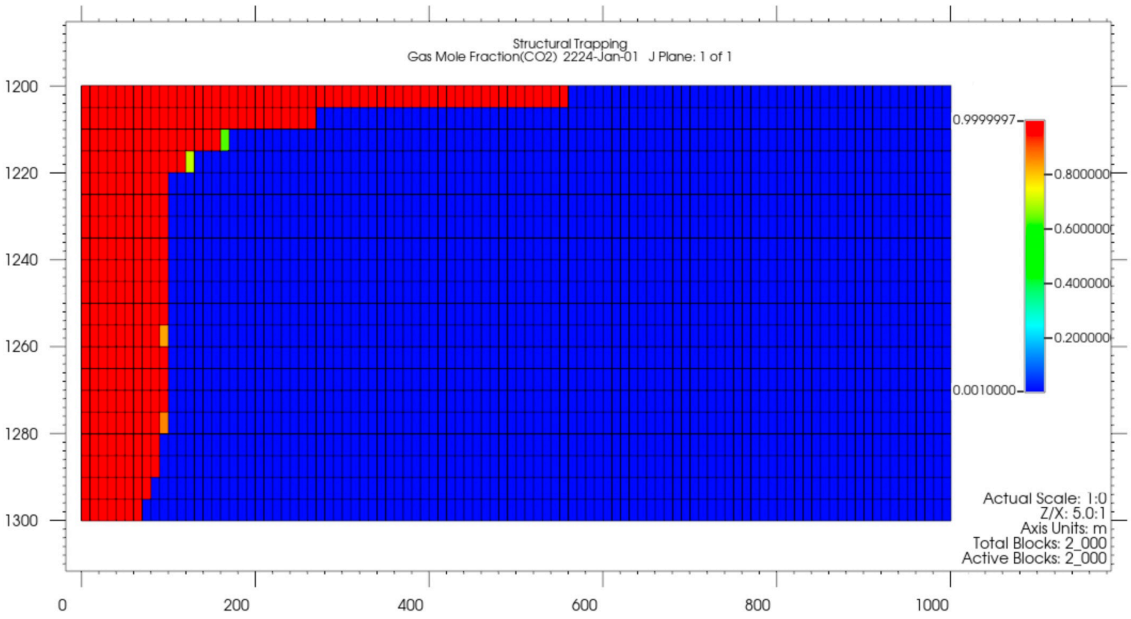

Figure 12: CO_2 mole fraction at year 2224 after structural trapping.

The water mole fraction of CO_2 before injection shown in Figure 13, and after injection shown in Figure 14. Reflecting that no solubility trapping is occurring at this level.

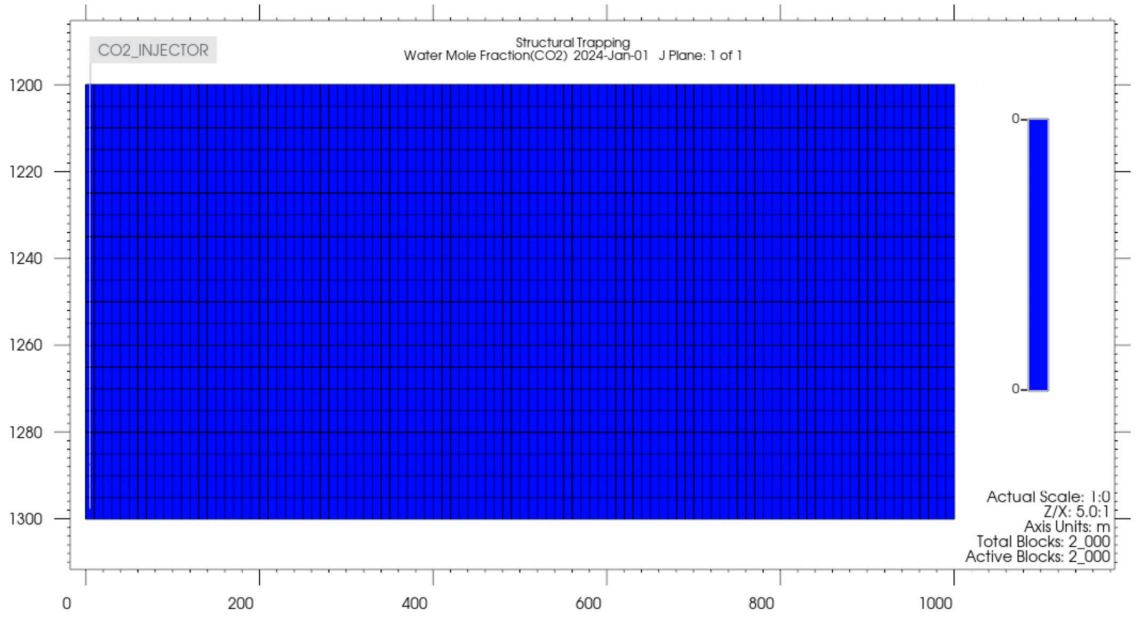

Figure 13: CO_2 fraction in water at year 2024 before structural trapping.

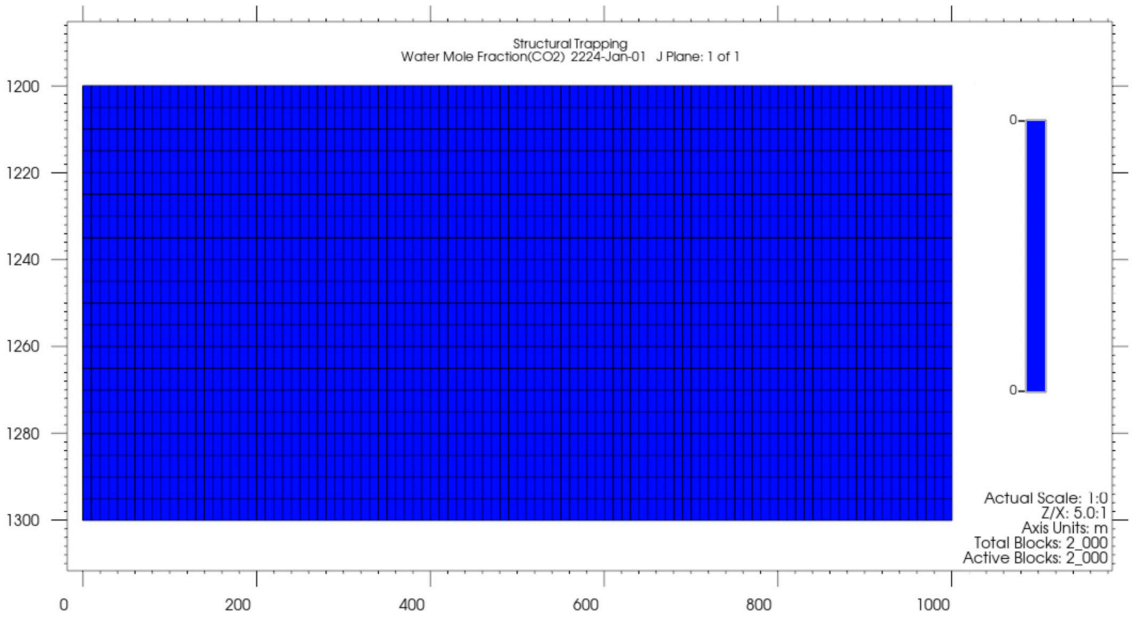

Figure 14: CO_2 fraction in water at year 2224 after structural trapping.

The relative permeability of gas due to hysteresis before CO_2 injection is shown in Figure 15, and after injection is shown in Figure 16. This reflects the absence of residual trapping (hysteresis).

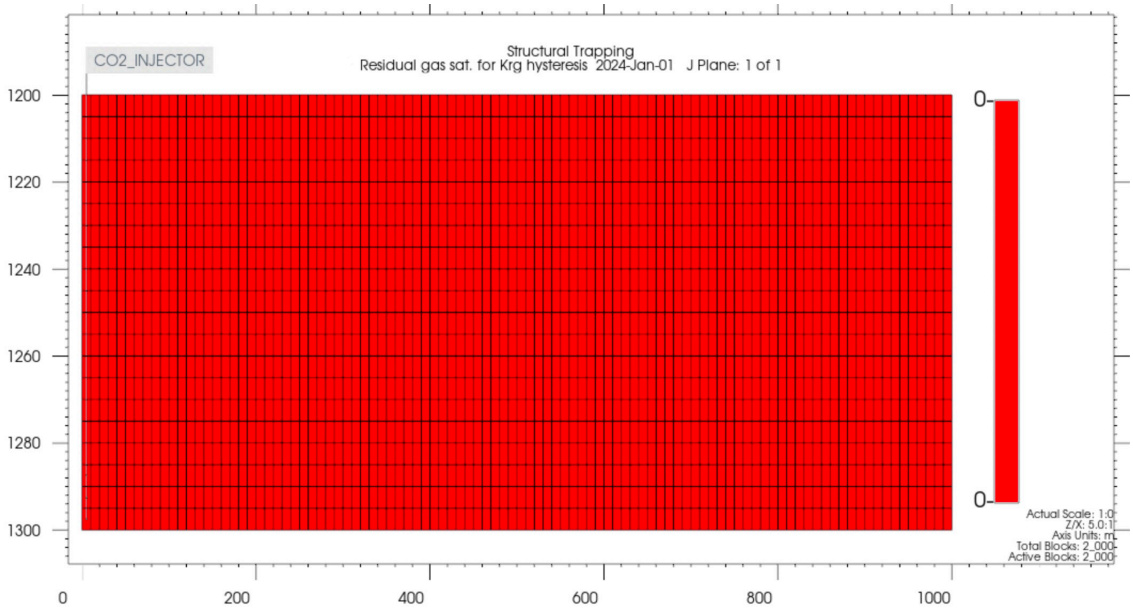

Figure 15: CO_2 relative permeability due to hysteresis at year 2024 before structural trapping.

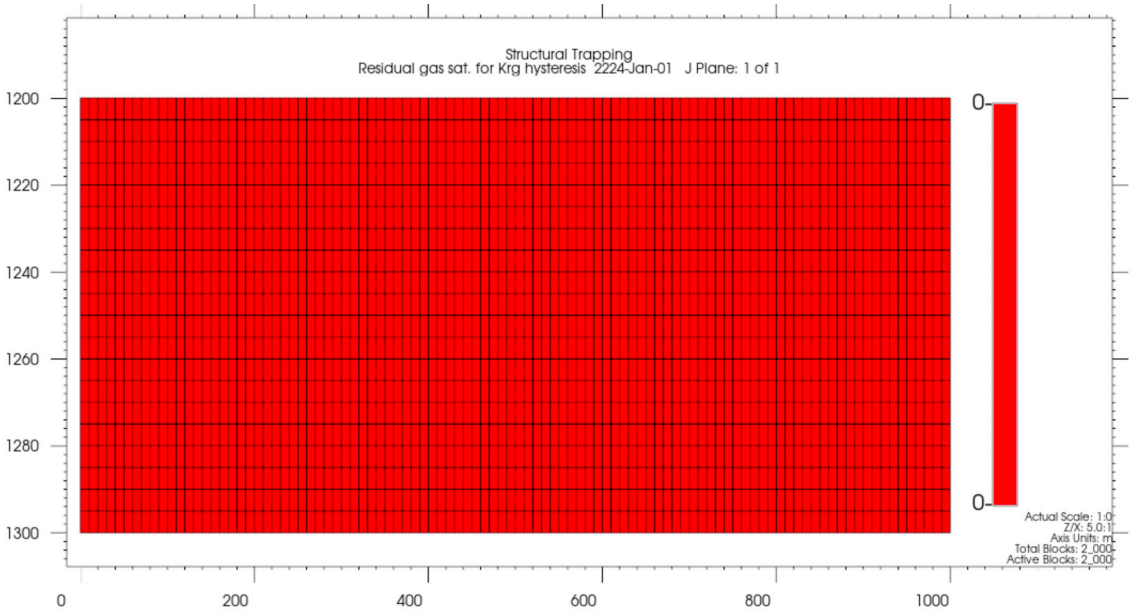

Figure 16: CO_2 relative permeability due to hysteresis at year 2224 after structural trapping.

In Figure 17 below, it is seen that there is no CO_2 trapped in minerals or aqueous ions yet. Confirming that at this stage the trapping of CO_2 is solely limited to structural trapping, which happens as CO_2 naturally migrate upwards, and gets confined physically in hosting structures.

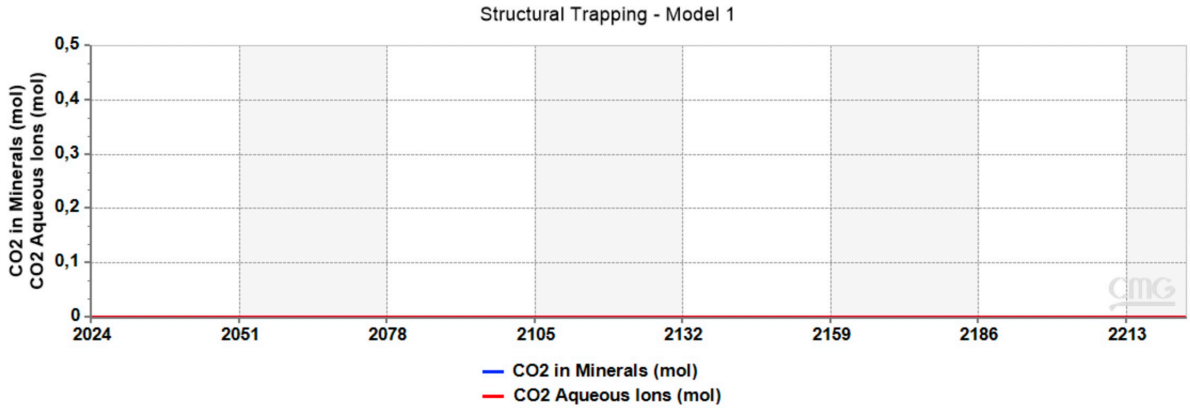

Figure 17: CO_2 trapped in minerals and aqueous ions after structural trapping.

4.1.2 Residual Trapping

In this section, the comparison should be between structural and residual trapping, instead of before and after CO_2 injection, to see how the CO_2 will move in the system considering now a 0.4 minimum residual saturation (hysteresis).

In Figure 18 below, it is clear compared to Figure 10 how the CO_2 is getting trapped more towards deeper layers and not just at the top, as CO_2 is getting trapped in pores due to capillary forces that immobilize CO_2 in small pores (hysteresis effect).
However, when it comes to CO_2 fraction in water and CO_2 trapped in minerals, it is the same as the previous mechanism.

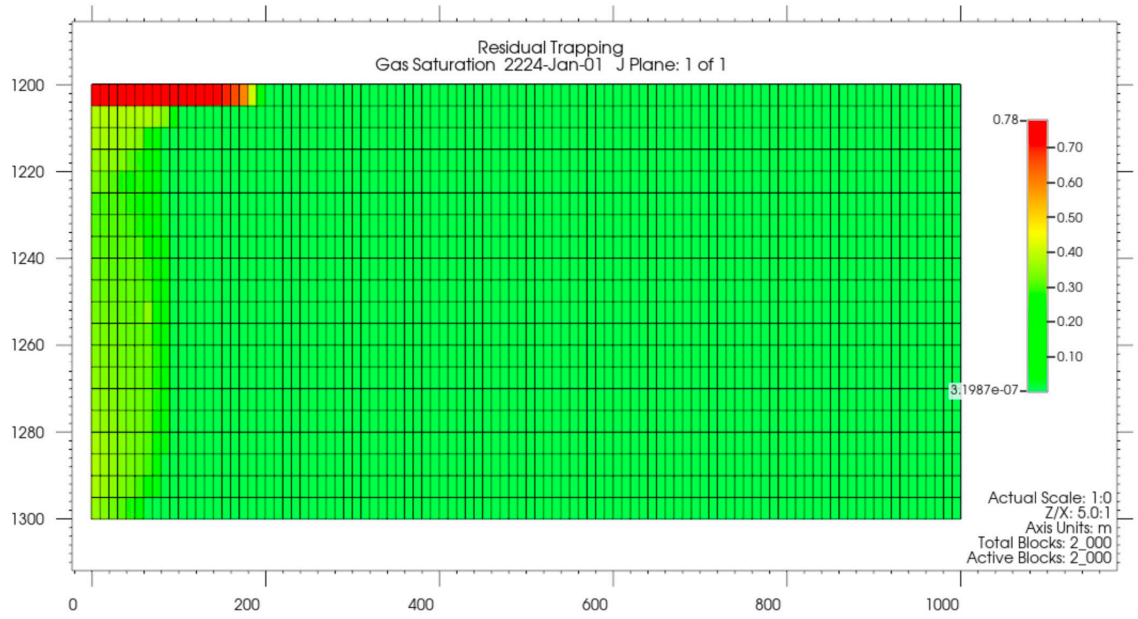

Figure 18: CO_2 saturation at year 2224 after residual trapping.

It gets clearer to see how there is more CO_2 in deeper layers and less at the grid top when comparing Figure 19 and Figure 12.

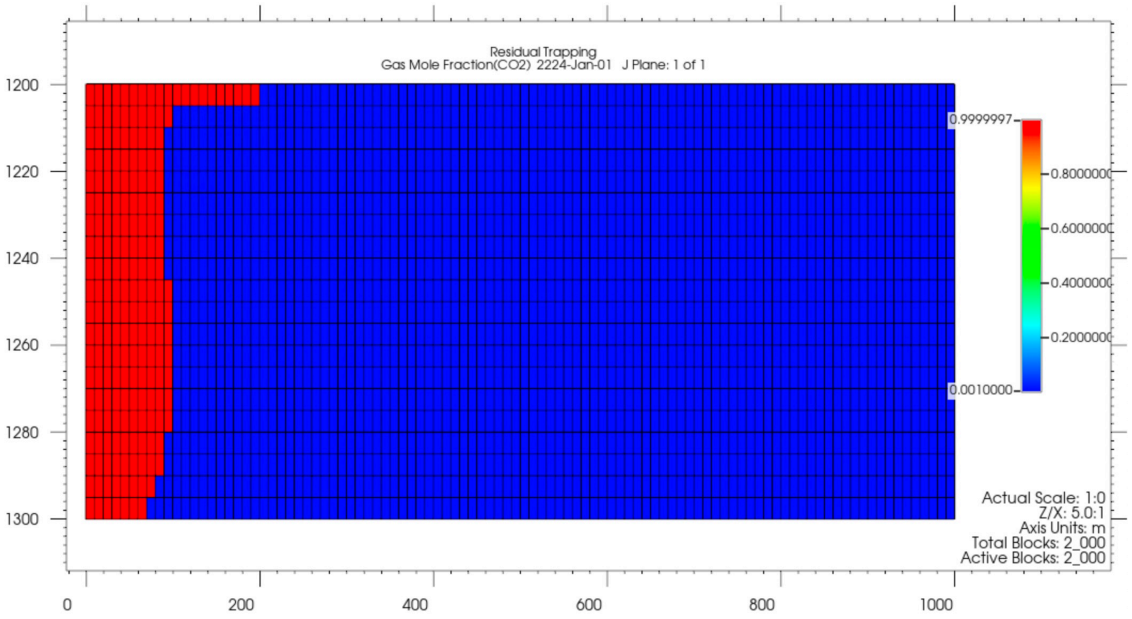

Figure 19: CO_2 mole fraction at year 2224 after residual trapping.

It is worth noting the difference between Figure 20 and Figure 16 when it comes to the relative permeability of CO_2 due to hysteresis. It is anticipated as a minimum residual saturation was added.

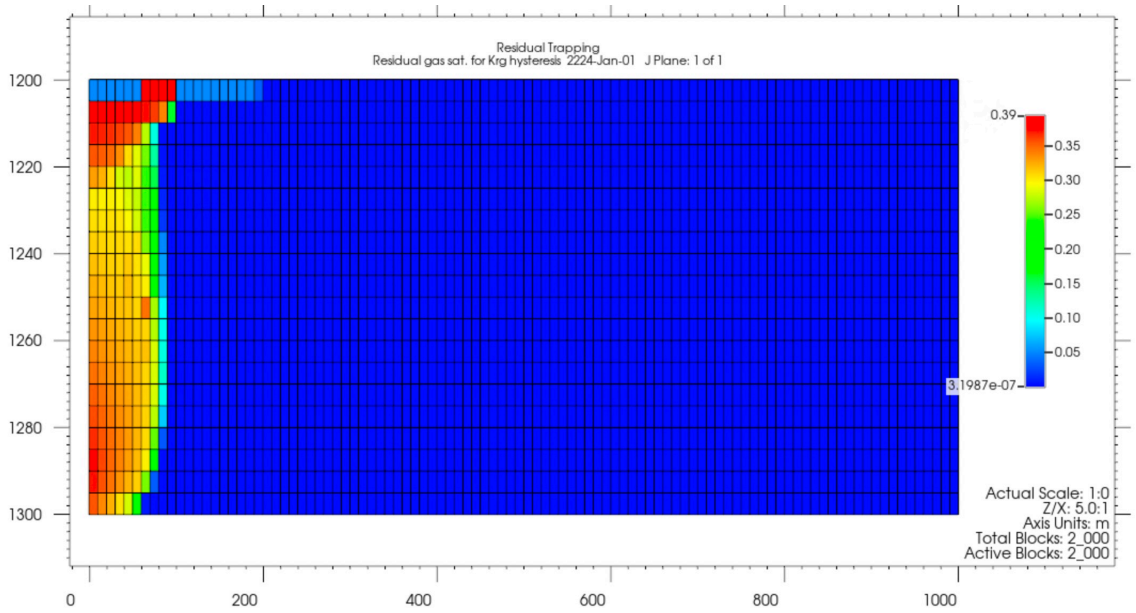

Figure 20: CO_2 relative permeability due to hysteresis at year 2224 after residual trapping.

4.1.3 Solubility Trapping

As previously done, the comparison should be done now between solubility trapping Figures and that of residual trapping.

When CO_2 gets dissolved in water, it tends to remain in the formation due to its increased density. This is seen in Figures 21, 22, and 23 compared to, Figures 18, 19 and 14 respectively. In addition to Figure 24 showing how the density of water is higher in areas where CO_2 is trapped.

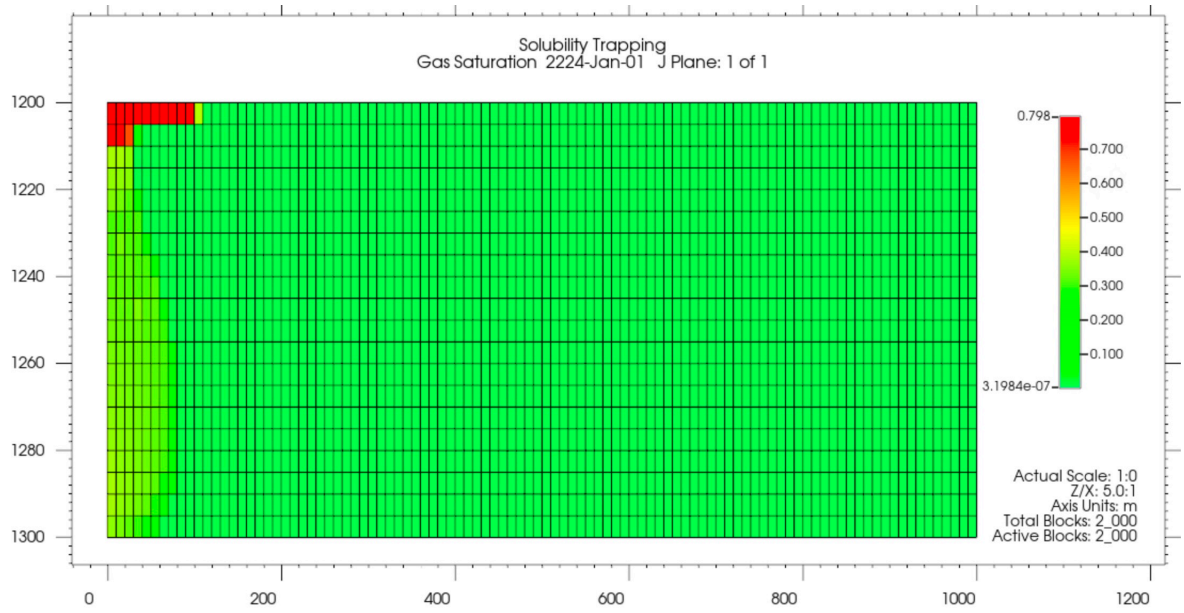

Figure 21: CO_2 saturation at year 2224 after solubility trapping.

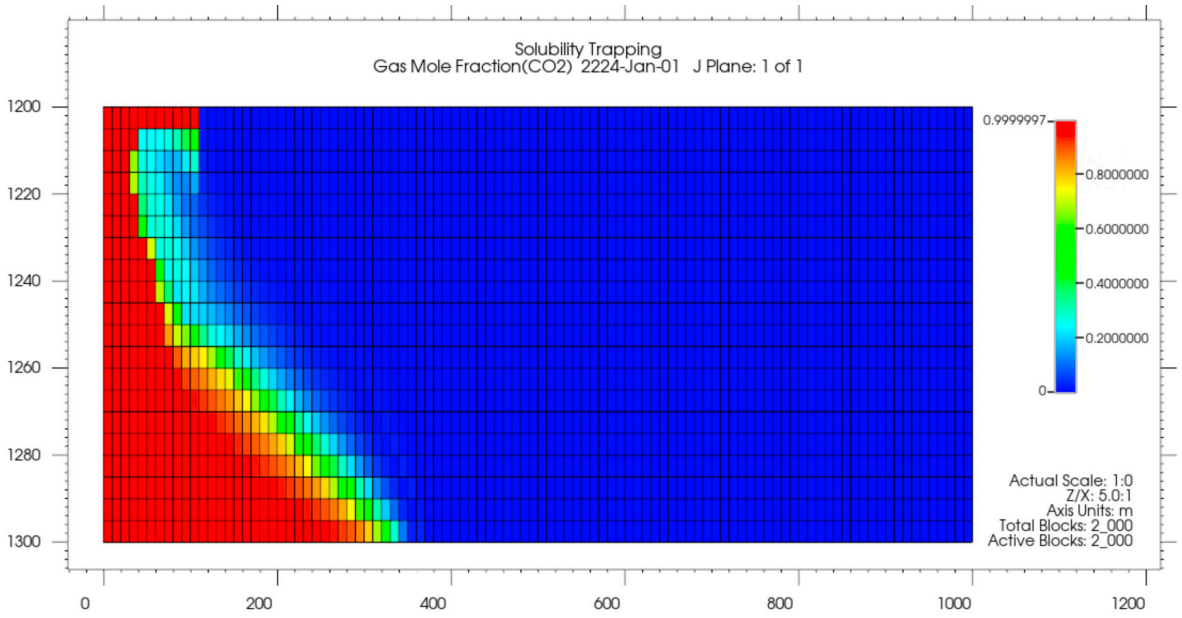

Figure 22: CO_2 mole fraction at year 2224 after solubility trapping.

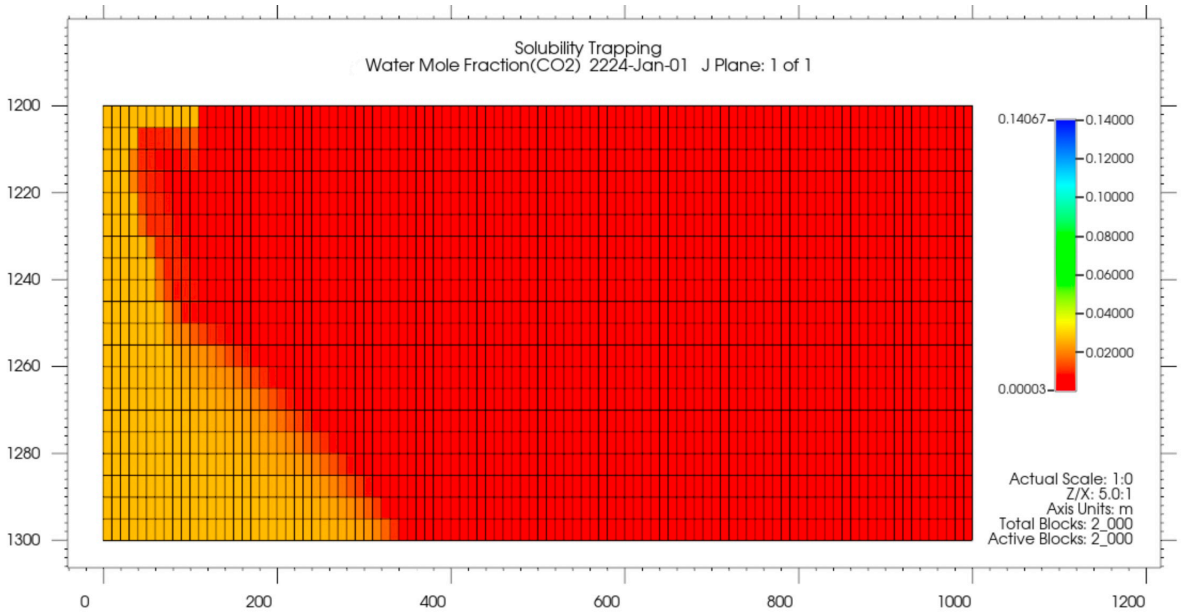

Figure 23: CO_2 fraction in water at year 2224 after solubility trapping.

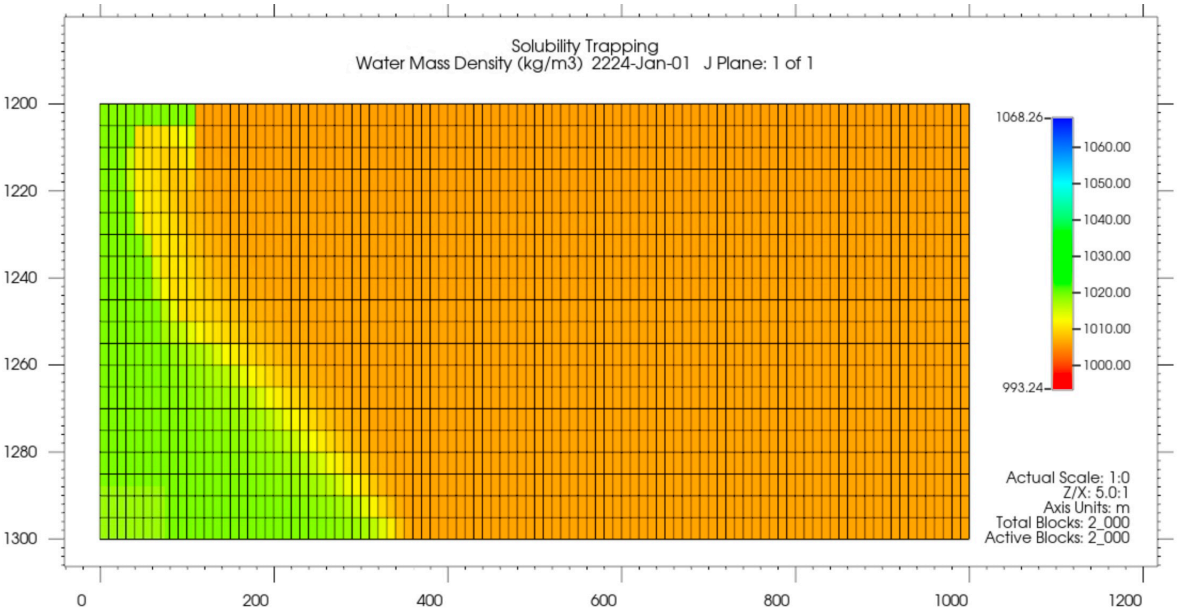

Figure 24: Water density at year 2224 after solubility trapping.

4.1.4 Mineral Trapping

Some mineral reactions, mentioned in the methodology part, were added to CMG GEM™ at this level to add the mineralization effect, this means that CO_2 now can react with minerals present in the rock to form solid carbonates.
What's different about this mechanism is the exponentially long time needed to achieve the mineralization of CO_2 to ensure permanent storing. However, CMG GEM™ was able to show some effect of CO_2 mineral trapping only after 200 years.
Some of the effects include the alteration of pH due to some geochemical and mineral reactions that are mentioned in the theory part.
In Figure 25 below, the pH of this model is compared with that of the previous case with no mineral reactions included, showing a decrease in pH to around 4.403 representing how some chemical reactions can make the environment more acidic.

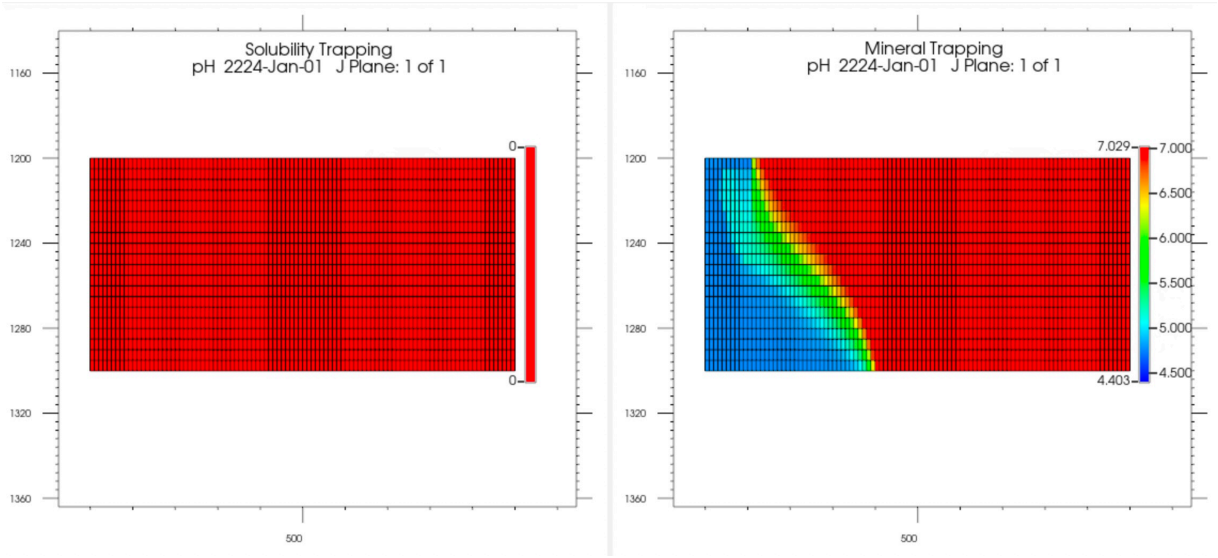

Figure 25: Comparison of pH in solubility and mineral trapping.

In addition, it is important to note that in CMG RESULTS™, there is an option to visualize the amount of CO_2 in moles trapped in minerals and in aqueous ions.
This is shown in Figures 26 and 27 below.

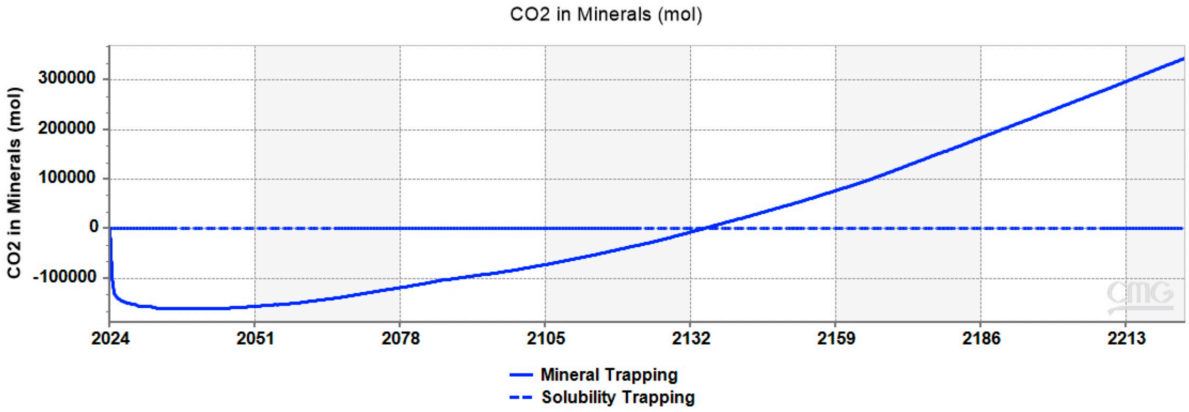

Figure 26: Comparison of CO_2 trapped in minerals in solubility and mineral trapping.

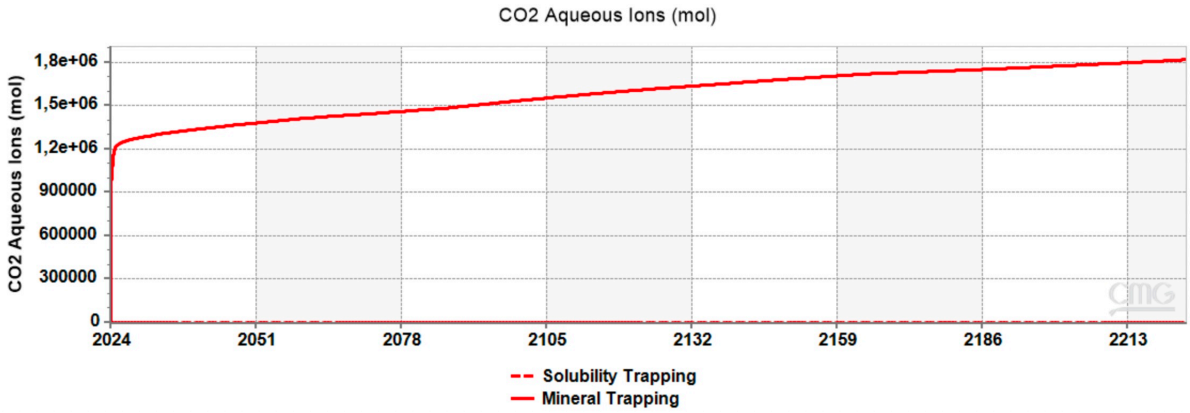

Figure 27: Comparison of CO_2 trapped in aqueous ions in solubility and mineral trapping.

What's worth noting from Figure 26 is the negative amount of CO_2 trapped in minerals in the first 108 years when there is mineral reactions (blue solid line) compared to that with no reactions at all (blue dotted line).
This could be caused by the long time that the mineral surfaces take to react with CO_2, it could also be due to the dissolution of CO_2 after interacting with some minerals due to initial changes in pressure, temperature, or chemical conditions triggered by the injection.

4.2 Fracture pressure calculation

4.2.1 Model 2: Bryne and Sandnes formations

Calculating the fracture pressure is required to set an operational constraint for CO_2 injection, Eaton's method was chosen for this reason. To calculate the fracture pressure, equation 10 was used. Before estimating the fracture pressure, Poisson's ratio, overburden pressure, and hydrostatic pressure should be calculated.

Using the well logs available for Wellbore 2/6-3, and specifically the sonic log, the average compressional velocity for the Bryne formation was found to be 100 µs/ft at the corresponding depth. (Click here to view the full log). Assuming a ratio of Vp = 1.75 Vs, the shear velocity would be equal to 57.14 µs/ft. Therefore, the Poisson's ratio is calculated using equation 11:

$$\nu = \frac{0.5 \cdot (V_{\mathrm{p}}/V_{\mathrm{s}})^2 - 1}{(V_{\mathrm{p}}/V_{\mathrm{s}})^2 - 1} = \frac{0.5 \cdot (100/57.14)^2 - 1}{(100/57.14)^2 - 1} = 0.2576 \tag{14}$$

Overburden pressure is calculated using 12 assuming an average formation density of 2.75 g/cm^{3}3 and a total depth of 3600 meters:

$$P_{ob}(z) = \int_0^z \rho_{\mathrm{formation}}(z) \cdot g \cdot dz = 2750 \cdot 9.81 \cdot 3600 = 971.2\, bar \tag{15}$$

The hydrostatic pressure is calculated using equation 13 assuming an average CO_2 density of 0.85 g/cm^3.

$$P_{\mathrm{p}} = \rho_{\mathrm{fluid}} \cdot g \cdot z = 850 \cdot 9.81 \cdot 3600 = 300.2\, bar \tag{16}$$

Finally the fracture pressure can be calculated using equation 10:

$$P_{\mathrm{f}} = \frac{\nu}{1-\nu} \cdot (OBG - P_{\mathrm{p}}) + P_{\mathrm{p}} = \frac{0.2576}{1 - 0.2576} \cdot (971.2 - 300.2) + 300.2 = 533\, bar \tag{17}$$

The maximum bottomhole pressure constraint should always be below the fracture pressure plus a safety margin. Thus, the chosen constrain for maximum bottomhole pressure is 515 bar.

4.2.2 Model 3: Frigg Formation

Fracture pressure of Frigg formation was calculated following the same steps taken for the previous model.
Using the well logs available for Wellbore 25/1-8S, and specifically the sonic log, the average compressional velocity for the Frigg formation was found to be around 200 µs/ft at the targeted depth. (Click here to view the full log).
Assuming a ratio of Vp = 1.75 Vs, the shear velocity would be equal to 114.28 µs/ft. Therefore, the Poisson's ratio is calculated using equation 11:

$$\nu = \frac{0.5 \cdot (V_{\mathrm{p}}/V_{\mathrm{s}})^2 - 1}{(V_{\mathrm{p}}/V_{\mathrm{s}})^2 - 1} = \frac{0.5 \cdot (200/114.28)^2 - 1}{(100/114.28)^2 - 1} = 0.2576 \tag{18}$$

This ratio works for both formations as they are both sandstone formations.
Overburden pressure is calculated using equation 12 assuming an average formation density of 2.3 g/cm^3 and a total depth of 2000 meters:

$$P_{ob}(z) = \int_0^z \rho_{\mathrm{formation}}(z) \cdot g \cdot dz = 2300 \cdot 9.81 \cdot 2000 = 451.26\, bar \tag{19}$$

The hydrostatic pressure is calculated using equation 13 assuming an average CO_2 density of 0.031 g/cm^3.

$$P_{\mathrm{p}} = \rho_{\mathrm{fluid}} \cdot g \cdot z = 30 \cdot 9.81 \cdot 2000 = 5.886\, bar \tag{20}$$

Finally the fracture pressure can be calculated using equation 10:

$$P_{\mathrm{f}} = \frac{\nu}{1-\nu} \cdot (OBG - P_{\mathrm{p}}) + P_{\mathrm{p}} = \frac{0.2576}{1-0.2576} \cdot (451.26 - 5.886) + 5.886 = 160.42\, bar \tag{21}$$

The maximum bottomhole pressure constraint should always be below the fracture pressure plus a safety margin. Thus, the chosen constrain for maximum bottomhole pressure is 150 bar.
The pressure is relatively low and this is highly influenced by the injection conditions and by the targeted depth.

4.3 Calibrating Model 2

In this section, the effects of calibrating model 2 will be presented and discussed.

4.3.1 Initial Conditions

As mentioned in the methodology, two options for initial conditions have been assessed. In Figure 28 below, it is clear that the bottomhole pressure of the model using the 'Vertical Depth Average' mode (blue dotted line) has reached the operational constraint (bottomhole pressure of 515 bara) at day 241, which is 562 days earlier than that of the 'USER INPUT' mode (blue solid line).
Thus, the injection of 10,000 m^3/d will be extended for an extra 562 days for the same exact parameters if the 'USER INPUT' mode was chosen, which will be the case for future analysis.

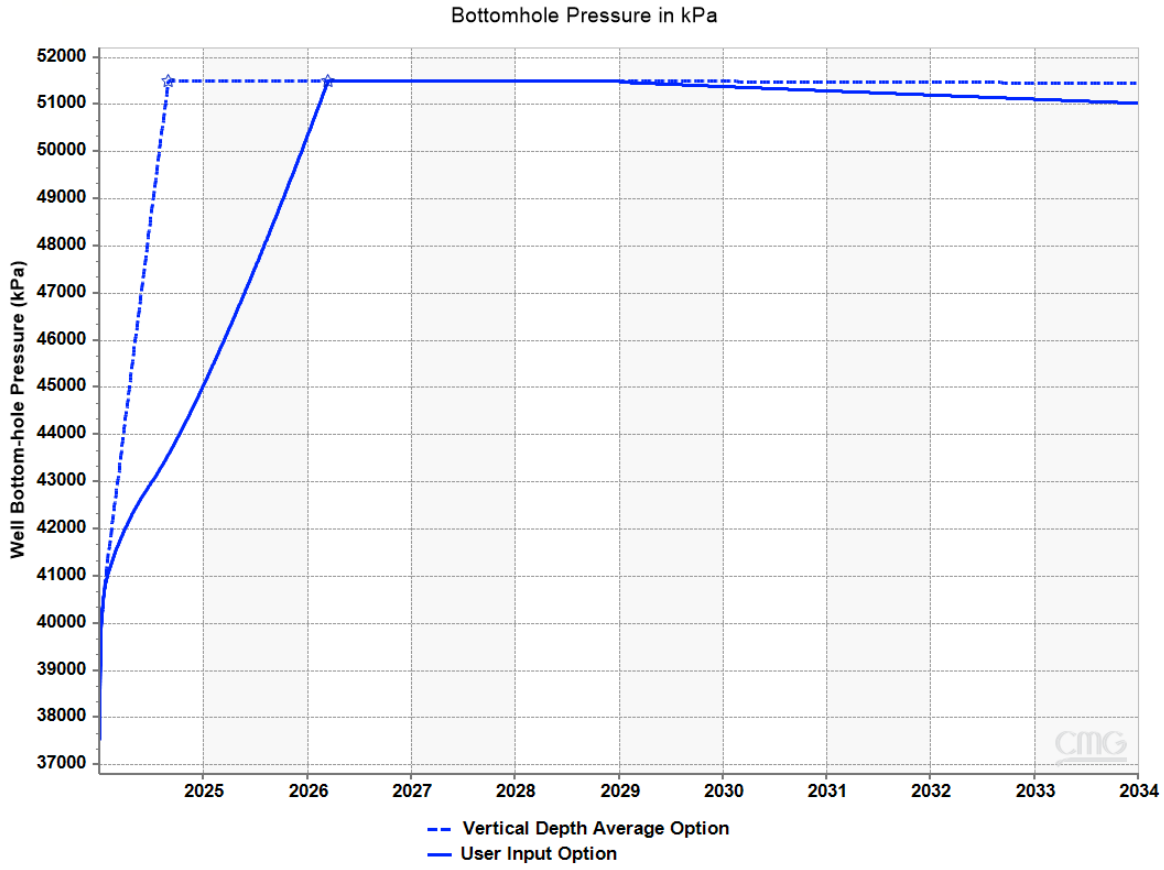

Figure 28: Bottomhole pressure comparison.

When comparing the cumulative CO_2 injected for both options at standard conditions, it is worth noting that for exactly the same well placement, grid properties, and every other parameter, choosing 'USER INPUT' for initial reservoir calculations gave privilege to inject 9.01154e+06 m^3 of CO_2 compared to 2.76716e+06 m^3 of CO_2 for the other mode.

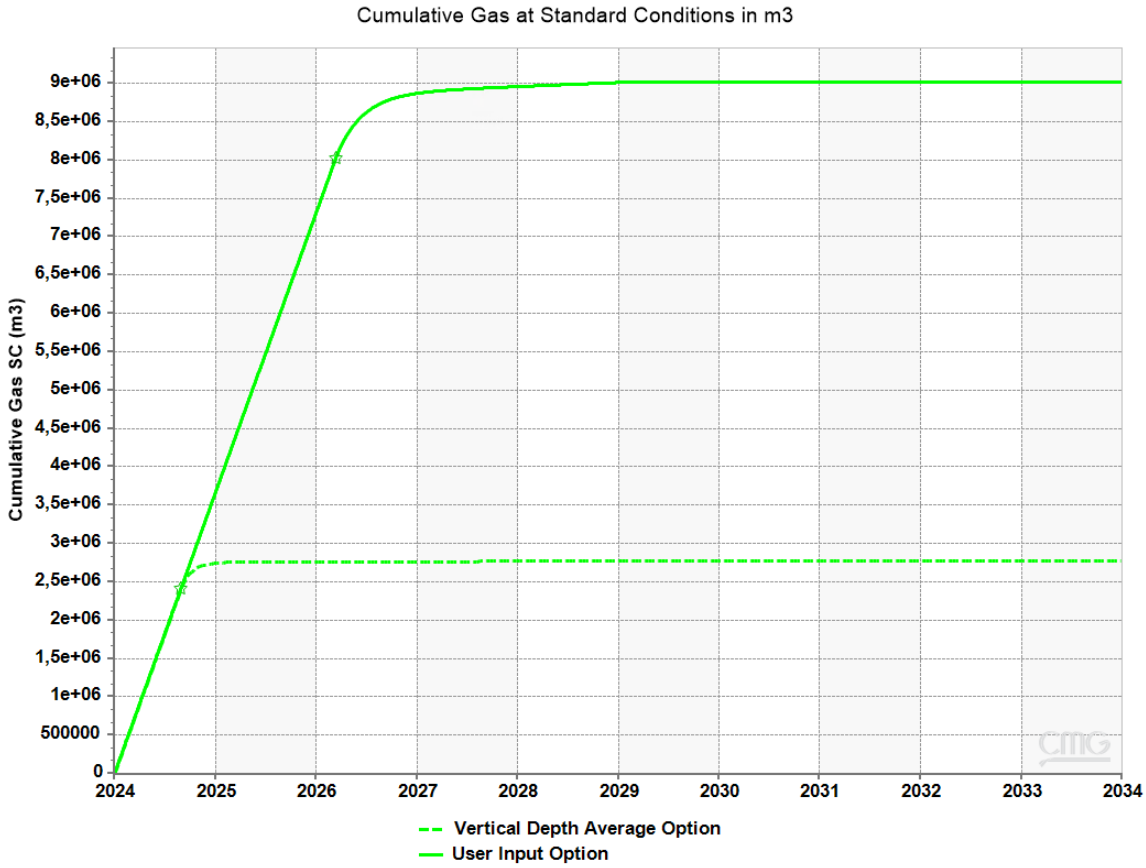

Figure 29: Cumulative CO_2 injected at standard conditions comparison.

Finally, when it comes to wellhead plots, it is shown in Figure 30 below that both options meet the operational constraint of having a minimum wellhead pressure of 100 bar. However, the 'USER INPUT' curve (red solid line) has a smoother increase in wellhead pressure compared to the other option, where the increase is sharp and fluctuating (red dotted line). This can be seen in a closer look at the plot in Figure 31. When considering all the three constraints, 'USER INPUT' option is most suitable with model 2.

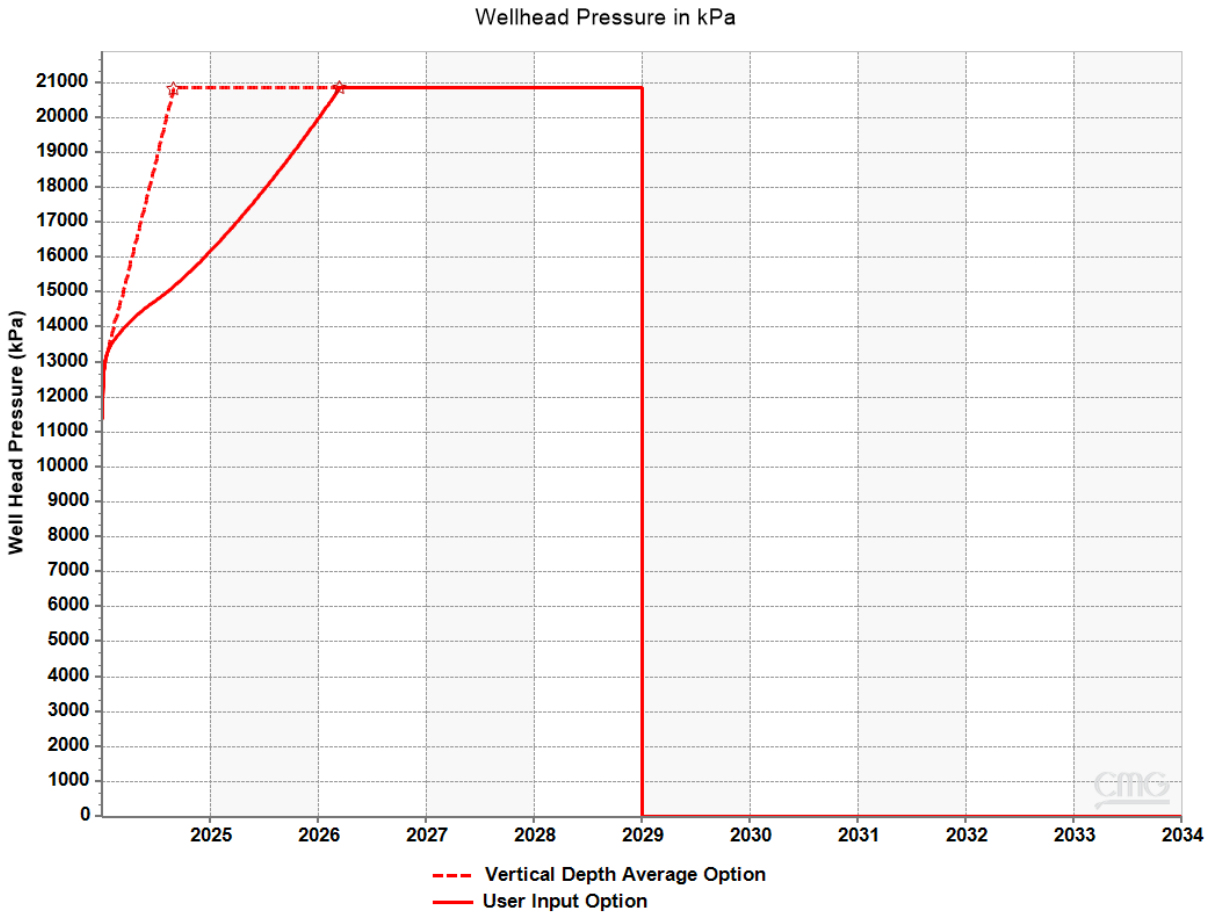

Figure 30: Wellhead pressure comparison.

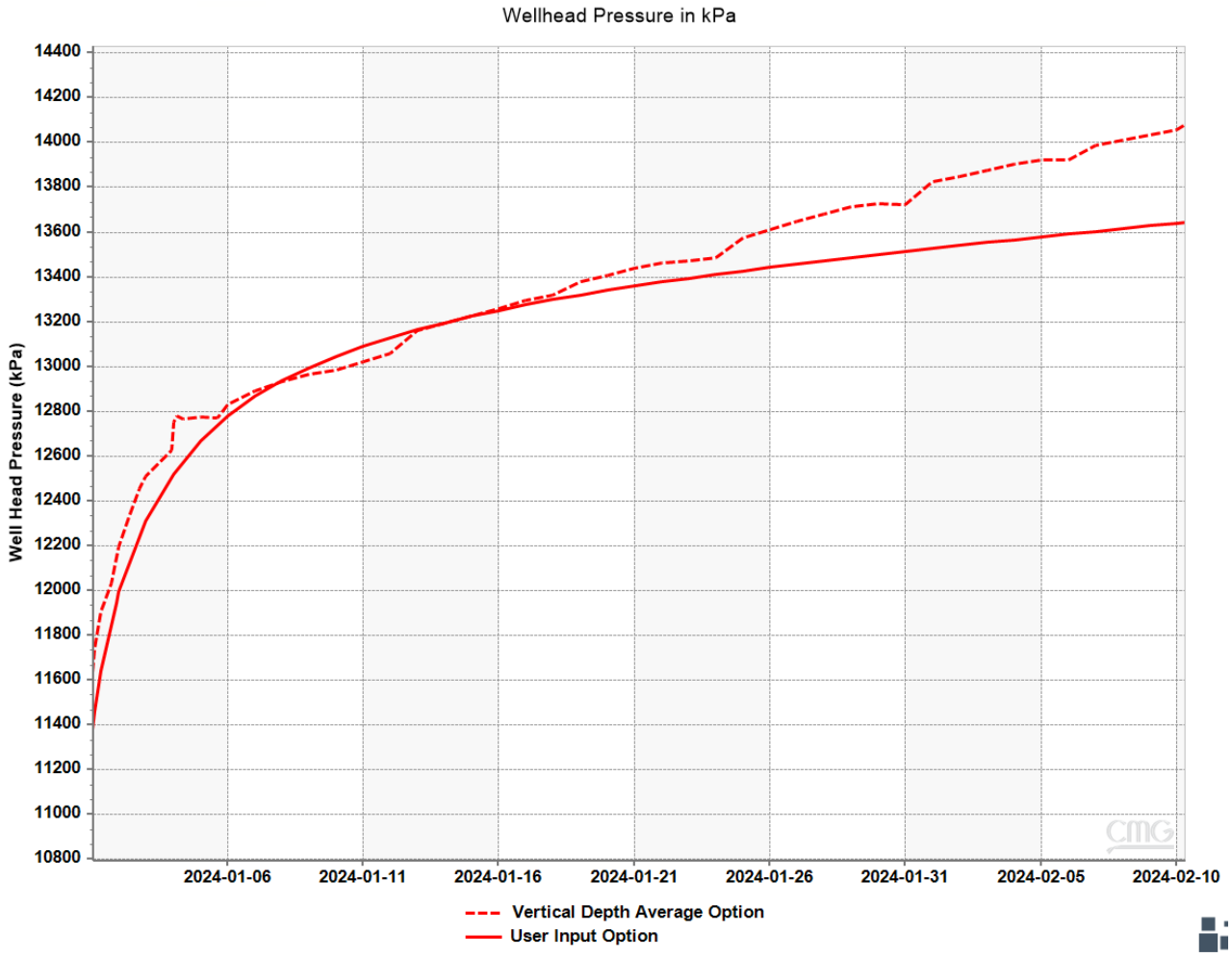

Figure 31: Wellhead pressure comparison zoomed-in.

4.3.2 Well placement

Well placement is considered a critical step before injecting CO_2, as numerous scenarios could be encountered if the features of the formation are not taken into account.
This step requires plenty of data about the formation, the presence of faults, fractures, coal or shale layers, etc.. As any unexpected feature could threaten the integrity of the wellbore thus the safety of the whole project.
However, since not enough data are available to add to the model at this level, some grid refinement and heterogeneous distribution of porosity and permeability around the model have been implemented.
In this section, 10 different well placements were tried along the 100-meter-thick formation, assuming three perforations were done on all cases and that there will be no well placement at the top layers.
The well placement iterations are as follows:

Well placement iteration	First Perforation in [i,j,k]	Second Perforation in [i,j,k]	Third Perforation in [i,j,k]
1	[1,1,8]	[1,1,9]	[1,1,10]
2	[1,1,18]	[1,1,19]	[1,1,20]
3	[50,1,8]	[50,1,9]	[50,1,10]
4	[50,1,18]	[50,1,19]	[50,1,20]
5	[100,1,8]	[100,1,9]	[100,1,10]
6	[100,1,18]	[100,1,19]	[100,1,20]
7	[150,1,8]	[150,1,9]	[150,1,10]
8	[150,1,18]	[150,1,19]	[150,1,20]
9	[200,1,8]	[200,1,9]	[200,1,10]
10	[200,1,18]	[200,1,19]	[200,1,20]

Table 5: Well placement iterations

The different iterations are represented in Figure 32.

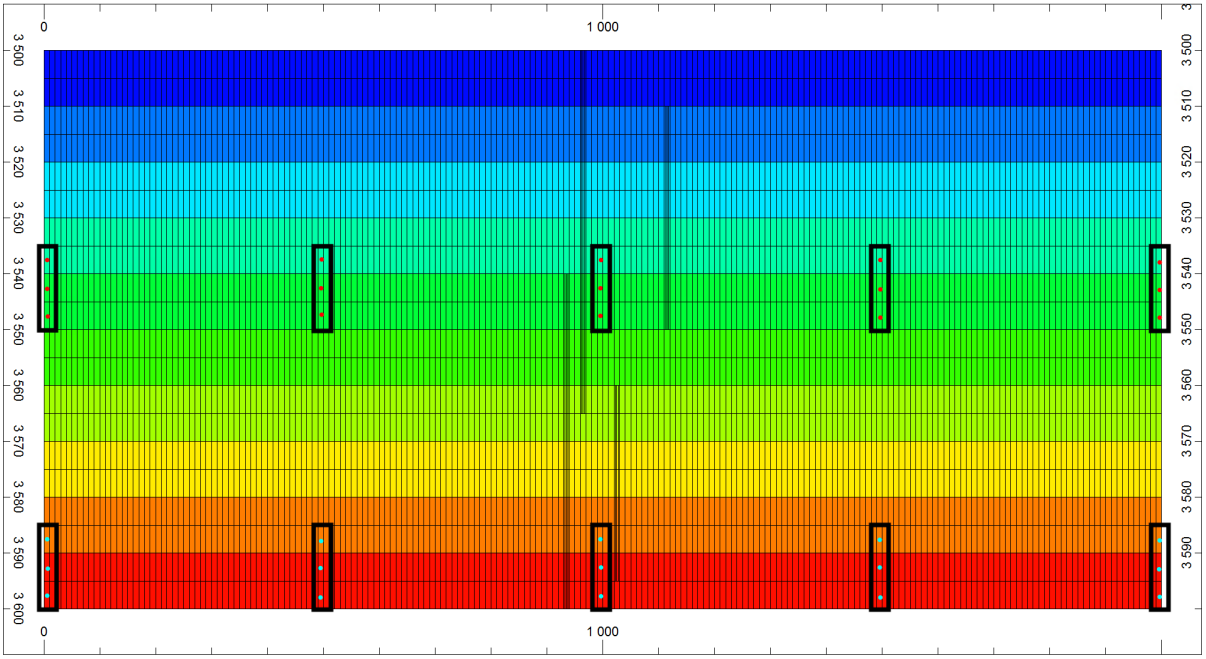

Figure 32: Different well placements on model 2.

After running simulations with the same injection plan, 10,000 m^3/d for 5 years, the results are displayed in Table 6 below:

Well Placement Iteration	**Time to reach the operational constraint (days)**	**Cumulative CO_2 injected (m^3)**
1	770	9.2733e+06
2	717	9.0027e+06
3	790	9.2753e+06
4	745	9.0044e+06
5	795	9.2747e+06
6	800	9.0104e+06
7	799	9.2770e+06
8	750	9.0026e+06
9	780	9.2759e+06
10	722	9.0037e+06

Table 6: Well placements results

Well placement number 6, which corresponds to perforations at [100,1,18], [100,1,19], and [100,1,20], was chosen as a reference placement for the rest of the study. This placement lays in the middle of the system and at the lowest layers, and it has the longest time of injection before reaching the maximum flowing bottomhole pressure of 515 bar. However, the cumulative CO_2 injected of this placement is not the highest, but this is due to the presence of refined blocks around the wellbore as shown in Figure 32.

Some placements had relatively shorter time of injection such as iterations 2 and 10, this could be explained by their placement at the boundaries. When the well is close to the edges of the system, the boundaries restrict the flow and spread of the injected CO_2 . This results in a relatively faster buildup of pressure as the CO_2 accumulates in the limited available space.

In addition, when looking in detail at every plot from all the iterations listed in Appendix .2, there is one common feature for all the wells that are placed at the deepest layers, which is a smoother increase in the bottomhole pressure compared to those in the middle layers. This could be explained by the gravitational stability in the lower layers, where denser CO_2 tends to accumulate naturally, leading to a more gradual and stable integration of injected CO_2 into the system. Also, the middle layers have more heterogeneous properties affecting the pressure response of the system.

4.4 Injection Rate Optimization

The step-rate injection test was applied to find the optimal injection rate, maximizing injection efficiency while considering the operational constraint of having the bottom-hole pressure less than fracture pressure to ensure the integrity of the wellbore.
The details of the step-rate injection test were already specified in the methodology part 3.5.1. The following graph in Figure 33 was obtained using CMG RESULTS™:

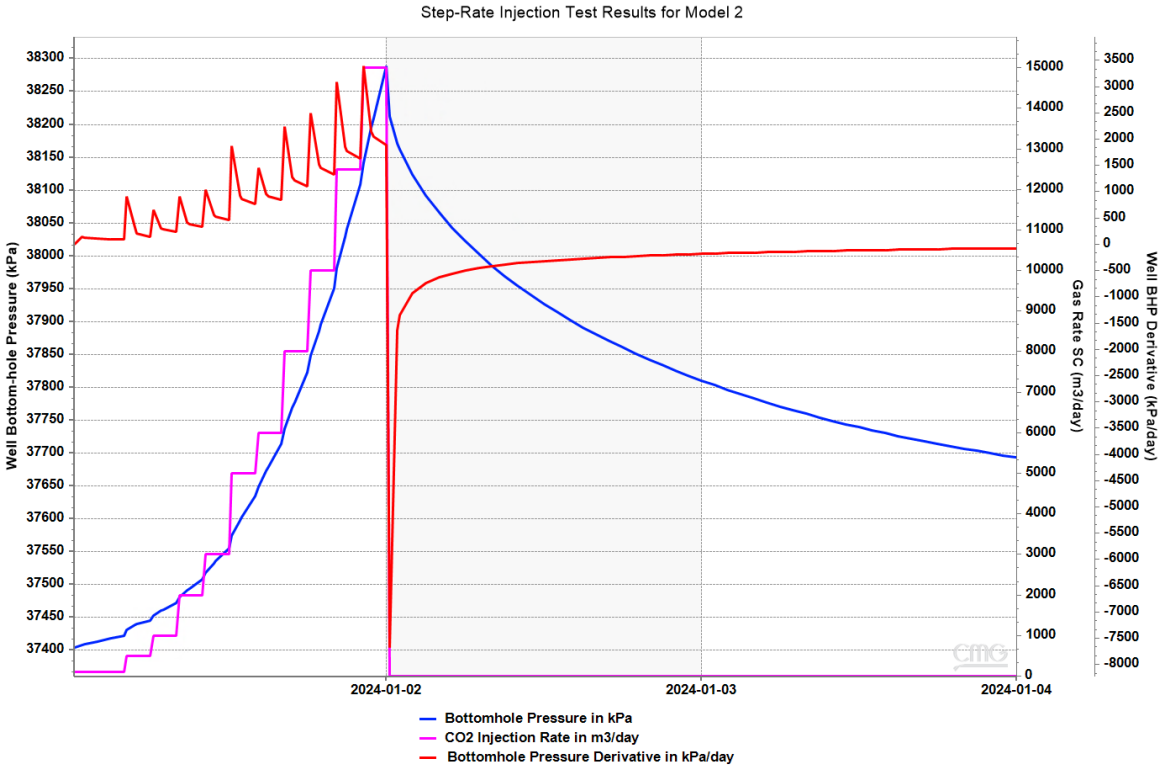

Figure 33: Step-rate injection test results for model 2.

This section is crucial, as choosing the injection rate without reaching the operational constraints is considered challenging. However, this test reflected good results as seen in Figure 33 above, where no spikes were recorded when the injection rate was increased from 100 m^3/day to 15,000 m^3/day in a period of 24 hours.

4.4.1 Pressure Profile

In Figure 34 below, it is clear that the bottomhole pressure is increasing from 374 bara to 382 bara with increasing injection rates from 100 m^3/day to 15,000 m^3/day, and then decreasing with shut-in to 376 bara. There are no significant spikes or fluctuations, which reflects a consistent response from the system to even the highest rate of CO_2 injection.

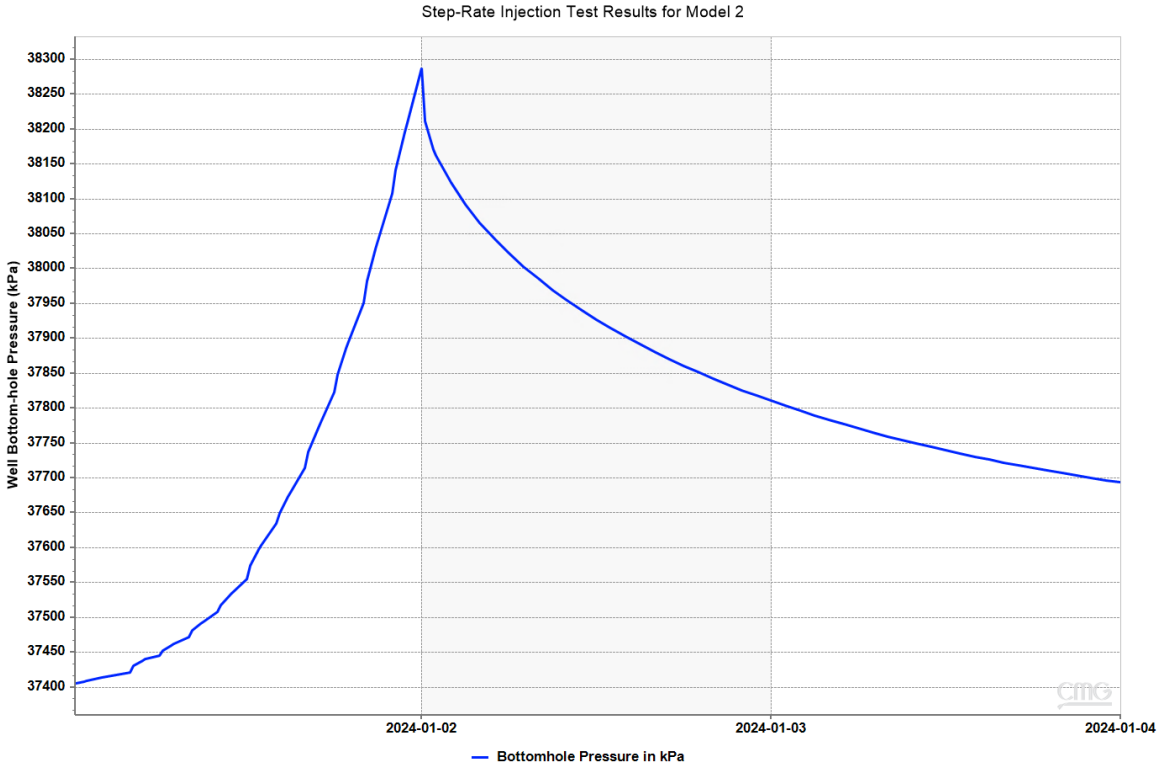

Figure 34: Pressure build-up and shut-in for model 2.

The system shows that any injection rate from 100 to 15,000 m^3/day would be accepted and not cause any apparent damage. Therefore, based on the simulation done on PIPESIM, and the data chosen for the reservoir simulator, an injection rate of 10,000 m^3/day will be chosen for model 2 to perform any further analysis. Changing the scheduled rate from 5,000 m^3/day as previously mentioned in section 3.5.1, to 10,000 m^3/day as mentioned earlier.

4.5 Non-Isothermal Effects in Model 2

Assessing the thermal effects of CO_2 injection helps in understanding the impacts and risks associated with CO_2 injection into saline aquifers. Some parameters to be assessed include temperature profiles, CO_2 phase behavior, thermal expansion coefficients of the reservoir rock and fluids, and solubility of CO_2 in brine. Model 2 was used for this section, however the comparison is done based on a small adjustment done in cEDIT, where a *THERMAL mode is turned on in one of the two versions being compared to visualize the thermal effects on the system.

4.5.1 Temperature and Pressure Profiles

Seeing the temperature profile in Figure 35 below, it is clear that the temperature for the thermal version (blue dotted line) decreases from 110°C all the way to around 100 and then increases to 106°C. Unlike the curve for the isothermal version (blue solid line) where the temperature stays at 110°C throughout the 10 years.
The temperature profiles are generated at a depth of 3600 meters (grid bottom).

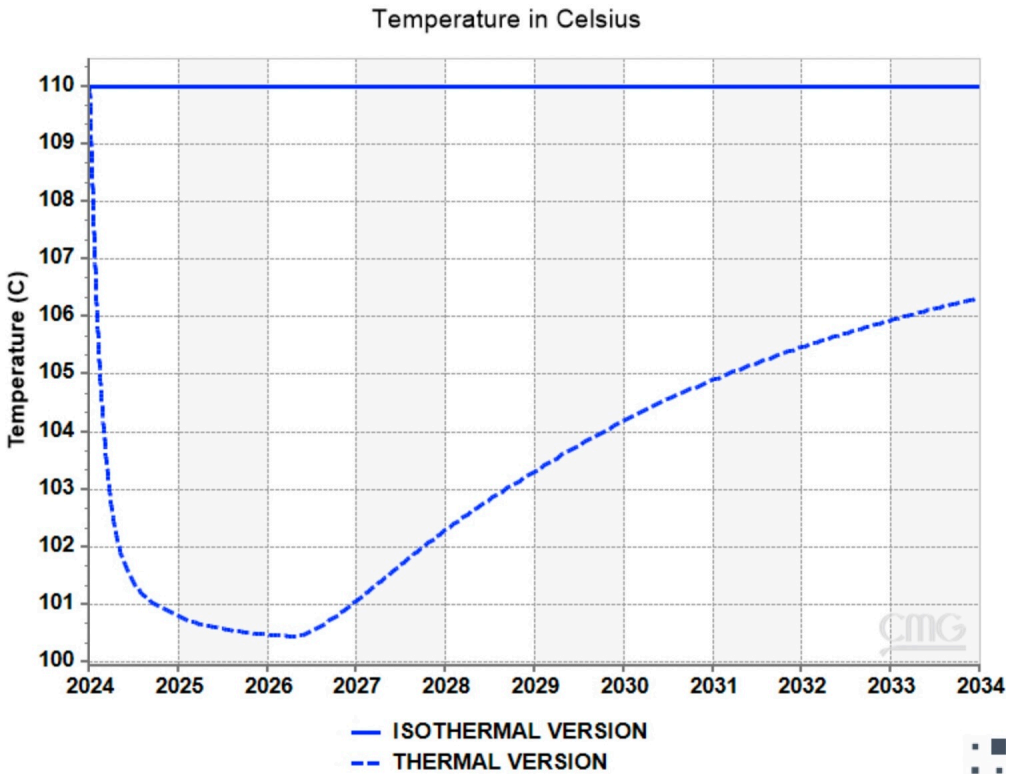

Figure 35: Temperature profile for thermal and isothermal models.

This is expected for the thermal version as after injecting cold CO_2 into a warmer formation, thermal contraction of the CO_2 and the surrounding rock would take place. This could induce stress changes in the rock matrix, possibly leading to thermal fracturing. On the other hand, as the CO_2 warms up to the ambient temperature of the formation, thermal expansion could occur, affecting the stress distribution within the reservoir. This is presented in the trend of the thermal curve (blue dotted line).

When looking at the bottomhole pressure profiles for both versions, in Figure 36 shown below, the bottomhole pressure of the thermal model (red solid line) reached the operational constraint of maximum flowing bottomhole pressure of 515 bara in 803 days, 37 days prior to the isothermal model (red dotted line).

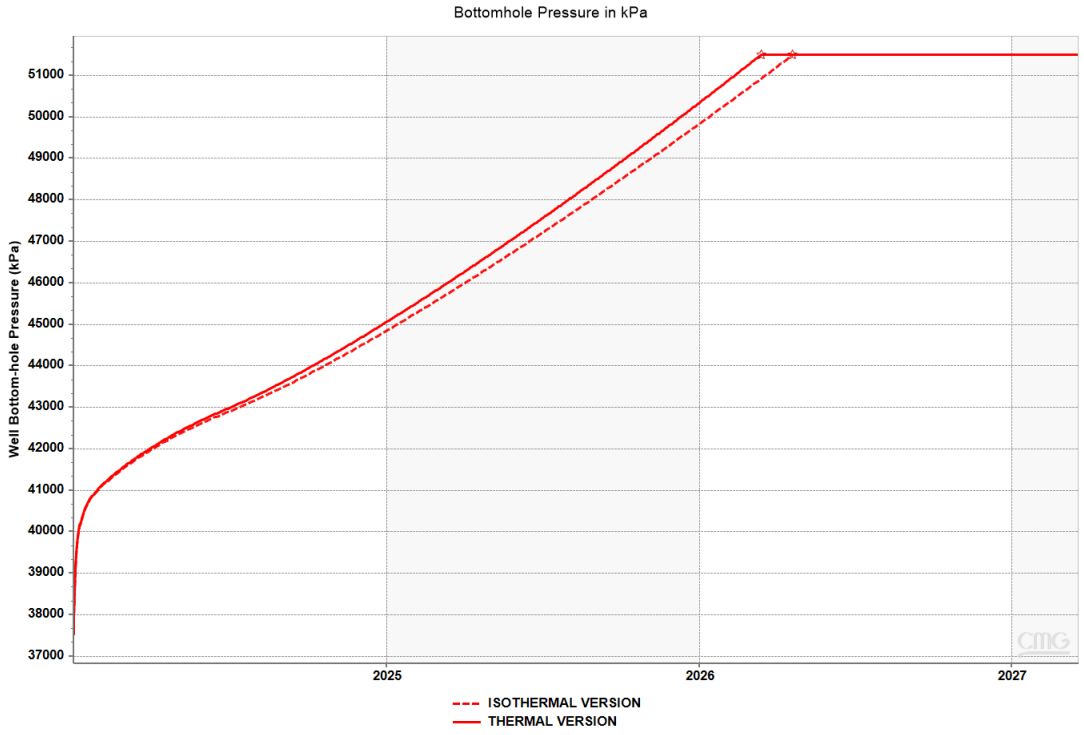

Figure 36: Bottomhole pressure for thermal and isothermal models.

This could have two explanations, the first is that in non-isothermal cases, the changes in temperature after injecting cold CO_2 into a warm system, cause the fluids and the surrounding rock to expand thermally, which causes a reduction in the available pore volume for the injected CO_2 due to the increase in the volumetric strain within the porous medium.

Therefore, the reduction in pore volume leads to a faster buildup of pressure compared to the isothermal model where such thermal expansions are not considered.
The second reasonable explanation is that due to thermal changes, the viscosity and density of CO_2 and brine get affected, the density and viscosity of CO_2 get typically higher because of the cooling effect caused by the expansion of injected CO_2, leading to a reduced mobility of the CO_2. This reduction in mobility can contribute to a quicker pressure increase as the resistance to flow is higher.

4.5.2 CO_2 phase behavior

GEM is not capable of explicitly producing a phase diagram for CO_2. However, after extracting the pressure and temperature data, the following Figures were generated using excel.

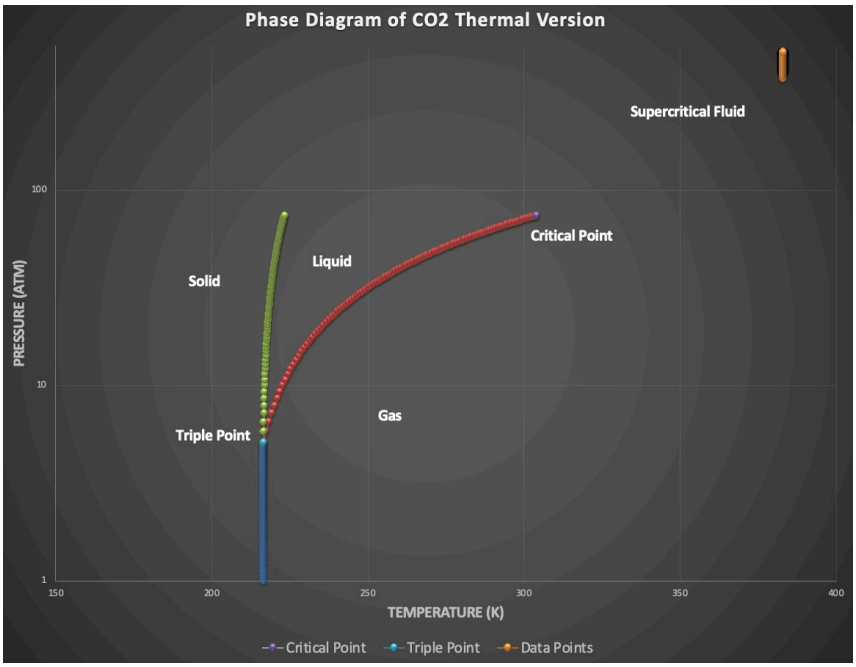

Figure 37: CO_2 phase diagram with isothermal data points.

In Figure 37 above, the data points from the isothermal version show a straight line (yellow points), confirming that the temperature is fixed at 110°C when the pressure is increasing from 375 bara to 515 bara. The CO_2 is in supercritical conditions at all times, meaning no phase change has occurred.

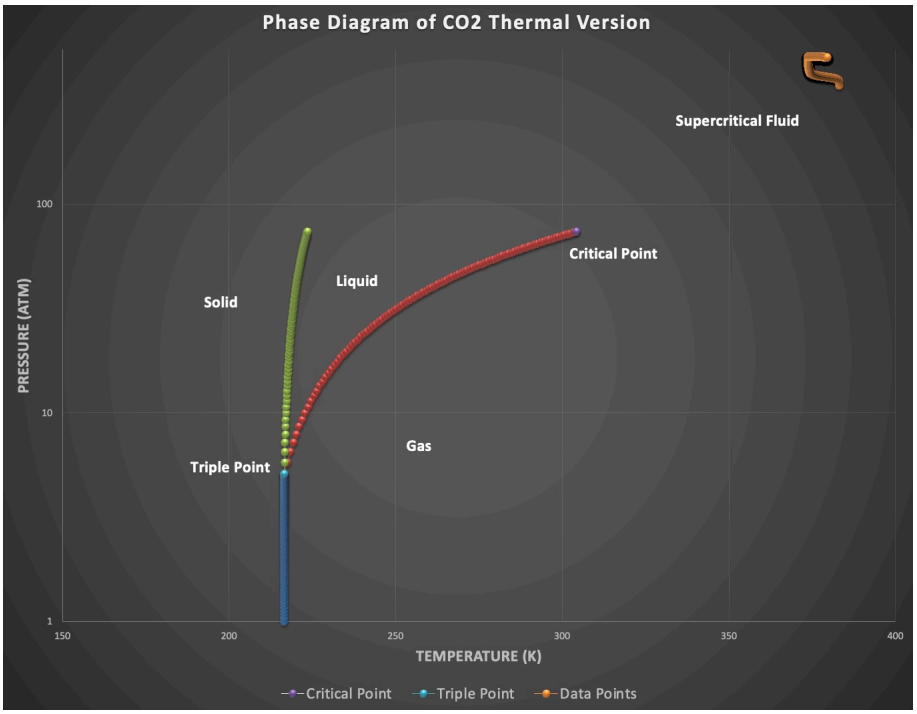

Figure 38: CO_2 phase diagram with thermal data points.

For the thermal version, the data points presented in Figure 38 show a fluctuating trend, aligning with the temperature and pressure profiles. However, the CO_2 stayed in supercritical conditions throughout the whole project. Maintaining CO_2 in a single phase minimizes the risk of phase transitions, which can cause complications to the injection operations and reduce efficiency.

In addition, the density and viscosity curves will be assessed for deeper understanding of the behavior of CO_2 under thermal effects. For a time-series comparison, a 'UBA' has to be chosen, which is a specific set of grid blocks [i,j,k]. To evaluate the thermal effects, it is better to choose grid blocks around the wellbore and at the lowest layers. For that, UBA [100,1,20] was chosen to conduct the comparison between the thermal and isothermal versions of model 2. As it was expected, the density of CO_2 in the thermal version (red solid line) is higher than that of the isothermal version (red dotted line) as observed in Figure 39. Both starting at a an initial density of almost 700 kg/m^3 at reservoir conditions, and ending up after 10 years of monitoring at 824 kg/m^3 for the thermal version and 812 kg/m^3 for the isothermal one. This is the case because, as previously mentioned, the density and viscosity of CO_2 get higher as an effect of the cooling caused by the expansion of injected CO_2.

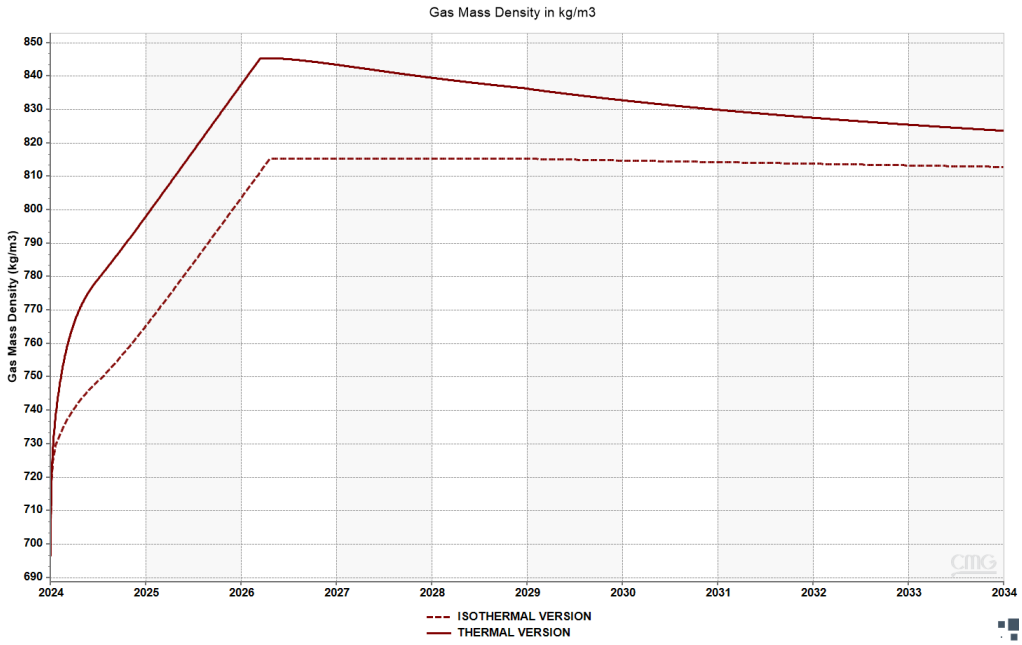

Figure 39: CO_2 density comparison for thermal and isothermal versions.

It is the same when it comes to the viscosity of CO_2 in both versions, the viscosity of CO_2 in the thermal version is higher than in the isothermal version, as shown in Figure 40 below.

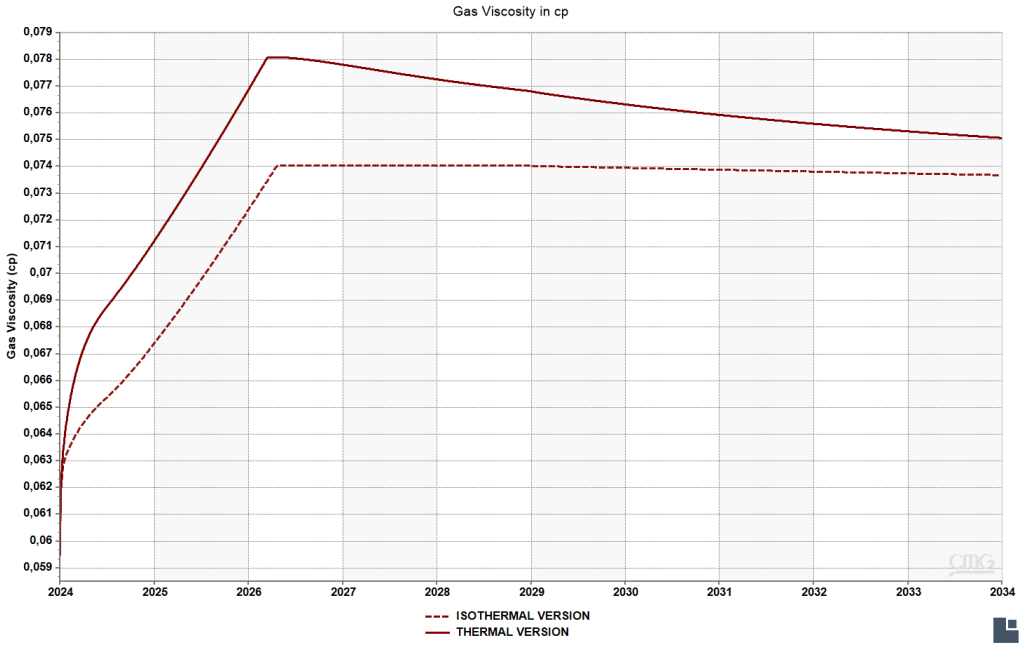

Figure 40: CO_2 viscosity comparison for thermal and isothermal versions.

4.5.3 CO_2 solubility in brine

To see how the thermal effects are altering the solubility of CO_2 in brine, comparing the curves of water density in thermal and isothermal versions would highlight the effects. As seen in Figure 41 below, the water density of the thermal version (blue solid line) is higher than that of isothermal version (blue dotted line), this is anticipated as when CO_2 dissolves in water, water density will eventually increase.

This is the general case regardless of the thermal effects. Injected CO_2 will dissolve in water as a natural trapping mechanism. According to Henry's Law [19], the increase in partial pressure of CO_2 significantly enhances its solubility, the amount of dissolved gas in a liquid is proportional to its partial pressure in the gas phase, assuming constant temperature.

However, thermal effects increased the solubility of CO_2 in brine, due to the potential decrease in kinetic energy allowing cold CO_2 molecules to easily dissolve into the warmer water's molecular structure.

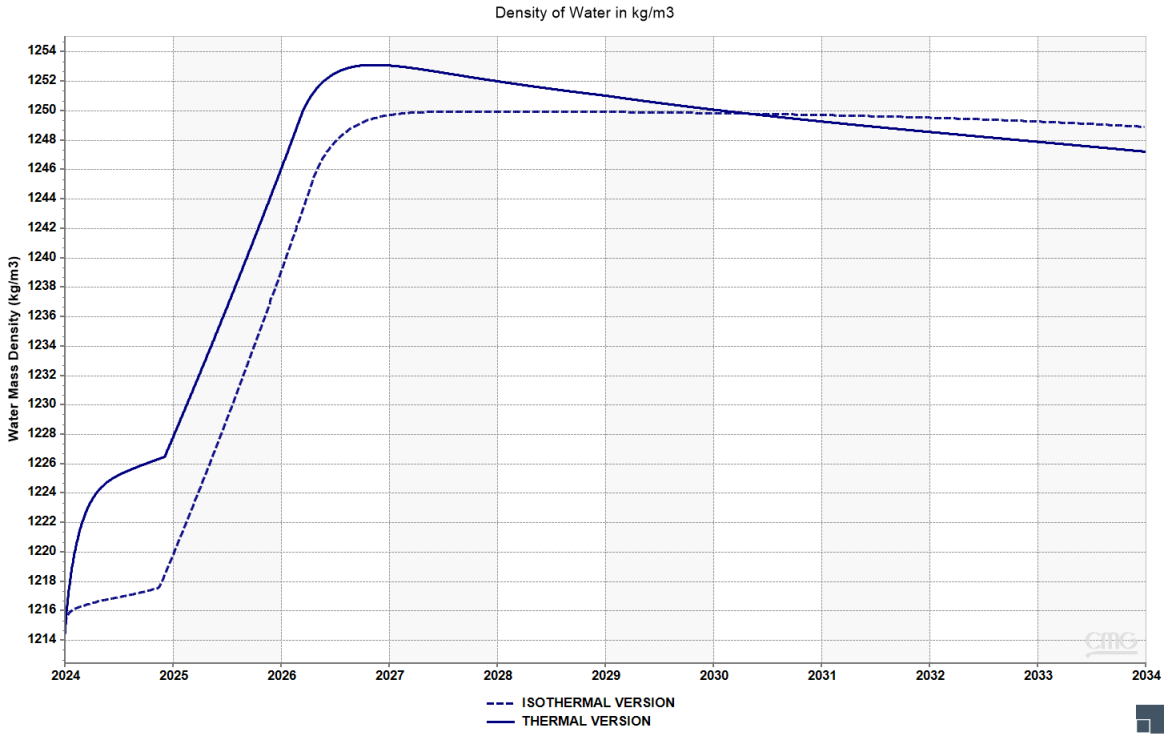

Figure 41: Density of water comparison for thermal and isothermal versions.

4.5.4 Geochemical reactions

What's important to compare here, is the pH difference and the amount of CO_2 trapped in minerals. Starting with the comparison of pH for thermal and isothermal models in Figure 42, it is clear that the pH is getting more acidic for both versions with time, as a result of the formation of carbonic acid when CO_2 dissolves in water.

$$CO_2(g) + H_2O(l) \longrightarrow H_2CO_3(aq) \tag{22}$$

$$H_2CO_3(aq) + H_2O(l) \rightleftharpoons HCO_3^-(aq) + H^+(aq) \tag{23}$$

However, the pH of the thermal version is slightly lower (red solid line) than the the isothermal version, due to thermal effects on reaction kinetics and solubility, leading to an increase in acidity. As mentioned previously, the thermal changes increases the solubility of CO_2 in brine, and based on the chemical equations 22 and 23, more acid will be formed, decreasing the pH.

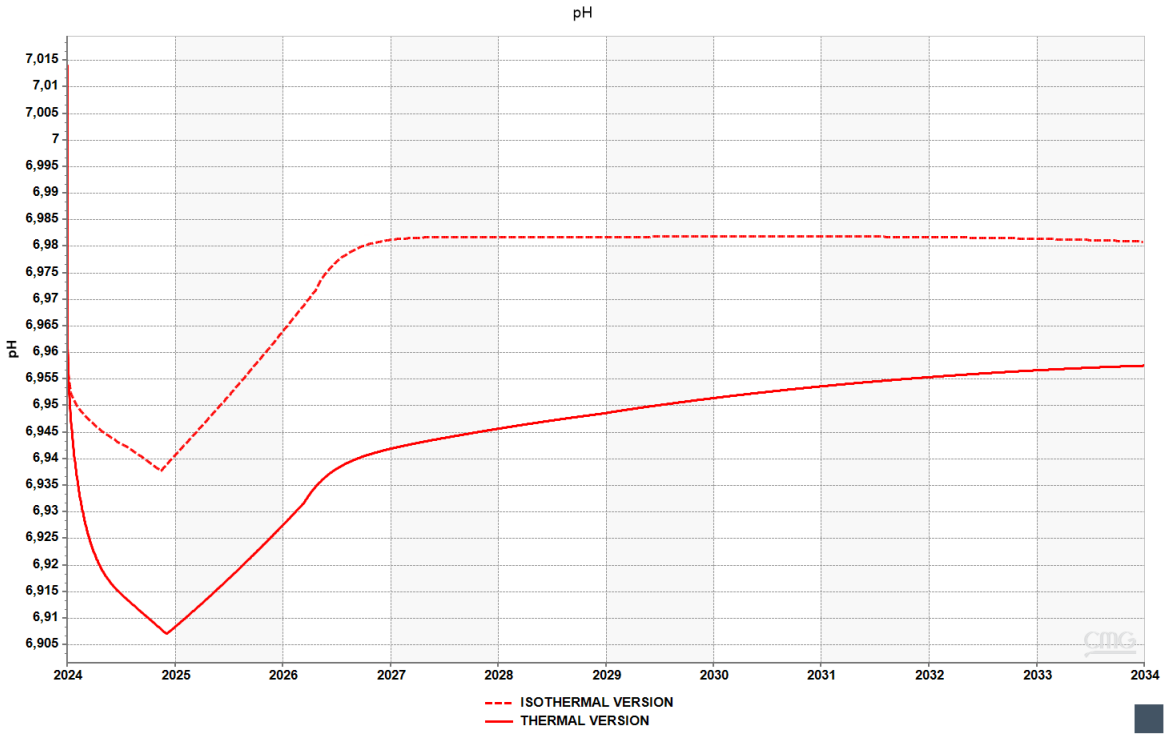

Figure 42: pH comparison for thermal and isothermal versions.

Thermal effects are also affecting how much of the injected CO_2 is trapped in minerals. As seen in Figure 43 below, both cases had the same trapping in minerals until 2025 and then the gap started increasing significantly until the end of the monitoring. For the thermal version, there was 1.934e+07 moles of CO_2 trapped inside of the minerals, compared to 1.81e+07 moles in the isothermal version.

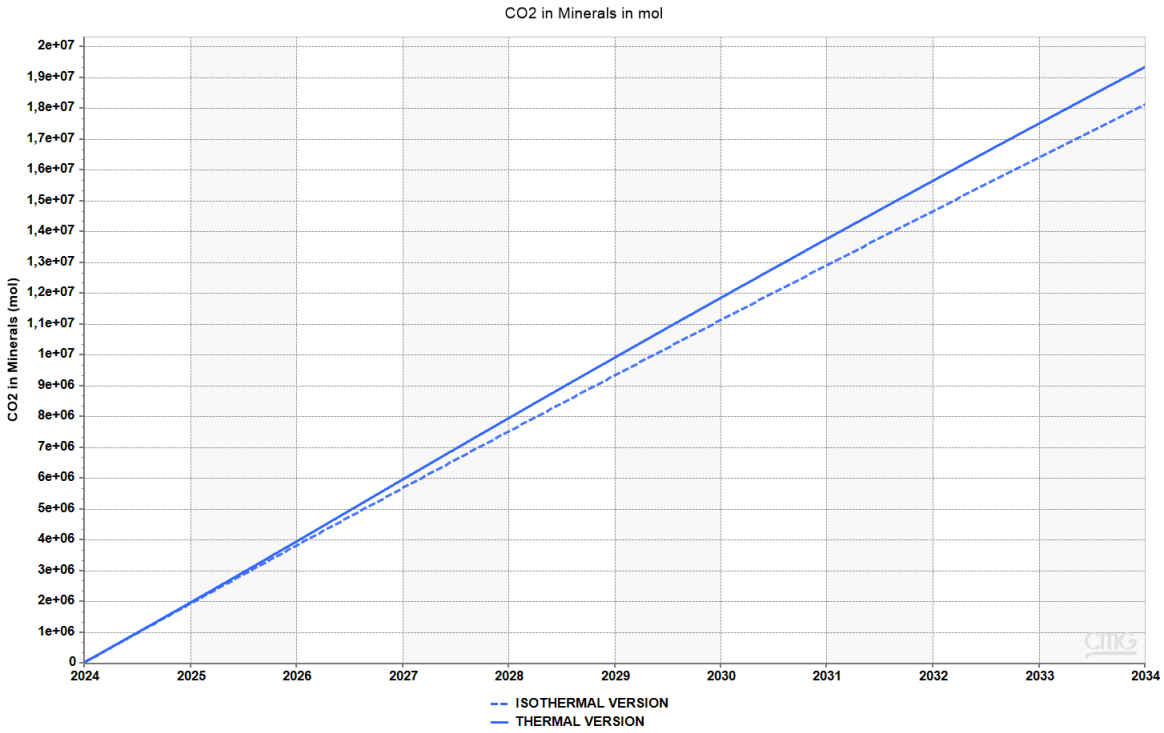

Figure 43: CO_2 trapped in minerals comparison for thermal and isothermal versions.

This could be explained by the increasing solubility of CO_2 in water due to the cooling effect in the system after injecting cold CO_2. More dissolved CO_2 can participate in chemical reactions that lead to mineral formation. The time needed for this to happen is reasonable, because as the injected CO_2 and the formation reach thermal equilibrium, the increased temperature in the system enhances for instance the kinetics of carbonate mineral formation reactions, such as reaction 24 needed for the trapping of CO_2.

$$Mg^2 + CO_2 + H_2O \longrightarrow MgCO_3 + {}_2H^+ \tag{24}$$

In addition, there is a significant difference in water viscosity curves when comparing thermal and isothermal versions, as shown in Figure 44. For the isothermal case, the water viscosity is more or less constant at 0.2713 cp, compared to the thermal case where the water viscosity increases to 0.2976 cp and then decreases to around 0.28 cp.

In isothermal conditions, the brine viscosity could be slightly affected by the change in brine's composition due to dissolution of CO_2 in brine, or due to the formation of carbonic acid that could react with some minerals and potentially change the ionic strength and composition of the brine.
Whereas in thermal conditions, the cold CO_2 injected into the aquifer would cool the surrounding brine and by that increase the viscosity of the brine due to the reduced molecular activity in colder temperatures. However, after thermal equilibrium, the viscosity will decrease again as the effects of the cooling will diminish, which perfectly represented in the blue solid line in Figure 44.

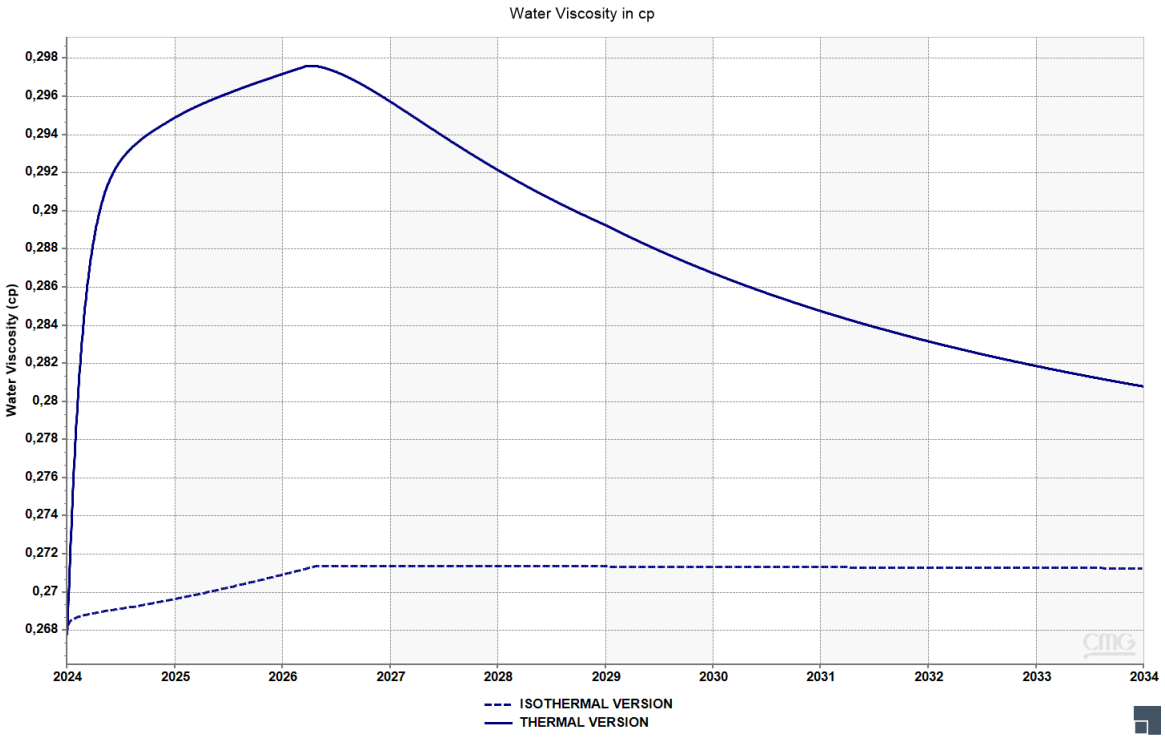

Figure 44: Water viscosity comparison for thermal and isothermal versions.

4.5.5 Porosity and Permeability

Porosity and permeability of the aquifer are highly affected by the goechemical changes as a result of thermal effects, influencing fluid flow paths and storage capacity.
When comparing the effective porosity changes for thermal and isothermal versions, it is clear from Figure 45 below that the effective porosity is slightly increasing for both cases, somewhat more when considering thermal changes (red solid line).

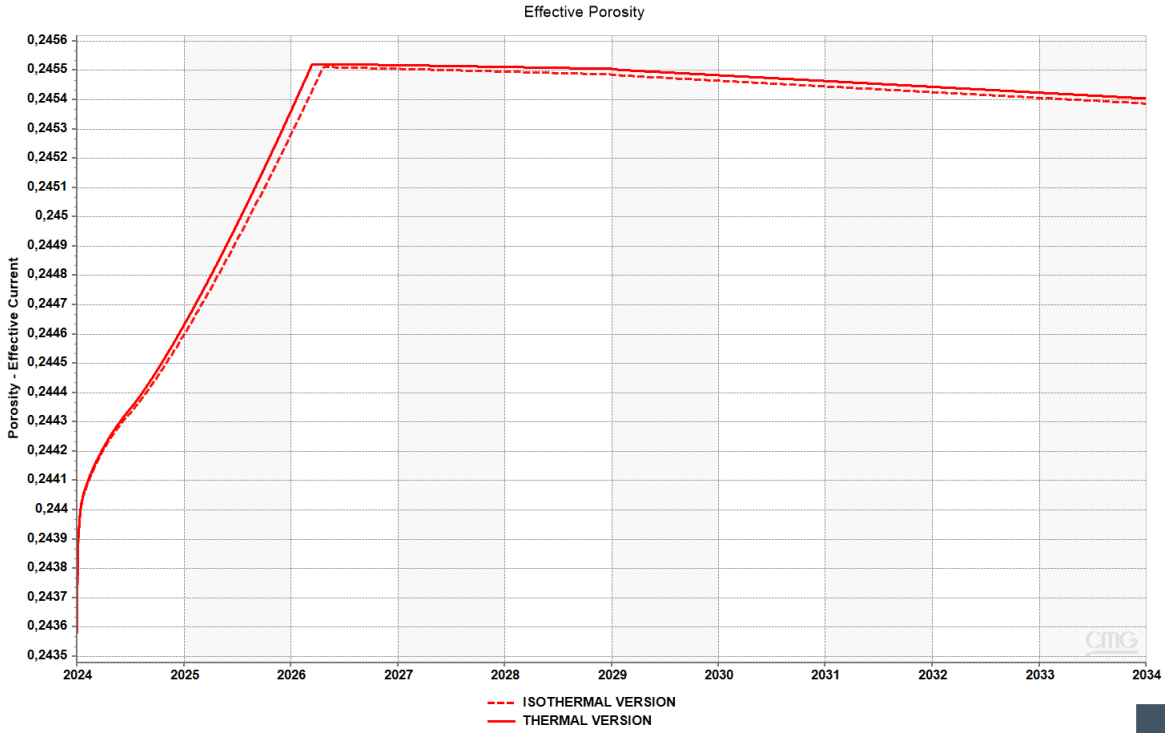

Figure 45: Effective porosity comparison for thermal and isothermal versions.

The subtle increase in porosity could be a result of injecting compressed CO_2 and inducing some fractures in the system. Another reason to this increase is the chemical dissolution of some minerals, which is more significant in the thermal version, as the formed carbonic acid from reaction 22, can cause the dissolution of calcite as shown in reaction 25 and other carbonate minerals present in the aquifer matrix.

$$CaCO_3 + H_2CO_3^- \longrightarrow Ca^{2+} + {}_2HCO_3^- \tag{25}$$

The porosity will eventually increase as a result of minerals dissolution. However, this process is more relevant in carbonate reservoirs.

When it comes to permeability, it should theoretically be affected by CO_2 injection and thermal changes similarly to porosity. However, CMG GEM™ couldn't show any changes in permeability as shown in Figure 46. The permeability remained constant at 150 mD for both thermal and isothermal versions throughout the whole injection and shut-in periods.

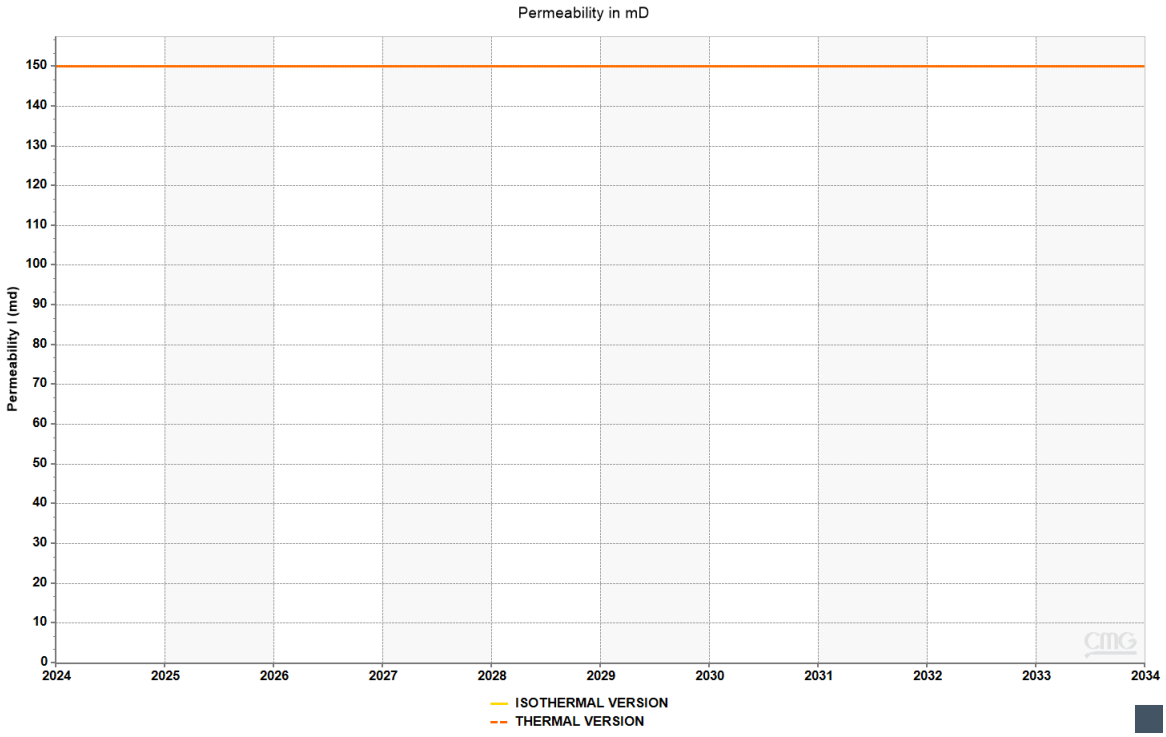

Figure 46: Permeability comparison for thermal and isothermal versions.

This could be explained by either, the lack of some particular geochemical and petrophysical data needed when building the model, or the inability of CMG GEM™ to perform detailed geochemical modeling that involves complex interactions leading to permeability changes.

Because mineral dissolution and/or precipitation would eventually affect the permeability, in addition to the changes in permeability due to induced fracturing in brittle formations from the injection of CO_2.

Temperature differences between the injected CO_2 and the formation could also alter the permeability through thermal expansion or contraction of the rock.

4.6 Sensitivity Analysis for Model 2

In this part, a series of parameters will be altered to assess how they will affect the efficiency of CO_2 storage in model 2. This does not imply that some changes could be viable in real life or even voluntarily executed. However, this analysis provides a general, comprehensive understanding of how CO_2 would behave under different conditions. Model 2 representing the Bryne and Sandnes formations serves as a reference for this analysis. The analysis will be done using radar plot to find the best storage conditions for the same injection scenarios, taking three values of each parameter, low, medium, and high respectively.

4.6.1 Changing reservoir pressure

The first parameter to analyze is the reservoir or formation pressure, as this is highly variable from one site to another, and from one depth to another. Considering the same depth with the same fracture pressure, three values for reservoir pressure were assessed.

A low value of 60 bara was analyzed first, followed by a medium value of 150 bara, and finally a high value of 375 bara which is the base case. For the same injection schedule, injecting 10,000 m^3/day of CO_2 for 5 years, the following bottomhole pressure profiles were generated for the three different values of reservoir pressure.

As shown in Figure 47 below, the curves for reservoir pressures 60 and 150 bara did not reach the operational constraint for a maximum bottomhole pressure of 515 bara, unlike the reservoir pressure 375 bara that reached the constraint in 800 days. Therefore when comparing the cumulative CO_2 injected, it is 9.01042e+06 m^3 of CO_2 for the base case (around 7.65 Mt) and 1.827e+07 m^3 for the two other cases (around 15.5 Mt).

To compare how much CO_2 could be possibly injected for each of the two reservoir pressures 60 and 150 bara, longer injection periods were tried. A trial to inject 10,000 m^3/day of CO_2 for 20 years for both cases resulted in the bottomhole pressure curves shown in Figure 48 below.

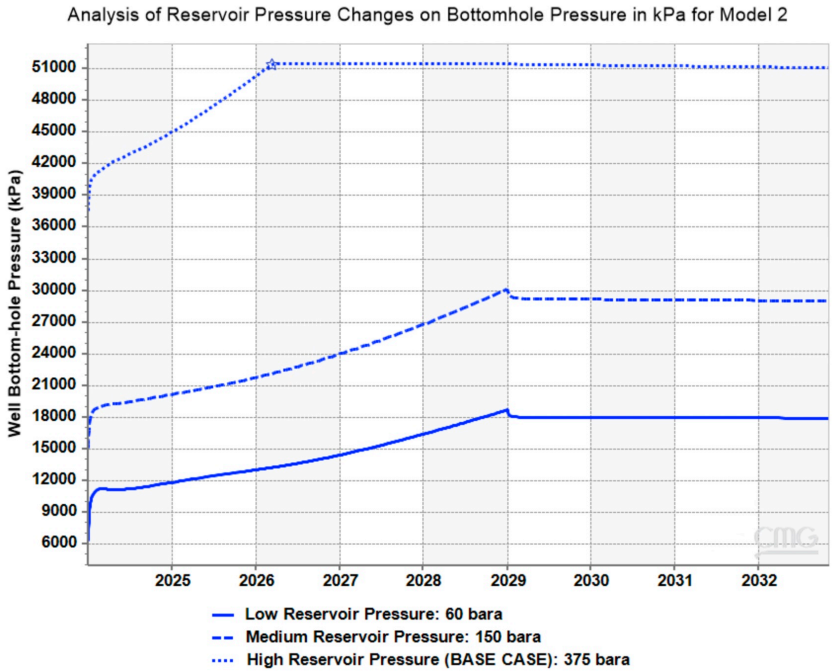

Figure 47: Effects of reservoir pressure changes on bottomhole pressure in Model 2.

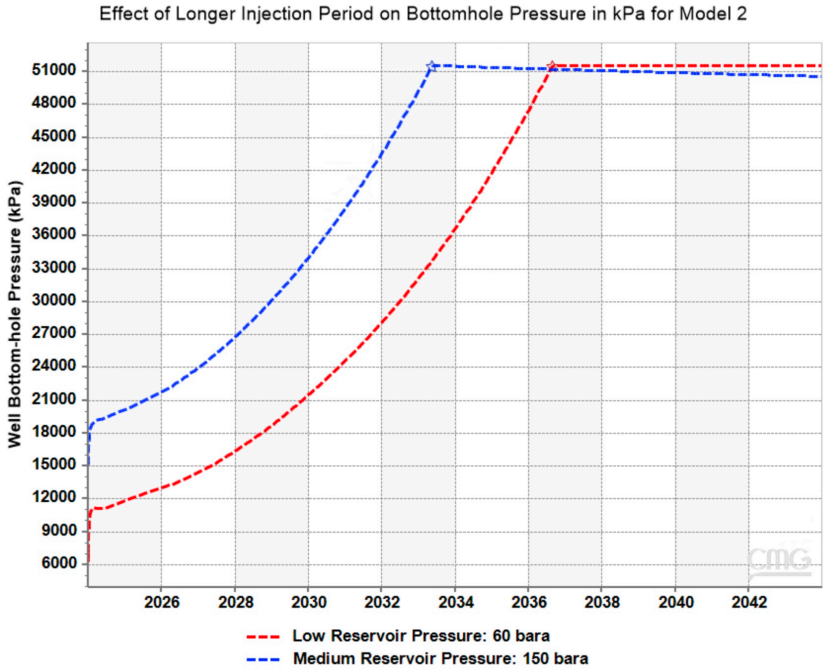

Figure 48: Effects of longer injection periods on reservoir pressures 60 bara and 150 bara in Model 2.

As shown in Figure 48 above, for a low reservoir pressure of 60 bara (red dotted line), the system was able to handle CO_2 injection for 4616 days before reaching the maximum bottomhole pressure, with around 4.68932e+07 m^3 of injected CO_2 (around 40 Mt), unlike the higher value of 150 bara (blue dotted line), where the system reached the constraint in 3421 days, with a cumulative 3.46876e+07 m^3 of injected CO_2 (around 30 Mt). This is predicted as with lower initial reservoir pressure, the pressure build-up until reaching the fracture pressure will take longer, allowing larger amounts of CO_2 to be injected in the formation.

Considering that the first case of reservoir pressure (60 bara) is below the critical pressure of CO_2 (73.8 bara), it is seen when plotting the bottomhole pressure with respect to the wellhead pressure in Figure 49 below that there is a sharp increase in bottomhole pressure from 60 to 280 bara between wellhead pressures of 30 to 70 bara, unlike the case for the base case (375 bara) shown in Figure 50, where the increase in bottomhole pressure is much smoother.

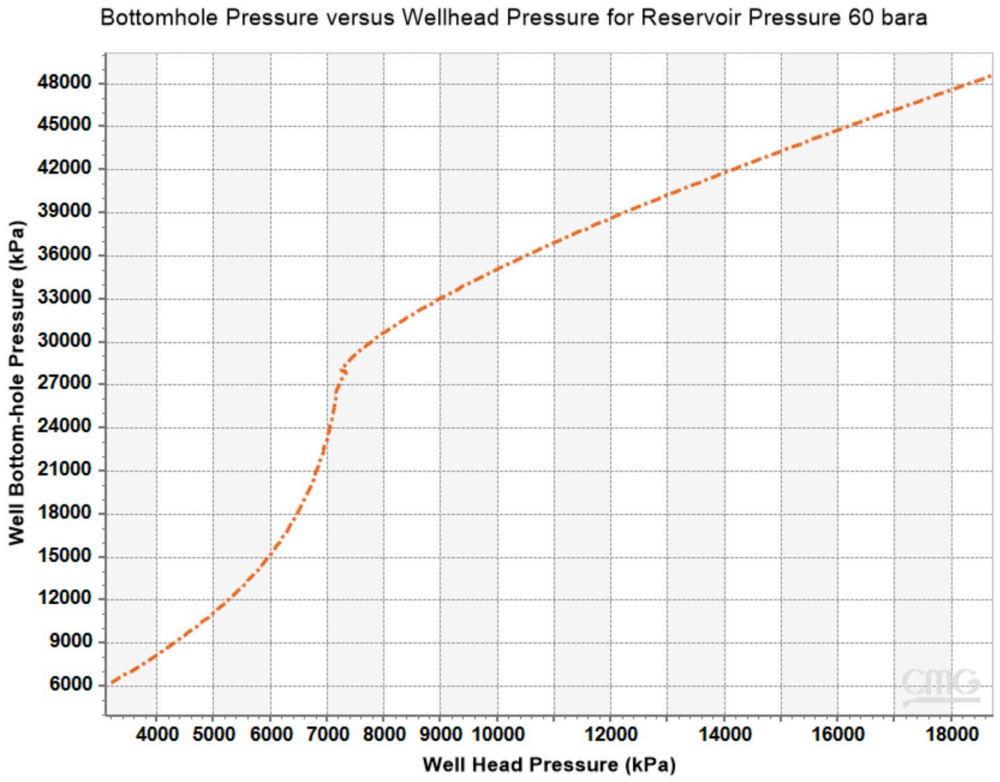

Figure 49: Bottomhole pressure with respect to wellhead pressure plot for a reservoir pressure of 60 bara.

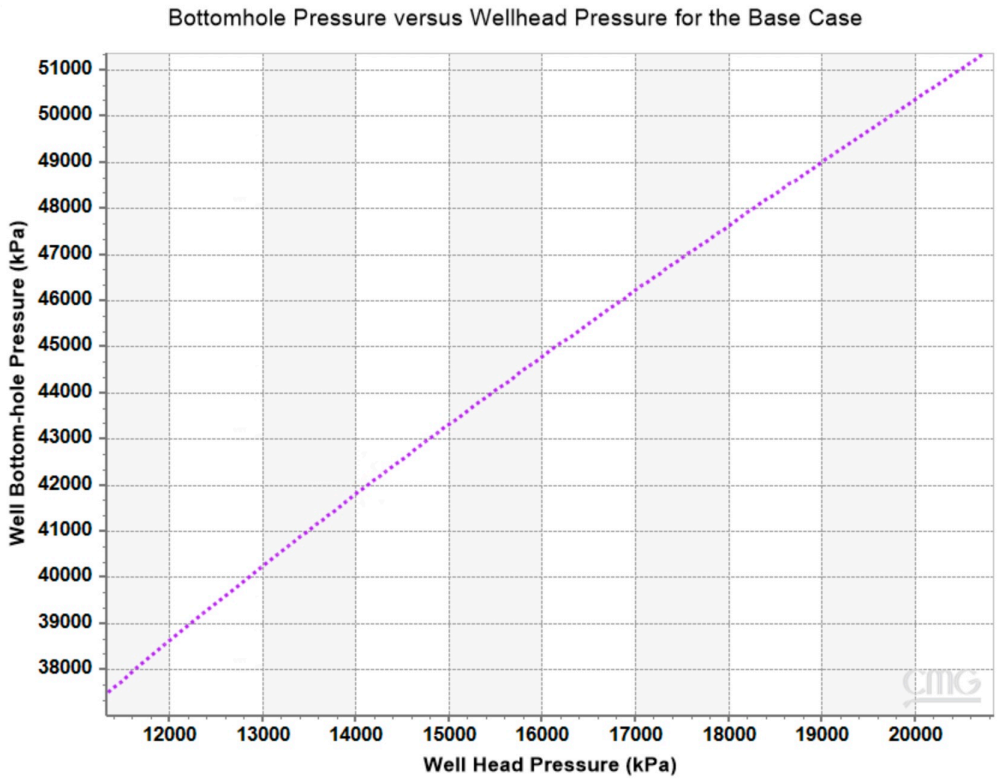

Figure 50: Bottomhole pressure with respect to wellhead pressure plot for the base case.

This could be caused by CO_2 transitioning from a gas phase to a liquid phase. This is assessed by analyzing the CO_2 gas mole fraction plot that represents how much CO_2 is in gas phase, and how much is in the liquid or supercritical phase, depending on pressure and temperature conditions.

As shown in Figure 51 below, the gas mole fraction was 1 initially, indicating that CO_2 was still in a single gaseous phase. The fraction started decreasing after 1730 days of injection until reaching a low 0.5. This reflects that a significant fraction of CO_2 is transitioning to a liquid phase.
Given that the bottom-hole pressure is higher than the critical pressure of CO_2 at this time, and the temperature is around 90°C which is above the critical temperature (31.1°C), CO_2 is in the supercritical phase at the bottomhole.

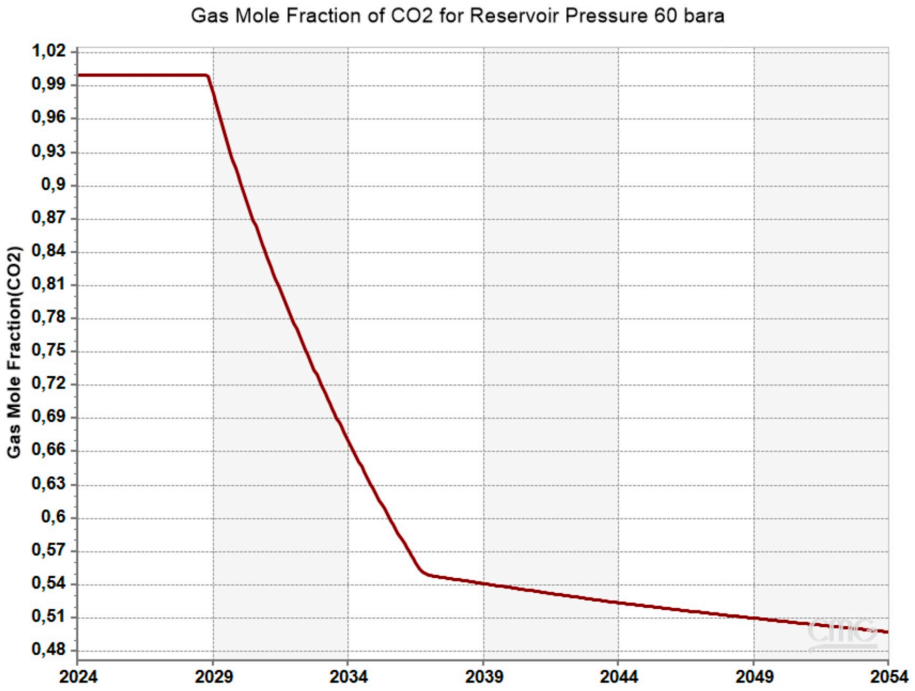

Figure 51: Gas mole fraction of CO_2 for a reservoir pressure of 60 bara.

This aligns with the density plot shown in Figure 52 below, where the density of CO_2 is increasing from 90 kg/m^3 to around 485 kg/m^3, representing a denser fluid.
This is not the case for both reservoir pressures 150 and 375 bara, as originally they are above the critical pressure, meaning that no phase change has occurred.
This could be highlighted by plotting the data points from the low reservoir pressure model on the phase diagram of CO_2. As shown in Figure 53, the CO_2 for this case is transitioning from gas to supercritical fluid, which explains the decrease in CO_2 gas fraction and the increase in density.

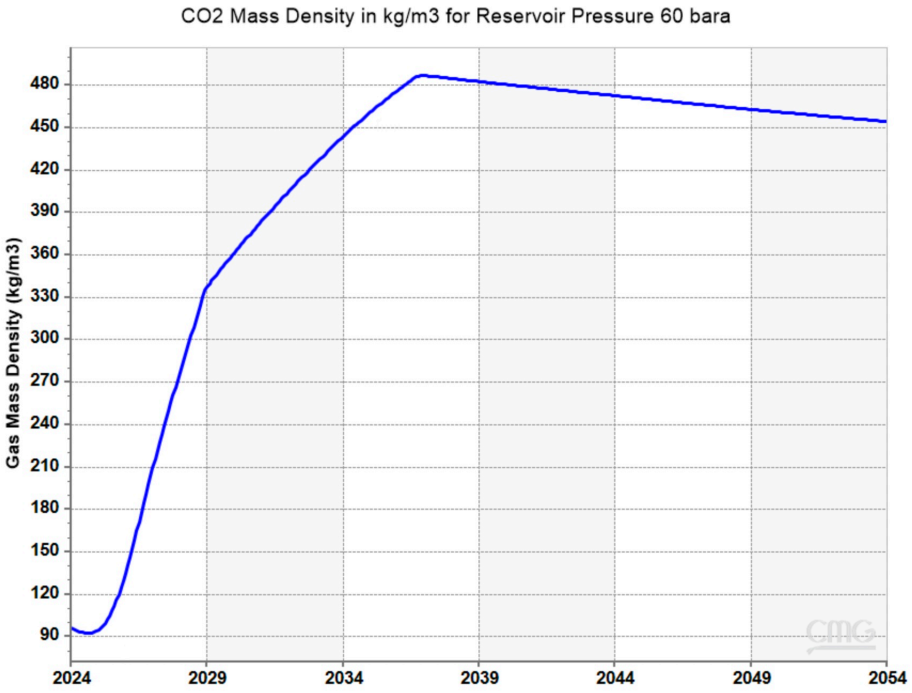

Figure 52: CO_2 mass density for a reservoir pressure of 60 bara.

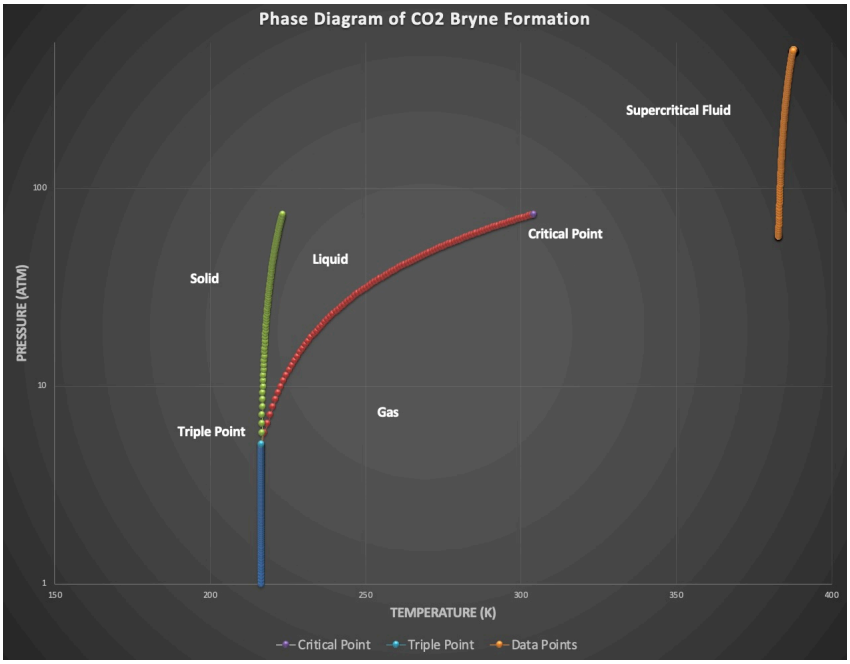

Figure 53: CO_2 phase diagram for a reservoir pressure of 60 bara.

4.6.2 Changing the porosity

The effects of porosity on cumulative CO_2 injected and the time needed to reach the operational constraint have been analyzed with a lower value of 0.1 and a higher value of 0.4 compared to the base case which is 0.24.

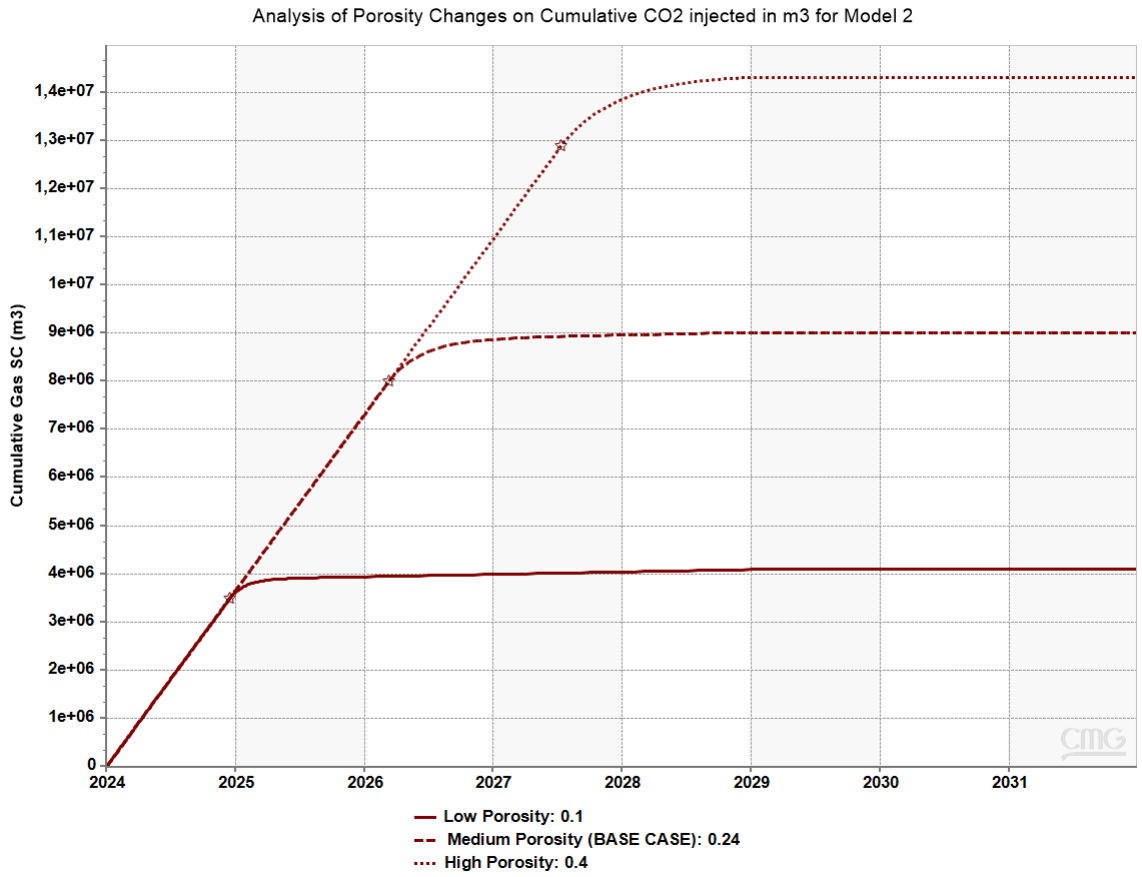

Figure 54: Effects of porosity changes on cumulative CO_2 injected in Model 2.

As shown in Figure 54 above, for a low porosity of 0.1 the time needed by the system to reach the fracture pressure is 349 days, injecting around 4.0e+06 m^3 of CO_2 (3.4 Mt), compared to the base case, and to the high porosity of 0.4, where the time needed was 1288 days, injecting around 1.43e+07 m^3 of CO_2 (12.15 Mt).
This is expected as more space is available for CO_2 to be stored, increasing the storage capacity of CO_2 in the system. In addition, higher porosity would cause the injected CO_2 to spread out easily, reducing the localized pressure build-up. Thus, increasing the injection time before reaching the fracture pressure of the formation.

4.6.3 Changing the permeability

To assess the effects of different permeability values on cumulative CO_2 injected and the time needed to reach the fracture pressure, three values have been analyzed. A low value of 50 mD, a medium value of 150 mD (base case), and a high value of 300 mD were chosen.

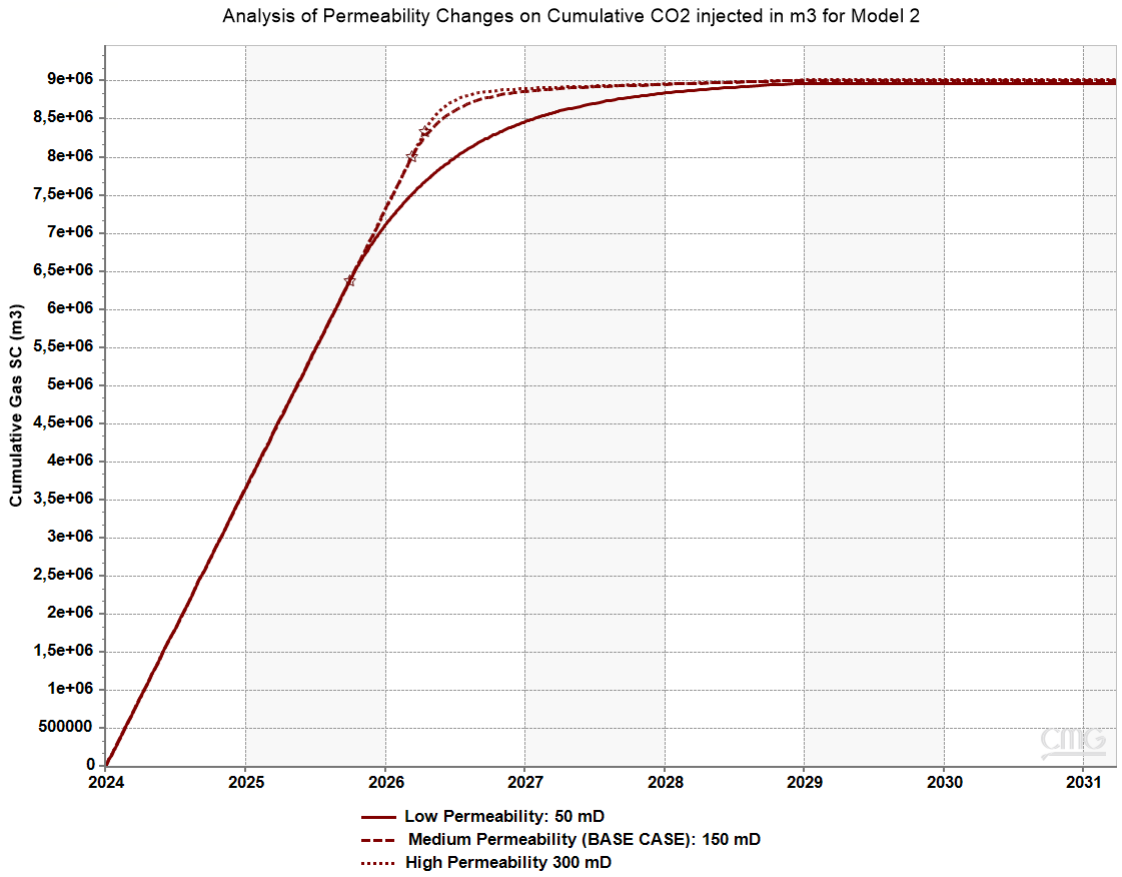

Figure 55: Effects of permeability changes on cumulative CO_2 injected in Model 2.

As shown in Figure 55 above, for a low permeability of 50 mD the time needed by the system to reach the fracture pressure is 637 days, injecting around 8.97047e+06 m^3 of CO_2, compared to the base case, and to the high permeability of 300 mD, where the time needed was 833 days, injecting around 9.01554e+06 m^3 of CO_2. The change in cumulative CO_2 injected is significantly less prominent than the case of changing the porosity as seen in Figure 54. The main reason behind this is that when permeability increases it doesn't add new storage space like porosity.

4.6.4 Changing the initial water saturation

Three values of initial water saturation were assessed, a low value of 0.6, a medium base case value of 0.8, and a high value of 1.

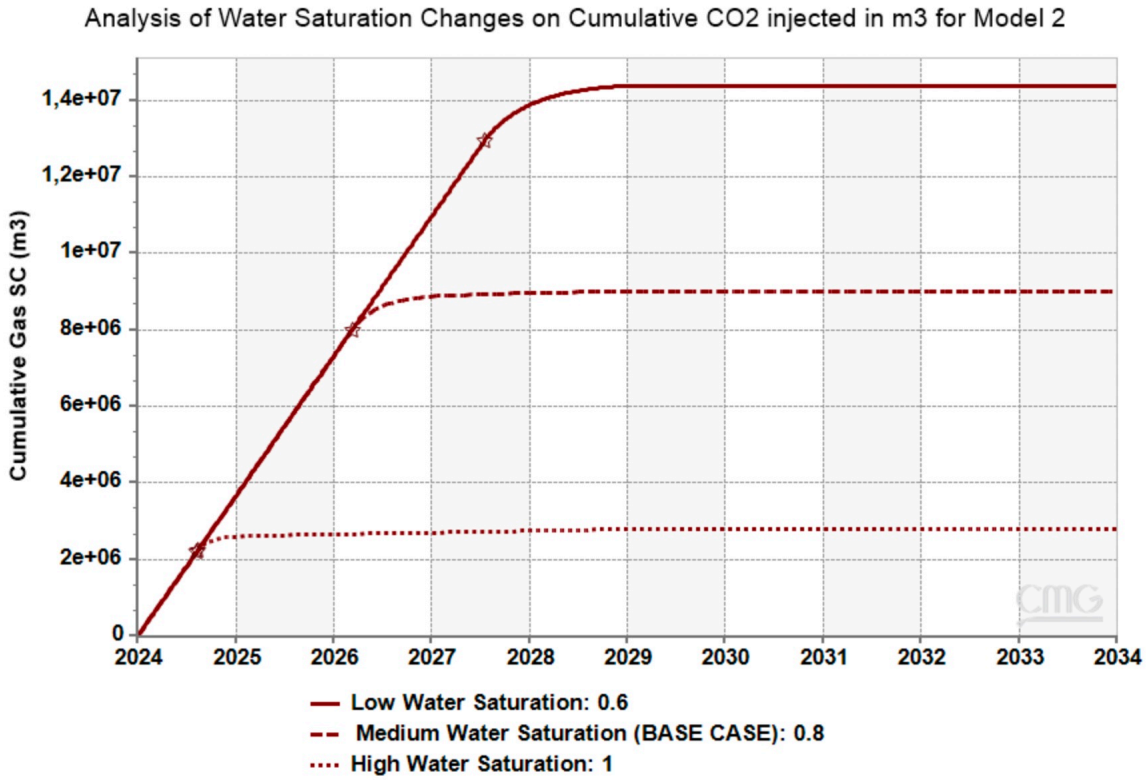

Figure 56: Effects of water saturation changes on cumulative CO_2 injected in Model 2.

As shown in Figure 56 above, for a low water saturation of 0.6 the time needed by the system to reach the operational constraint is 1292 days, injecting around 1.438+07 m^3 of CO_2, compared to the base case, and to the high water saturation of 1, where the time needed was 221 days, injecting around 2.788e+06 m^3 of CO_2.
The cumulative CO_2 stored decreases when the formation is fully saturated with water as more pore space is occupied by water, reducing the available space for CO_2 to be stored. In addition, the pressure build-up is quicker for a fully saturated formation as high water saturation means that most of the pore space is filled with water leaving limited space for the CO_2 to occupy, leading to a faster build-up of pressure.

After gathering the results from all the previously mentioned cases, Excel was used to create two radar plots to present the optimal conditions for CO_2 storage.
The results were normalized and distributed as shown in Table 7 below.

	Cumulative CO_2 Injected (m^3)	Time to reach the operational constraint (day)	Normalized CO_2 Injected	Normalized Time
Porosity Low	4086610	349	0.029933178	0.029124005
Porosity Medium	9010420	800	0.143443555	0.131740614
Porosity High	14312800	1289	0.265681243	0.243003413
Permeability Low	8970470	638	0.142522573	0.094880546
Permeability Medium	9010420	800	0.143443555	0.131740614
Permeability High	9015540	833	0.143561588	0.139249147
Water Saturation Low	14380200	1292	0.26723504	0.243686007
Water Saturation Medium	9010420	800	0.143443555	0.131740614
Water Saturation High	2788180	221	0	0
Reservoir Pressure Low	46165800	4616	1	1
Reservoir Pressure Medium	34212500	3421	0.724436242	0.728100114
Reservoir Pressure High	9010420	800	0.143443555	0.131740614

Table 7: Gathered results for sensitivity analysis.

The first radar plot created including the reservoir pressure changes is shown in Figure 57 below.

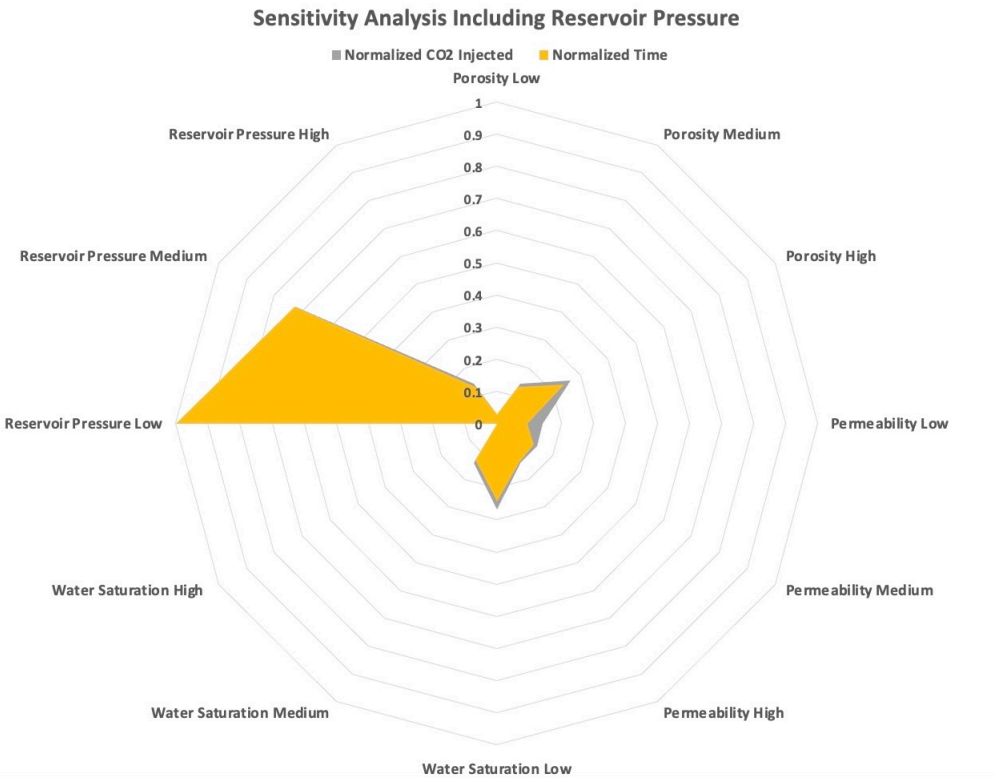

Figure 57: Radar plot including reservoir pressure changes.

The first radar plot shows that the changes in reservoir pressure have a significant influence on the whole sensitivity analysis. Therefore, another radar plot was created excluding the reservoir pressure parameter from the sensitivity analysis.
As shown in Figure 58 below, the effects of different parameters are more apparent. An optimal set of parameters would include low water saturation, high permeability, and high porosity.
It is challenging to find a prospective site with all the preferred parameters. However, a depleted gas field with low reservoir pressure and high porosity and permeability could be identified based on previous production data. The analysis on a depleted gas field is performed in section 4.7 on the depleted Frigg field located in the North Sea.

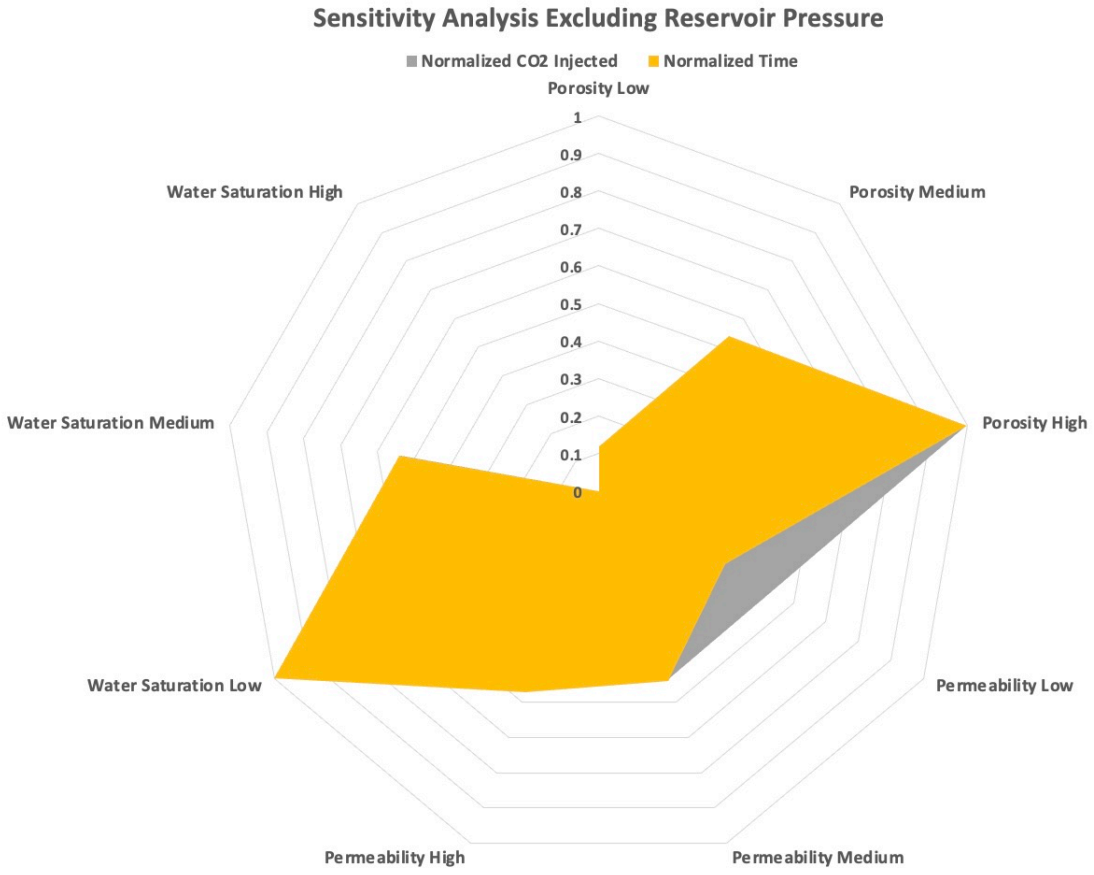

Figure 58: Radar plot excluding reservoir pressure changes.

4.7 Pressure profile analysis for model 3

After calculating the fracture pressure corresponding to Frigg formation in section 4.2.2, the maximum bottomhole pressure was set at 150 bara, and further simulations were ran accordingly.

Figure 59 showing the sharp increase in bottomhole pressure was generated on PIPESIM, after running an initial system analysis on a range of wellhead pressures from 20 bara to 100 bara with a fixed injection rate of 100,000 m^3/day. PIPESIM only gives instantaneous results along the depth without considering the time factor. Therefore, having a range of increasing wellhead pressure would simulate the real life scenario with time.

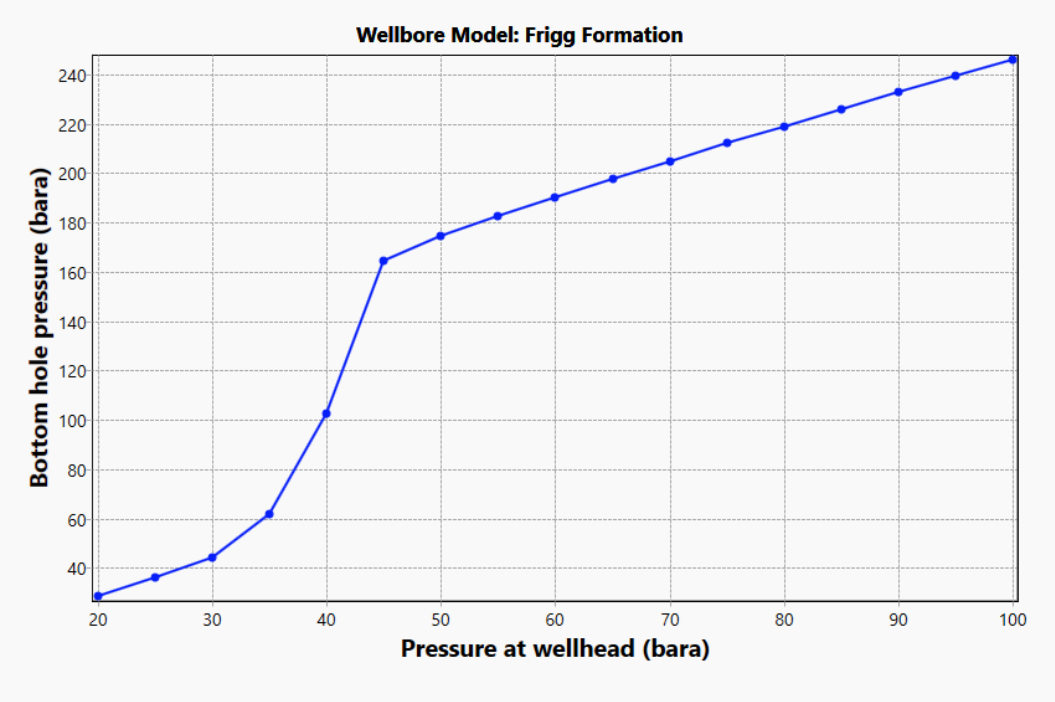

Figure 59: Bottomhole pressure with respect to wellhead pressure plot from PIPESIM.

This is not the case in CMG, as the simulation was ran over a period of 30 years, where CO_2 was being injected at a rate of 100,000 m^3/day for as long as the system could take it without reaching the fracture pressure. After injecting CO_2 for 670 days the system reached the constraint of maximum bottomhole pressure. The bottomhole pressure plot is shown in Figure 60 below:

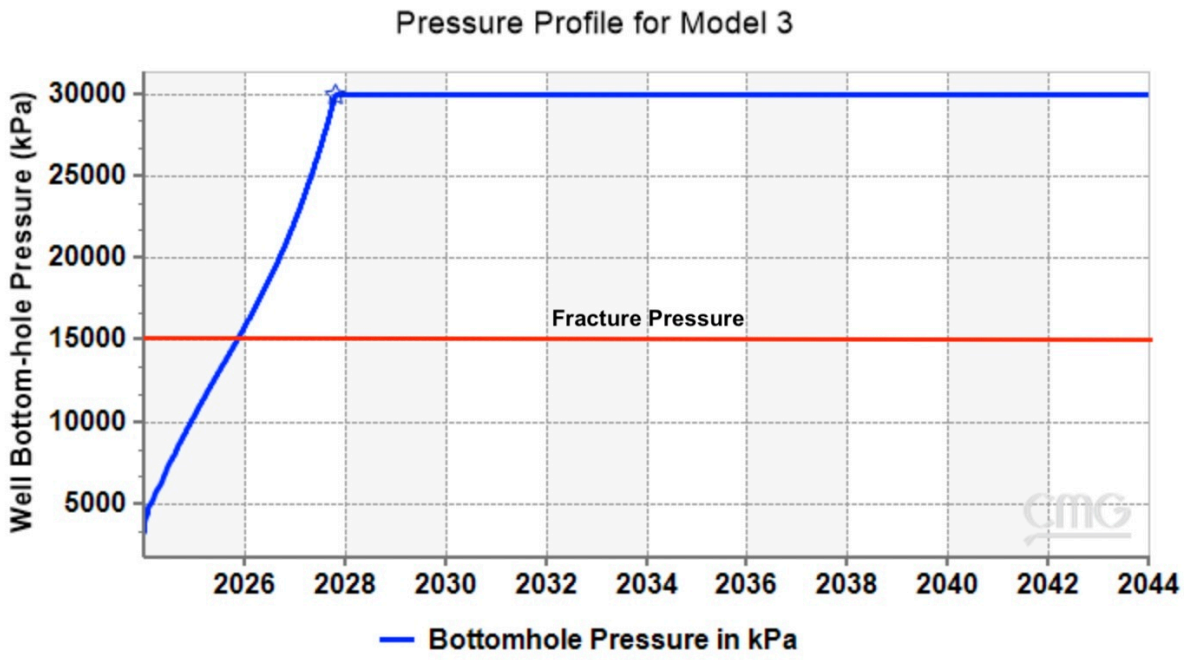

Figure 60: Bottomhole pressure plot for model 3.

It is worth noting that in a period of 2 years, around 6.7e+07 m^3 of CO_2 was injected, which is around 2.01 Mt of CO_2 (considering a density of 30 kg/m^3), with only a 120 bara pressure buildup.

When plotting the bottomhole pressure curve against the wellhead pressure using CMG RESULTS™, it is clear that there is a disturbance or unusual fluctuations between wellhead pressures 38 and 42 bara which corresponds to a range of bottomhole pressures from 60 to 145 bara, as shown in Figure 61.

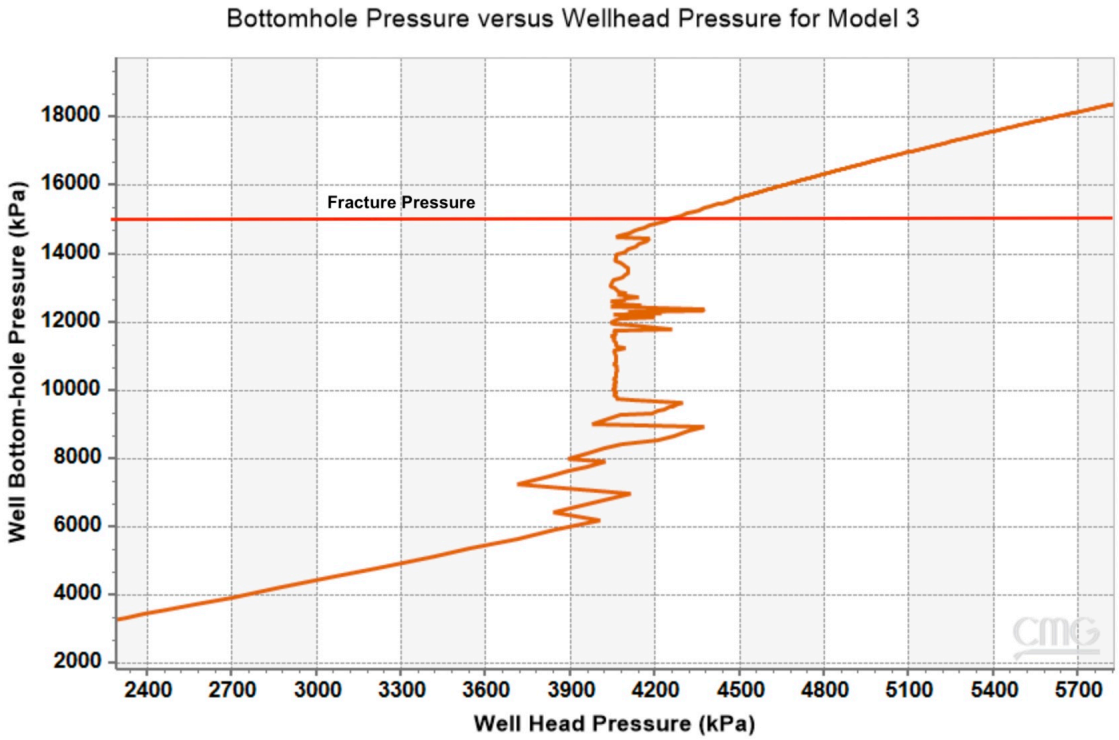

Figure 61: Bottomhole pressure with respect to wellhead pressure for model 3.

This matches the wellbore model built on PIPESIM, as when plotting the bottomhole pressure versus wellhead pressure, the curve shown in Figure 59 reflects somewhat the same behavior. When the wellhead pressure increases from 30 to 45 bara, the bottomhole pressure increases drastically from 40 to 160 bara which is beyond the fracture pressure. This uncontrolled surge could be risky to the integrity of the wellbore and the safety of the injection process. Therefore, it is important to know what is happening in the wellbore to try and mitigate any possible risk associated with CO_2 injection and storage. The surge in pressure, represented by fluctuations in wellhead pressure when the bottomhole pressure is ultimately increasing from 60 bara to 145 bara, as shown in Figure 61, indicates a phase transition of CO_2 from gas to supercritical fluid, causing the abrupt changes in pressure. This could be assessed by analyzing the following using CMG:

- Pressure versus temperature plot
- CO_2 phase diagram
- The density of CO_2 along the wellbore and with respect to time

Pressure versus temperature

When looking first at wellhead and bottomhole pressure plots in Figure 61, it is clear that both curves are increasing with time, and that the bottomhole pressure exceeded the critical pressure of CO_2 (73.7 bara) almost one year after injection, and this is when the fluctuations started happening. The initial bottomhole pressure was around 30 bara where CO_2 was still in the gas phase. The wellhead pressure stayed below the critical pressure along the whole injection indicating that the CO_2 stayed in the gas phase at the wellhead. Temperature plot would help to see if the critical temperature (31.1°) was crossed. Looking at Figure 62 below, it is shown that the bottomhole pressure is increasing with increasing temperature, in an expected trend.

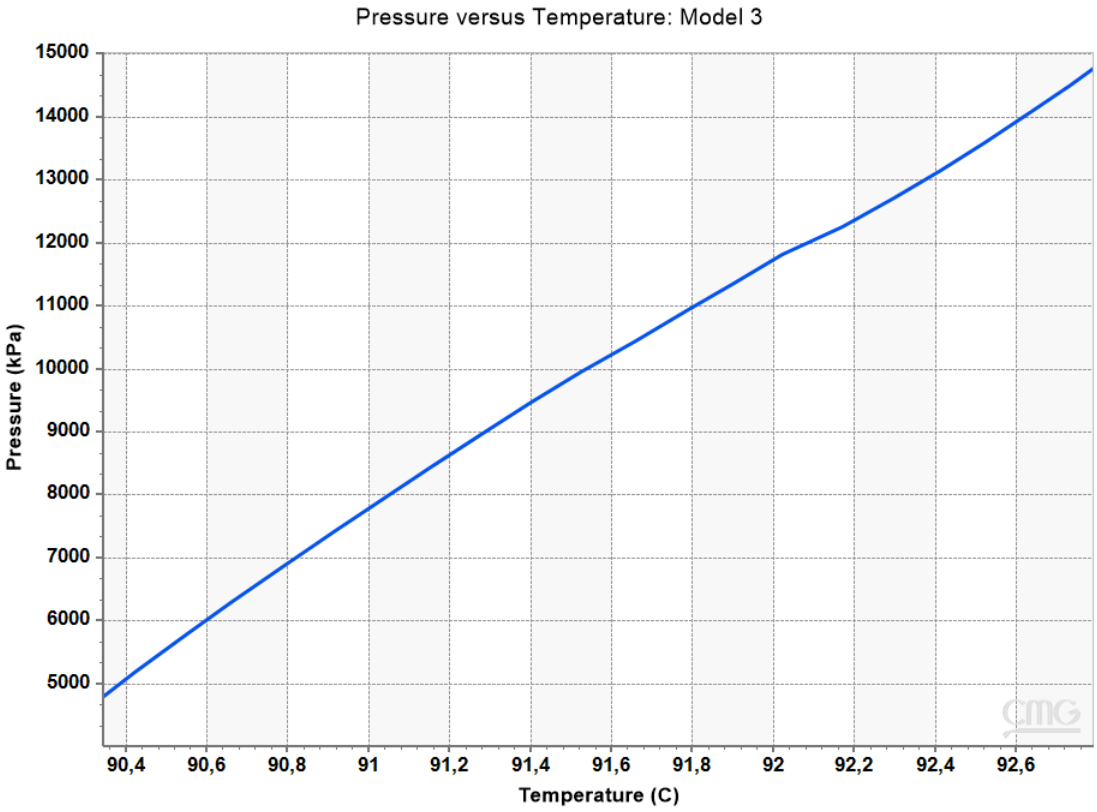

Figure 62: Bottomhole pressure with respect bottomhole temperature for Model 3.

Considering that the plot is only taking account for bottomhole conditions, the temperature was already above 90°C, therefore above the critical temperature of CO_2.

CO_2 phase fraction

As mentioned earlier, CMG GEM™ does not plot phase diagrams for the injected CO_2 under the varying pressure and temperature conditions. However, after extracting the pressure and temperature data points generated on CMG RESULTS™, a phase diagram was plotted using Excel.

The Figure below shows the CO_2 phase diagram corresponding to model 3. It is clear in Figure 63 how the CO_2 is transitioning from gas to a supercritical fluid as the pressure and temperature are increasing.

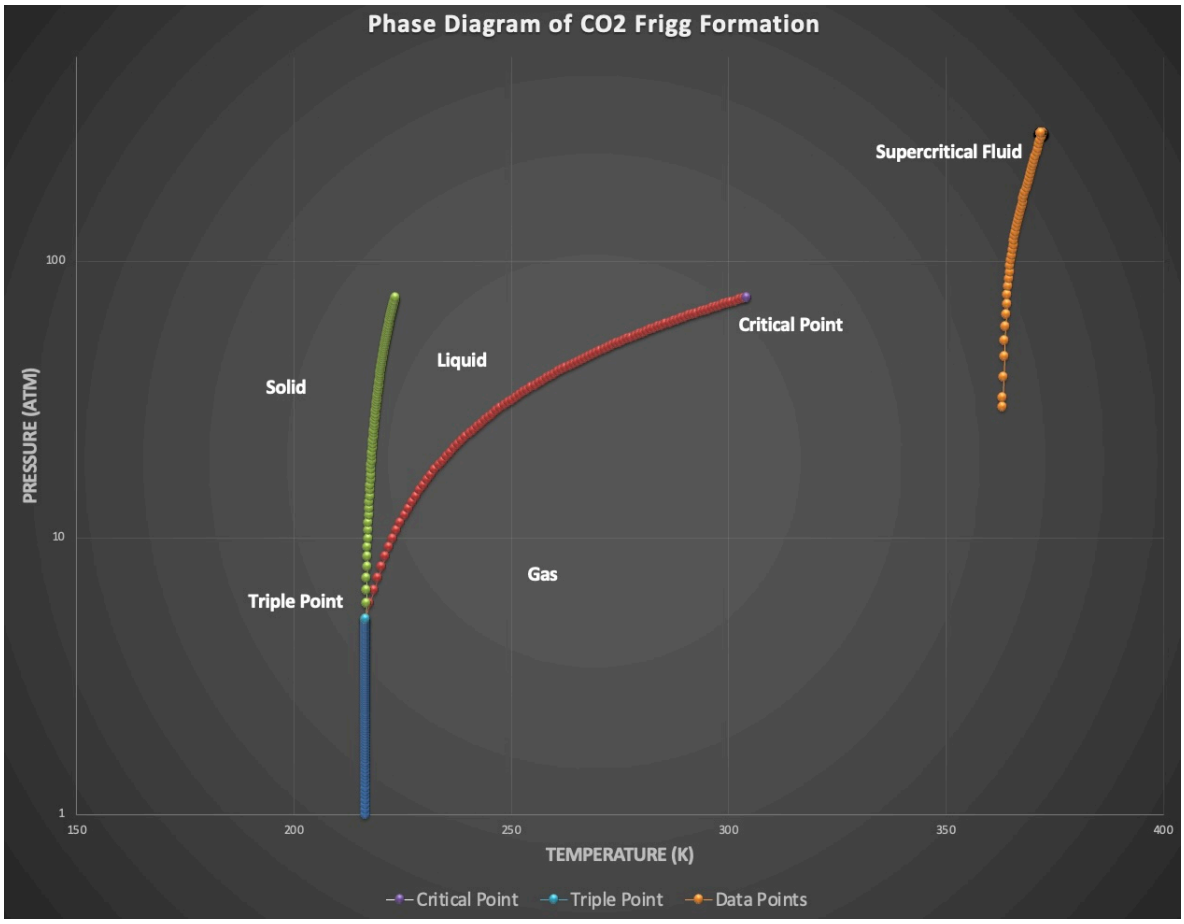

Figure 63: CO_2 phase diagram for Model 3.

CO_2 density

As shown in Figure 64 below, the CO_2 density curve has an increasing trend, which aligns with the fact the pressure is increasing from 30 bara to 150 bara, and with the fact that CO_2 is transitioning from gas to supercritical conditions.

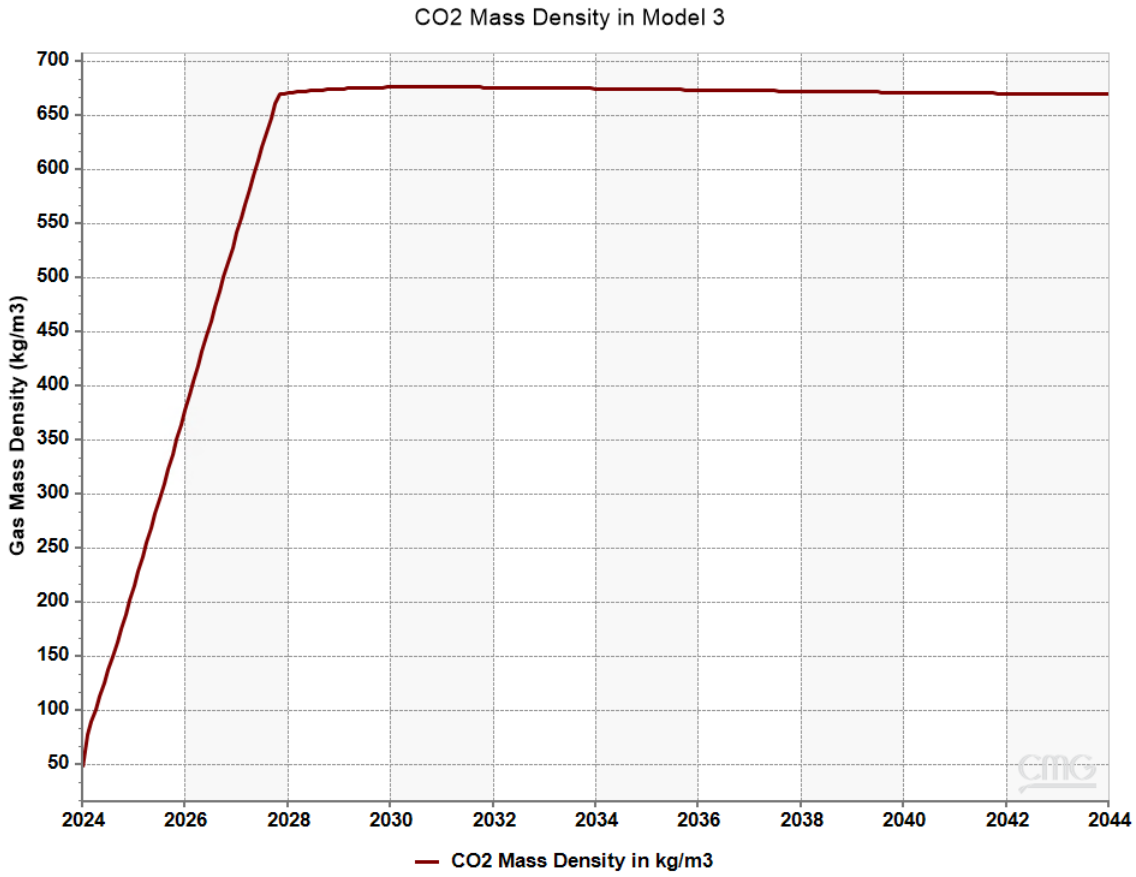

Figure 64: CO_2 mass density for Model 3.

Finally, coupling the wellbore model from PIPESIM with a detailed thorough reservoir model in CMG helped in investigating all the previous parameters and understanding what exactly happened during the pressure surge. As long as the phase change is taken into account with appropriate planning, the CO_2 injection would still be safe ensuring the integrity of the wellbore and the hosting formation.

5 Conclusion

This study presented a comprehensive analysis of CO_2 injection using a coupled wellbore-reservoir modeling approach in the context of carbon capture and storage (CCS). Wellbore models were built using PIPESIM and then coupled to reservoir models built using CMG GEM™. Bryne and Sandnes formations were chosen as a targeted deep saline aquifer, and Frigg formation as a depleted gas field. The study presents the different CO_2 trapping mechanisms, the calculation of fracture pressure, the estimation of an optimal CO_2 injection rate, the evaluation of thermal effects, and a sensitivity analysis on optimal storage conditions.

- The visualization of CO_2 trapping mechanisms provided an indication of how CO_2 will behave in a simulator under the system's conditions.

- The fracture pressures were calculated using Eaton's method. For the Bryne and Sandnes formations it was calculated at 515 bara, and for the Frigg depleted field, it was calculated at 150 bara. Calculating the fracture pressure is essential to ensure safe injection rates.

- Step-rate injection test was done to determine an optimal CO_2 injection rate of 10,000 m^3/day, not to compromise the formation integrity for higher CO_2 storage.

- Temperature variations, or thermal effects, caused an increase in CO_2 mass density, solubility in brine, acidity, and brine viscosity.

- Phase diagrams were generated showing no phase change in the Bryne and Sandnes model where the CO_2 stayed in a supercritical state, and phase change in the Frigg depleted field model where CO_2 transitioned from gas to supercritical fluid causing a surge in bottomhole pressure.

- Sensitivity analyses were done to highlight that lower reservoir pressure, higher porosity, and lower initial water saturation increase storage capacity by an average of 60%.

In conclusion:
- The simulations done on Bryne and Sandnes formations showed that they are good targets for CO_2 injection in saline aquifer, where CO_2 stayed in a single phase, and where no complications were faced.

- The Frigg formation is also a good target for CO_2 injection in a depleted gas field due to the large time needed for pressure build-up. However, phase changes occur in the bottomhole, which are not always favorable due to possible complications such as two-phase flow issues, including slugging. This complicates the predictability and control of the injection process. Additionally, the rapid expansion of CO_2 can lead to cooling due to the Joule-Thomson effect, potentially causing temperature drops significant enough to form hydrates or even freeze formation water, leading to blockages and damage to the well infrastructure.

- Using a simulator that accounts for both transient multi-phase flow and for thermal effects, like CMG STARS™ is key element in future studies, as it contributes to a thorough understanding of the CO_2 injection and storage, helping in mitigating any unexpected or unfavourable scenario.

- Pressure transient analysis could be used in future work to validate the model and to confirm the chosen injection strategy, such as Horner plot and diagnostic plot.

In summary, this thesis offered a thorough framework for CCS optimization, contributing to the broader goal of mitigating global warming by effectively managing CO_2 emissions.
Future studies could include refined models, considering more complex geological settings with additional reliable geomechanical data and longer-term monitoring to enhance the applicability and effectiveness of these findings.

References

[1] Sally M. Benson and David R. Cole. CO2 Sequestration in Deep Sedimentary Formations. *Elements*, 4(5):325–331, 2008.

[2] Jens Birkholzer, Quanlin Zhou, and Chin-Fu Tsang. Large-scale impact of co2 storage in deep saline aquifers: A sensitivity study on pressure response in stratified systems. *International Journal of Greenhouse Gas Control*, 3:181–194, 01 2008.

[3] David R. Boyd. Safe climate: A report of the special rapporteur on human rights and the environment, 2020. Presented to the Third Committee on Social, Humanitarian and Cultural Issues of the UN General Assembly at its 74th session.

[4] Howard Crumpton. Chapter one - introduction and well control fundamentals. In *Well Control for Completions and Interventions*, pages 1–64. Gulf Professional Publishing, Boston, 2018.

[5] Ben A. Eaton. Fracture gradient prediction and its application in oilfield operations. *Journal of Petroleum Technology*, 21:1353–1360, 1969.

[6] ExxonMobil. 2024 advancing climate solutions report, January 2024. Published January 8, 2024.

[7] Sigurdur Gislason and Eric Oelkers. Carbon storage in basalt. *Science (New York, N.Y.)*, 344:373–4, 2014.

[8] Marc Hesse, Hamdi Tchelepi, B. CANTWEL, and Franklin Orr. Gravity currents in horizontal porous layers: Transition from early to late self-similarity. *Journal of Fluid Mechanics*, 577:363 – 383, 2007.

[9] Hussein Hoteit, Marwan Fahs, and Mohamad Reza Soltanian. Assessment of co2 injectivity during sequestration in depleted gas reservoirs. *Geosciences*, 9(5), 2019.

[10] M. K. Hubbert and D. G. Willis. Mechanics of hydraulic fracturing. *Transactions of the AIME*, 210:153–168, 1957.

[11] Seyed Mostafa Jafari Raad, Don Lawton, Greg Maidment, and Hassan Hassanzadeh. Transient non-isothermal coupled wellbore-reservoir modeling of co2 injection — application to co2 injection tests at the cami frs site, alberta, canada. *International Journal of Greenhouse Gas Control*, 111:103462, 2021.

[12] Evgenii Kanin, Igor Garagash, Sergei Boronin, Svetlana Zhigulskiy, Artem Penigin, Andrey Afanasyev, Dmitry Garagash, and Andrei Osiptsov. Co2 storage in deep saline aquifers: evaluation of geomechanical risks using integrated modeling workflow. 2023.

[13] Qi Liu, Marcelo D. Benitez, Zhao Xia, and J. Carlos Santamarina. Pore-scale phenomena in carbon geological storage (saline aquifers—mineralization—depleted oil reservoirs). *Frontiers in Energy Research*, 10, 2022.

[14] Michael E Mann. *greenhouse gas*. 2024.

[15] Juerg Matter and Peter Kelemen. Permanent storage of carbon dioxide in geological reservoirs by mineral carbonation. *Nature Geoscience*, 2, 2009.

[16] Hannah Ritchie, Pablo Rosado, and Max Roser. Greenhouse gas emissions. *Our World in Data*, 2020.

[17] Haissam Rabih Sakr. A study to assess the limitations of using a steady-state wellbore simulator in showcasing the effect of different co2 injection scenarios on flow behavior. Specialization project, Department of Geoscience and Petroleum, NTNU, Norway, 2023.

[18] A.. Shchipanov, L.. Kollbotn, and M.. Prosvirnov. Step Rate Test as a Way to Understand Well Performance in Fractured Carbonates. 2017.

[19] The Editors of Encyclopedia Britannica. *Henry's law*. 2023.

[20] Victor Vilarrasa and Jonny Rutqvist. Thermal effects on geologic carbon storage. *Earth-Science Reviews*, 165, 2016.

[21] Jon Jincai Zhang. Chapter 9 - fracture gradient prediction and wellbore strengthening. In *Applied Petroleum Geomechanics*, pages 337–374. Gulf Professional Publishing, 2019.

Appendices

.1 Wells Diagrams

.1.1 Model 2: Bryne and Sandnes formations

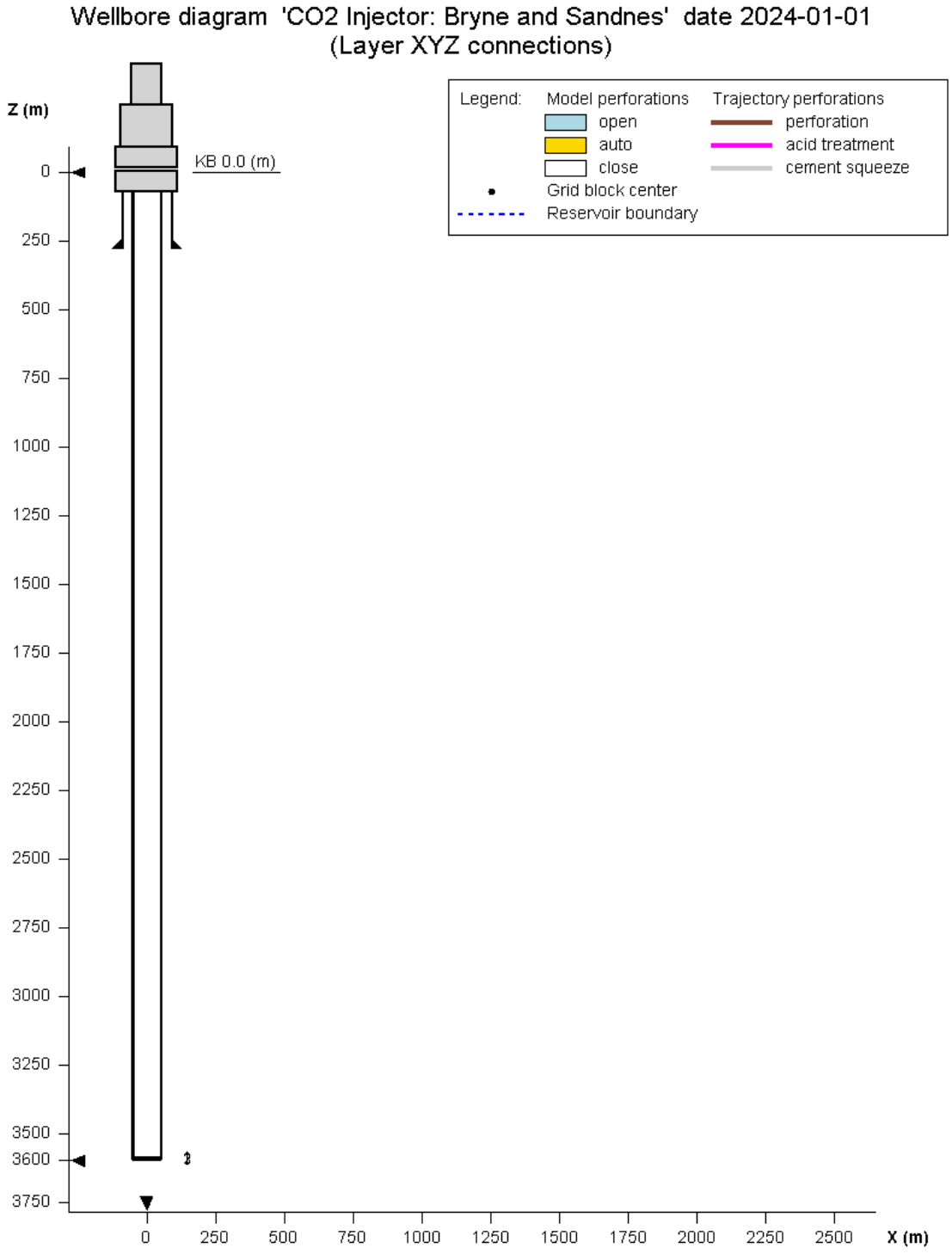

Figure 65: CO_2 Injector for Model 2.

.1.2 Model 3: Frigg field

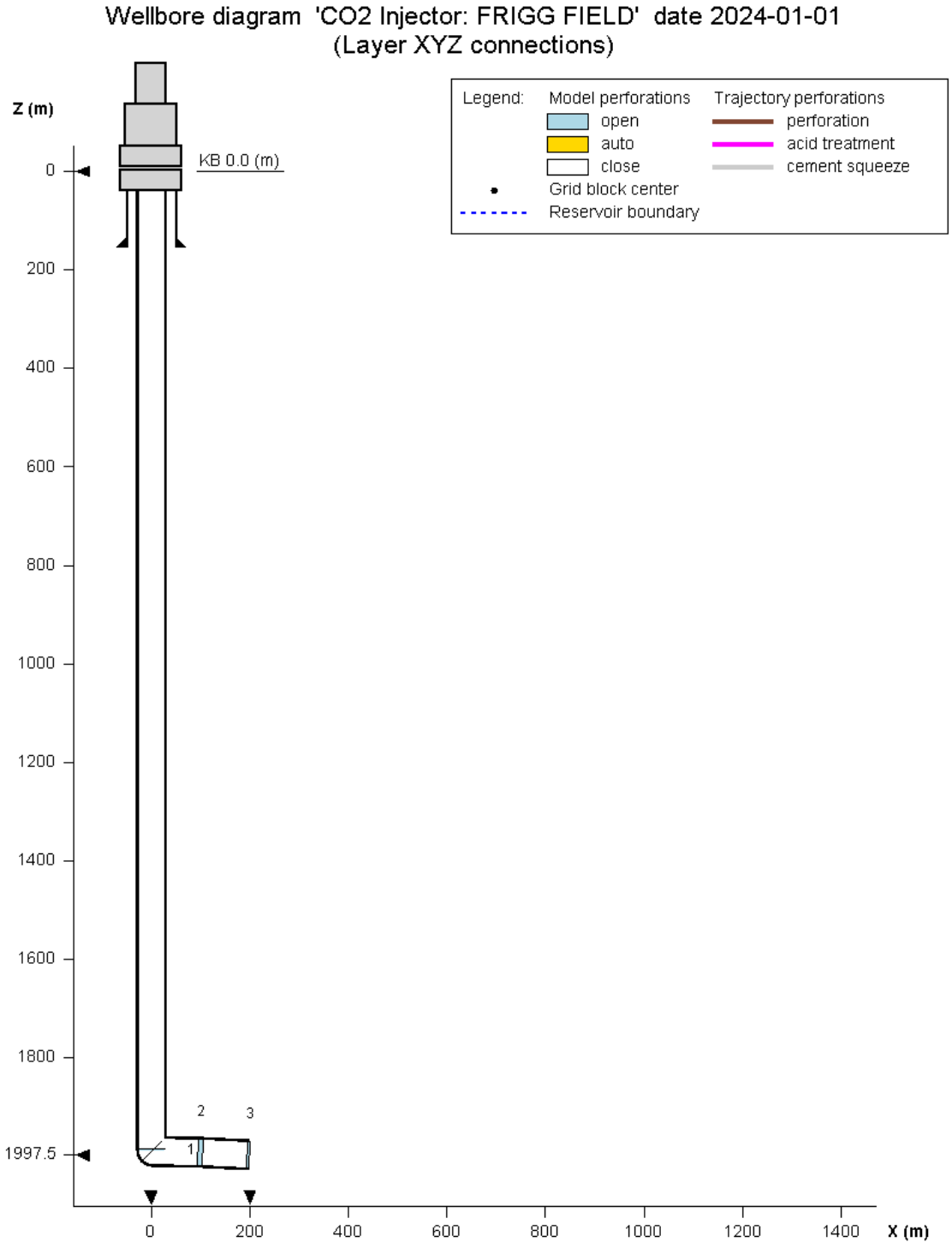

Figure 66: CO_2 Injector for Model 3.

.2 Well Placement Iterations Results

Well placement 1:

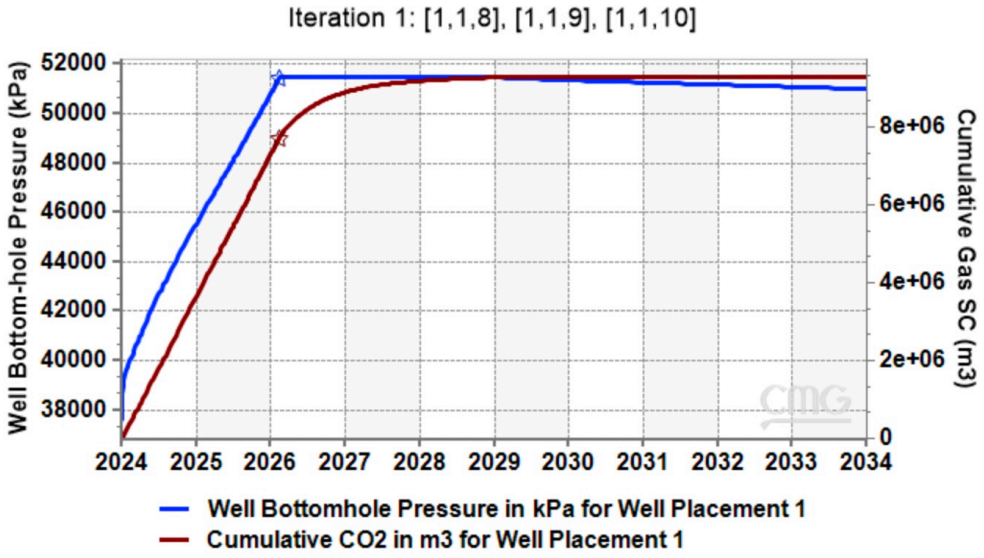

Figure 67: Well placement iteration 1.

Well placement 2:

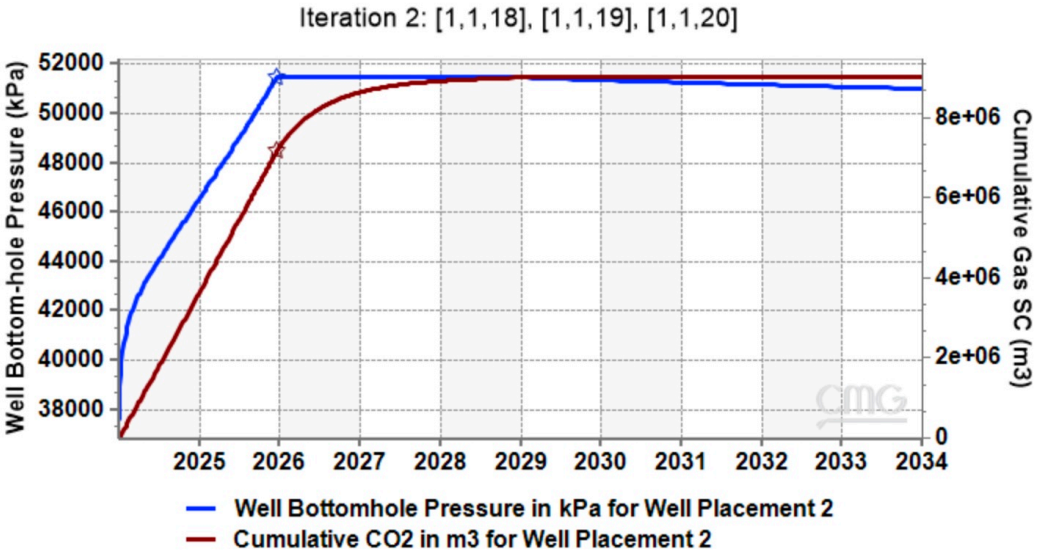

Figure 68: Well placement iteration 2.

Well placement 3:

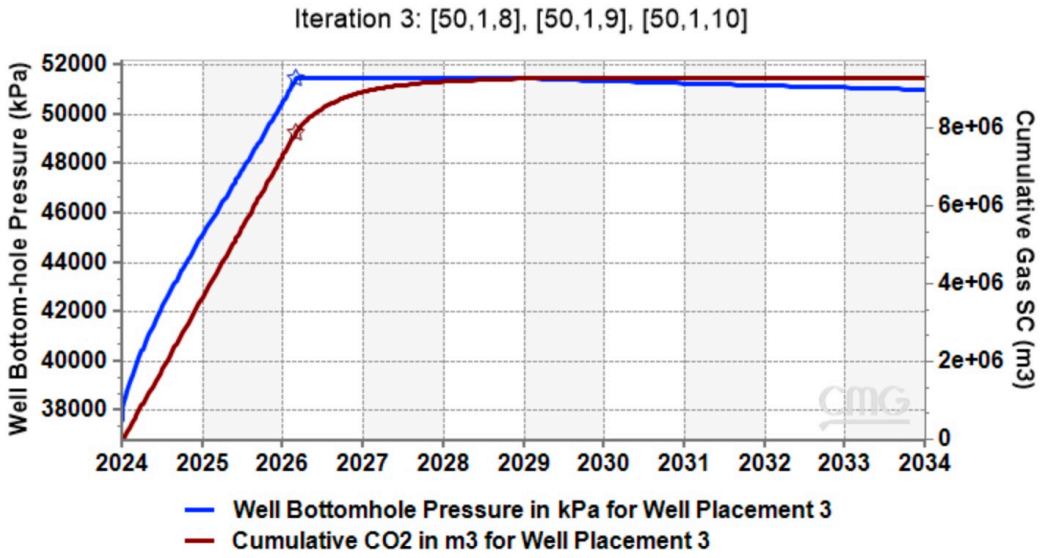

Figure 69: Well placement iteration 3.

Well placement 4:

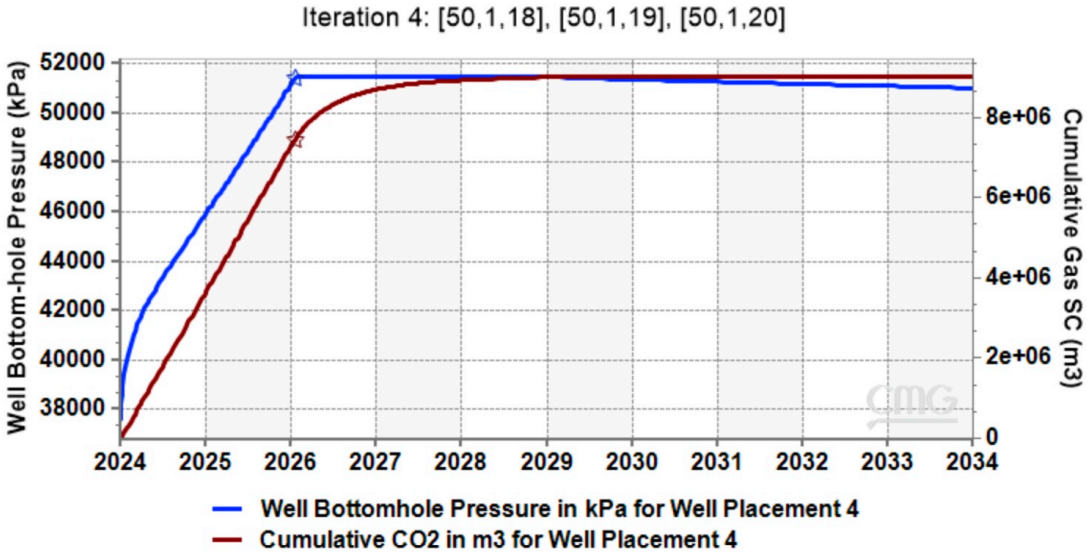

Figure 70: Well placement iteration 4.

Well placement 5:

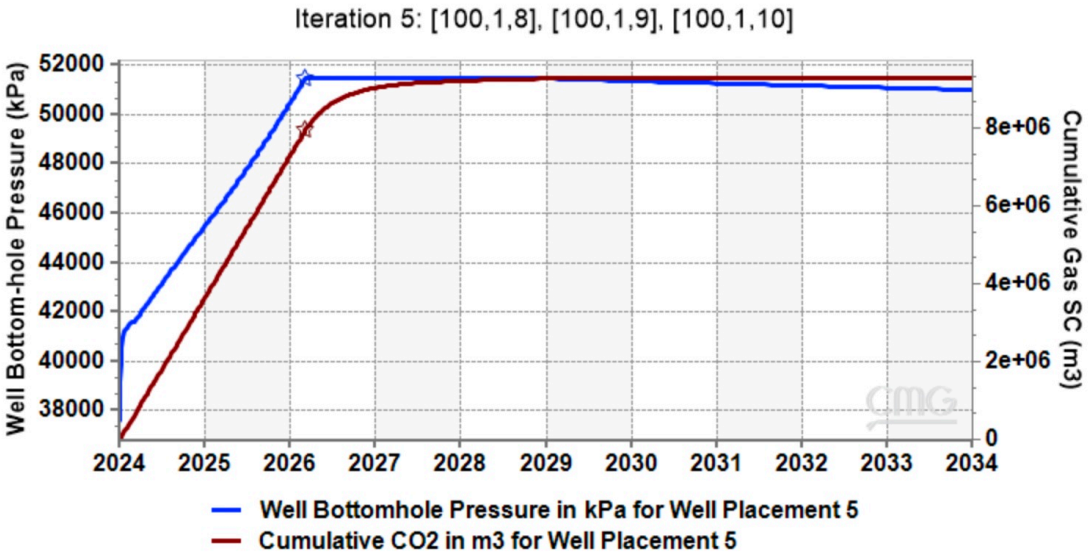

Figure 71: Well placement iteration 5.

Well placement 6:

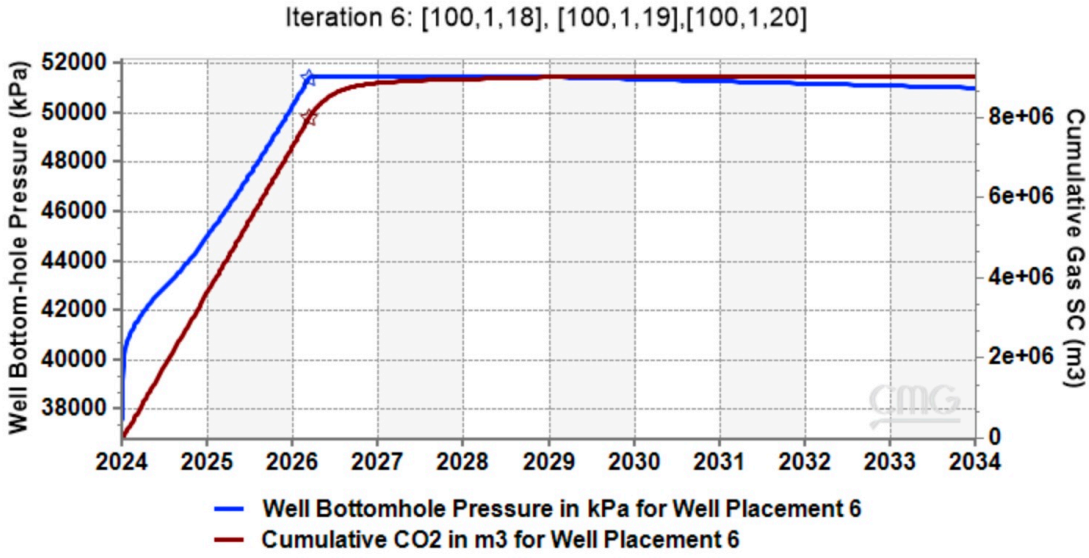

Figure 72: Well placement iteration 6.

Well placement 7:

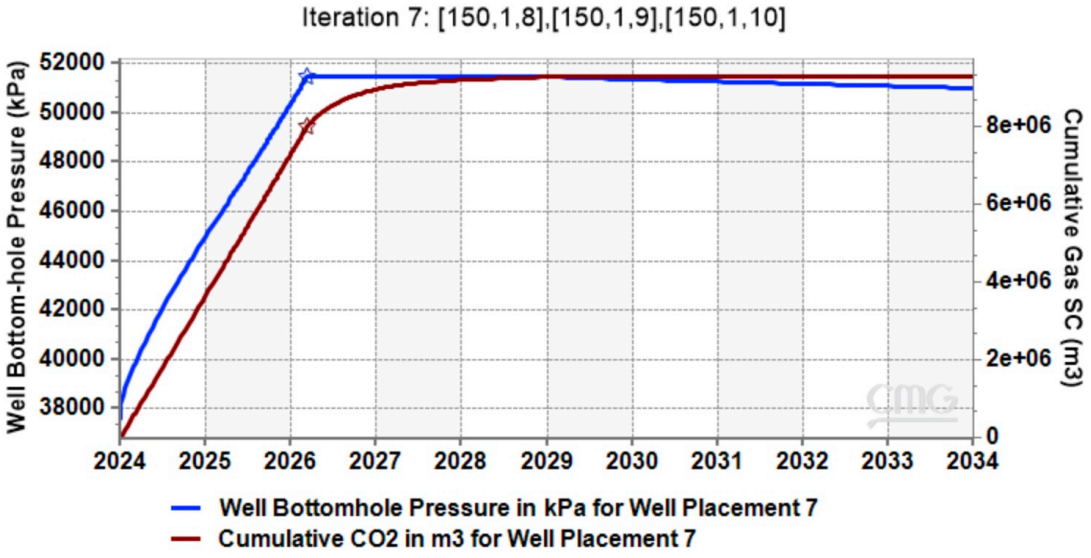

Figure 73: Well placement iteration 7.

Well placement 8:

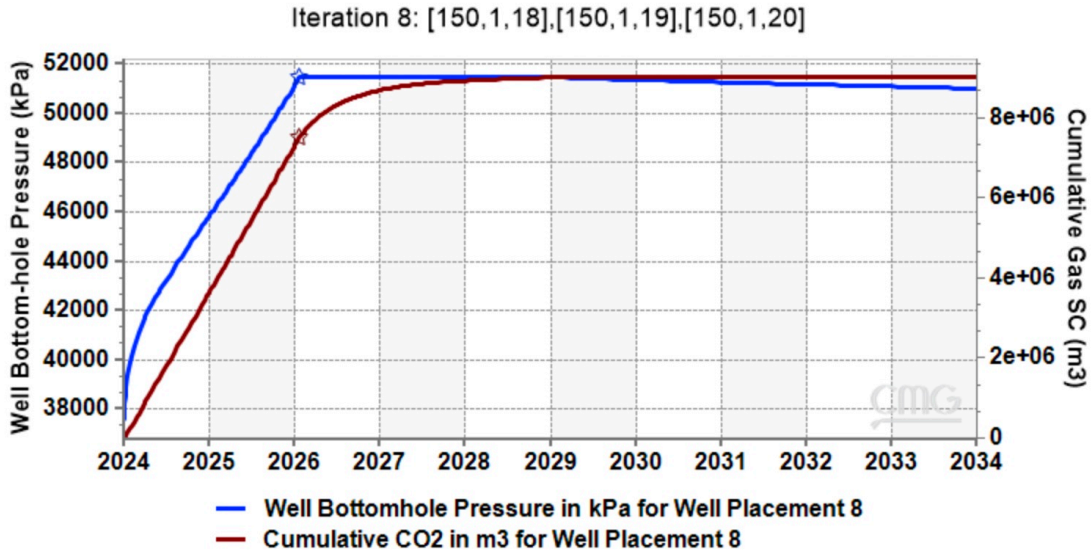

Figure 74: Well placement iteration 8.

Well placement 9:

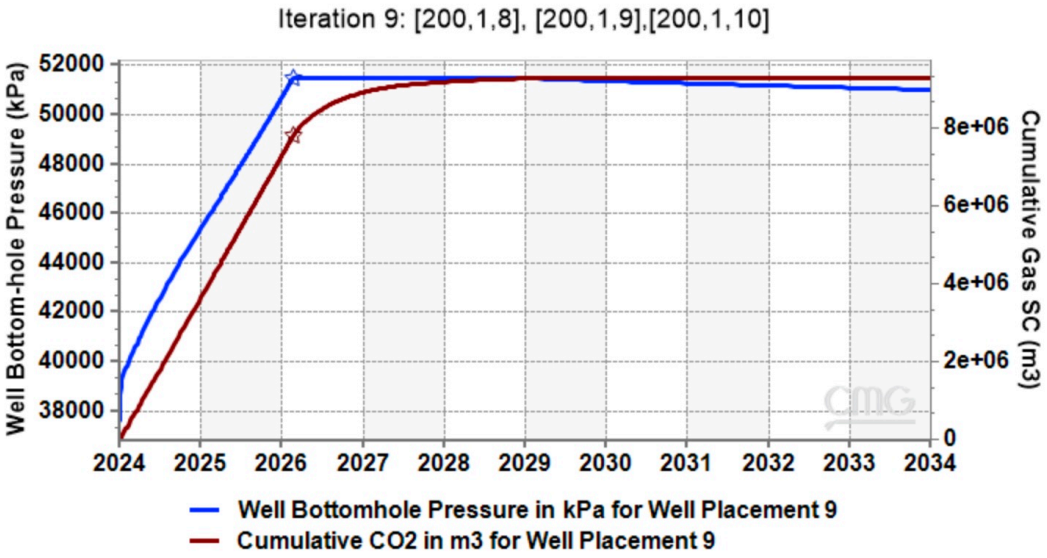

Figure 75: Well placement iteration 9.

Well placement 10:

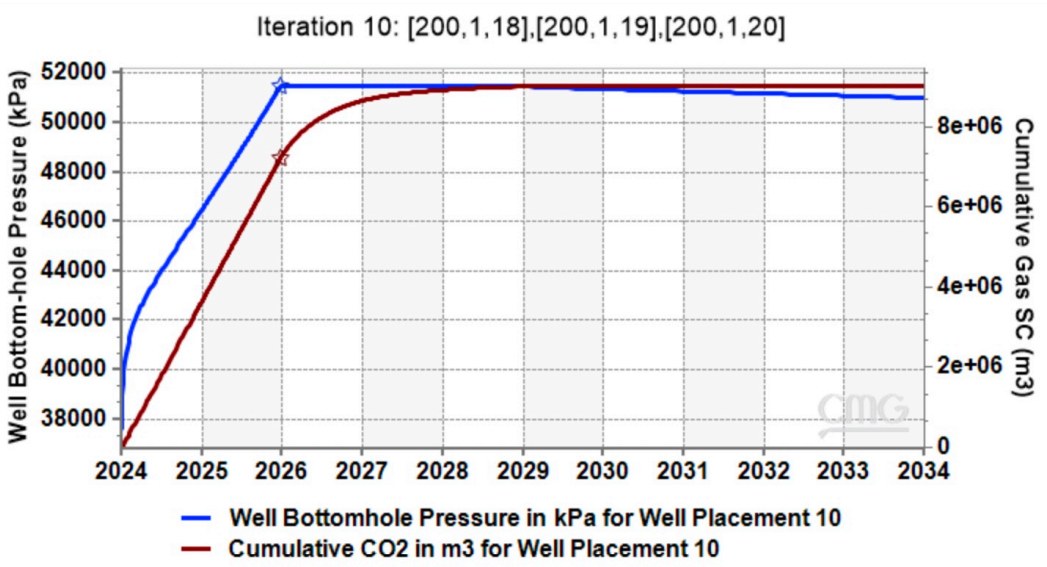

Figure 76: Well placement iteration 10.

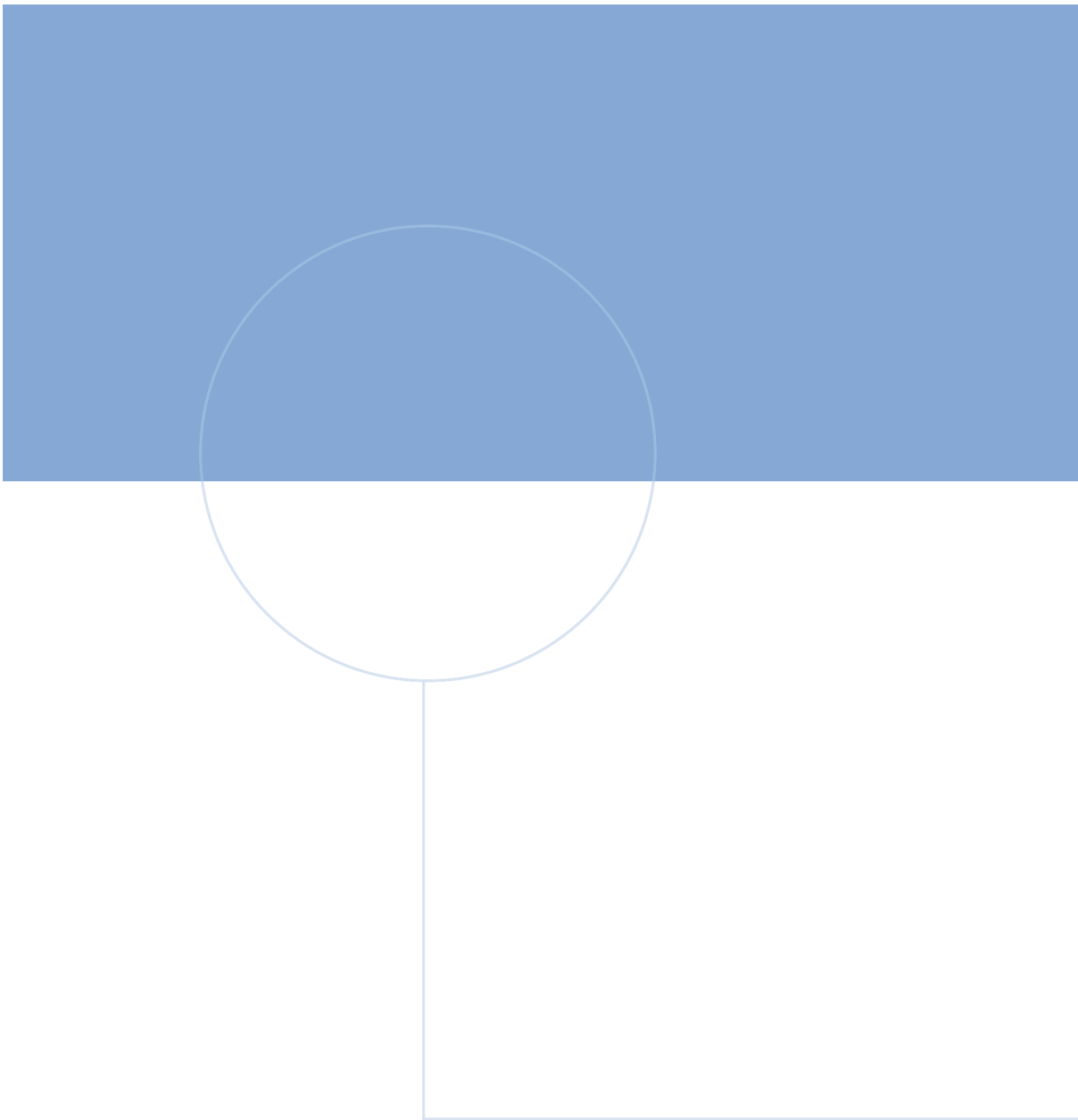

NTNU

Norwegian University of
Science and Technology